T cell specific function of the deubiquitinating enzyme A20 in murine listeriosis

Dissertation

zur Erlangung des akademischen Grades

doctor rerum naturalium
(Dr. rer. nat.)

genehmigt durch die Fakultät für Naturwissenschaften
der Otto-von-Guericke-Universität Magdeburg

von   M. Sc. Sissy Just

geb. am   14.03.1987   in   Eilenburg

Gutachter: Prof. Dr. med. Dirk Schlüter
                    Prof. Dr. rer. nat. Astrid M. Westendorf

eingereicht am: 24. Oktober 2016

verteidigt am: 14. Februar 2017

ACKNOWLEDGEMENT

PUBLICATIONS

Parts of this work are published under the following article:

Just S, Nishanth G, Buchbinder JH, Wang X, Naumann M, Lavrik I, Schlüter D. (2016) A20 curtails primary but augments secondary CD8$^+$ T cell responses in intracellular bacterial infection. *Sci Rep*. Dec 22;6:39796. doi: 10.1038/srep39796.

Other publications:

Nishanth G, Wolleschak D, Fahldieck C, Fischer T, Mullally A, Perner F, Schnöder TM, Just S, Heidel FH, Schlüter D. (2017) Gain of function in Jak2V617F positive T-cells. Leukemia. Feb; 31(2). doi: 10.1038/leu.2017.6.

Hrdinka M, Sudan K, Just S, Drobek A, Stepanek O, Schlüter D, Reinhold D, Jordan BA, Ginschel P, Schraven B, Kreutz MR. (2016) Normal development and function of T cells in Proline Rich 7 (Prr7) mice. *Plos One*. Sep; 11(9): e0162863 doi: 10.1371/journal.pone.0162863.

Wex K, Schmid U, Just S, Wang X, Wurm R, Naumann M, Schlüter D, Nishanth G. (2016) Receptor-interacting protein kinase-2 inhibition by CYLD impairs antibacterial immune responses in macrophages. *Front Immunol*. Jan; 6:650 doi: 10.3389/fimmu.2015.00650.

Wurm R, Just S, Wang X, Wex K, Schmid U, Blanchard N, Waisman A, Schild HJ, Deckert M, Naumann M, Schlüter D, Nishanth G. (2015) Protective dendritic cell responses against listeriosis induced by the short form of the deubiquitinating enzyme CYLD are inhibited by full-length CYLD. *Eur J Immunol*. May; 45(5):1366-76 doi: 10.1002/eji.201445116.

Wang X, Deckert M, Xuan NT, Nishanth G, Just S, Waisman A, Naumann M, Schlüter D. (2013) Astrocytic A20 ameliorates experimental autoimmune encephalomyelitis by inhibiting NF-κB- and STAT1-dependent chemokine production in astrocytes. *Acta Neuropathol*. Nov; 126(5): 711-724 doi: 10.1007/s00401-013-1183-9.

ABSTRACT

Under resting conditions, the immune system has to maintain a homeostasis, but responds rapidly to a wide range of pathogens. $CD8^+$ T cells, a subpopulation of leukocytes, play an important role in eliminating intracellular pathogens, such as *Listeria monocytogenes*, by targeting infected cells. Upon infection, $CD8^+$ T cells are activated, expand and produce effector molecules, such as interferon-γ and granzyme B. After successful elimination of the pathogen, the $CD8^+$ T cell pool contracts and leaves behind a small population of pathogen-specific memory $CD8^+$ T cells, persisting for many years or even lifelong in the host. Upon a secondary infection with the same pathogen, this population rapidly re-expands and mediates immediate protection. The major regulator of the $CD8^+$ T cell response is NF-κB, which mediates activation, expansion and production of effector molecules. The ubiquitin-modifying enzyme A20 (TNFAIP3) negatively regulates NF-κB activation.

To study the T cell-specific function of A20 in bacterial infection, we intravenously infected mice lacking A20 specifically in T cells (CD4-Cre A20^fl/fl) and A20-competent mice with *Listeria monocytogenes*. Interferon-γ and granzyme B-producing A20-deficient pathogen-specific $CD8^+$ T cells expanded stronger, resulting in an improved pathogen control at day 7 p.i. compared to the A20-sufficient counterparts. Surprisingly, upon secondary infection at day 50 p.i., expansion of pathogen-specific $CD8^+$ T cells and pathogen control were significantly impaired in CD4-Cre A20^fl/fl mice. Imaging flow cytometry revealed that the reduced secondary $CD8^+$ T cell response was caused by an increased apoptosis and necroptosis of A20-deficient pathogen-specific effector, effector memory and central memory $CD8^+$ T cells after day 7 p.i. *In vitro*, apoptosis and necroptosis of T cell receptor-stimulated A20-deficient $CD8^+$ T cells were strongly induced, accompanied by increased caspase-3/7 activity, caspase-3 cleavage and RIPK1/RIPK3 complex formation. Furthermore, A20-deficient $CD8^+$ T cells expressed significantly more CD95, which was completely abolished *in vitro* by inhibition of NF-κB. CD95L stimulation resulted in increased active caspase-3/7 and cell death of A20-deficient $CD8^+$ T cells indicating that A20 limited cell death by reducing NF-κB-dependent CD95 expression.

In conclusion, this study uncovers that T cell-specific A20 limits the expansion of *Listeria*-specific $CD8^+$ T cells but reduces apoptosis and necroptosis resulting in an impaired clearance of *Listeria* in primary but improved control in secondary infection. Understanding mechanisms of T cell responses and development of memory T cells will be helpful in designing new vaccination strategies to boost T cell immune responses.

TABLE OF CONTENTS

TABLE OF CONTENTS

LIST OF FIGURES

LIST OF TABLES

ABBREVIATIONS

7

7-AAD. *7-Amino-Actinomycin D*

A

ABIN1. *A20-binding Inhibitor of NF-κB Activation 1*
ACAD. *Activated Cell-autonomous Death*
AD-EDA-ID. *Autosomal-dominant Anhidrotic Ectodermal Dysplasia With Immunodeficiency*
AICD. *Activation-induced Cell Death*
ALT. *Alanine Transaminase, Alanine Aminotransferase*
ANK. *Ankyrin*
APC. *Antigen Presenting Cell*
APS. *Ammonium Persulfate*
ATP. *Adenosine Triphosphate*

B

BAFF-R. *B cell Activating Factor Receptor*
BHI. *Brain Heart Infusion*
Blimp-1. *B Lymphocyte Induced Maturation Protein 1*
BSA. *Bovine Serum Albumin*

C

Carma1. *Caspase Rrecruitment Domain-containing Protein 1*
CBA. *Cytometric Bead Array*
CD. *Cluster of Differentiation*
CFSE. *Carboxyfluoresceindiacetatesuccinimidyl Ester*
CFU. *Colony Forming Unit*
cIAP. *Cellular inhibitor of apoptosis*
CTL. *Cytotoxic T Lymphocytes, Cytotoxic T Lymphocytes*
CYLD. *Cylindromatosis*

D

DC. *Dendritic Cell*
DISC. *Death Inducing Signaling Complex*
DMSO. *Dimethyl Sulfoxide*
dNTP. *Deoxynucleotide*
DPBS. *Dulbecco's Phosphate Buffered Saline*
DSS. *Dextran Sulphate Sodium*
DTT. *Dithiothreitol*
DUB. *Deubiquitinating Enzymes*

E

E1. *Ubiquitin-activating Enzyme*
E2. *Ubiquitin-conjugating Enzyme*
E3. *Ubiquitin Ligase*
EDTA. *Ethylenediaminetetraacetic Acid*
ERK. *Extracellular-signal Regulated Kinase*

F

FADD. *Fas-associated death-domain*
FcεRI. *High-affinity Receptor For The Fc Region Of Immunoglobulin E*
FCS. *Fetal Calf Serum*
FLIP$_L$. *Long Isoform Of FLICE –like Inhibitory Proteins*

G

GAPDH. *Glyceraldehyde 3-phosphate Dehydrogenase*

H

HBSS. *Hank's Balanced Salt Solution*
HEPES. *(4-(2-Hydroxyethyl)-1-piperazine-ethanesulfonic Acid*
HPRT. *Hypoxanthine guanine phosphoribosyl transferase*
HRP. *Horseradish Peroxydase*

I

IκB. *Inhibitor Of Kappa B*
IBD. *Inflammatory Bowel Disease*
IEC. *Intestinal Epithelial Cell*
IFC. *Imaging Flow Cytometry*
IFN. *Interferon*
IgE. *Immunoglobulin E*
IKK. *IκB Kinase*
IL. *Interleukin*
IRAK. *IL-1 Receptor Associated Kinases*

J

JAMM. *JAB1/MPN/Mov34 Metalloenzyme*

K

K. *Lysine*
KHCO$_3$. *Potassium Hydrogene Carbonate*
KLRG-1. *Killer cell lectin-like receptor subfamily G member 1*

L

L. monocytogenes. *Listeria monocytogenes*
Lck. *Lymphocyte-specific Protein Tyrosine Kinase*
Lm OVA. *ovalbumin-expressing Listeria monocytogenes*
Lm WT. *Listeria monocytogenes wildtype EGD*
LPS. *Lipopolysaccharide*
LTβR. *Lymphotoxin-Beta-Receptor*

M

MALT1. *Mucosa-associated Lymphoid Tissue Lymphoma Translocation Protein 1*
MgCl₂. *Magnesium Chloride*
MHC. *Major Histocompatibility Complex*
MJD. *Machado-Josephin Domain Protease*
MLKL. *Mixed Lineage Kinase Domain-like Protein, Mixed Lineage Kinase Domain-like Protein*
MPEC. *Memory precursor effector cells*
MyD88. *Myeloid Differentiation Primary-response 88*

N

NaCl. *Sodium Chloride*
NEAA. *Non-essential Amino Acids*
NF-κB. *Nuclear Factor 'kappa-light-chain-enhancer' Of Activated B cell*
NH₄Cl. *Ammonium Chloride*
NIK. *NF-κB Inducing Kinase*
NKT. *Natural Killer T Cell*

O

OTU. *Ovarian Tumor Protease*
OTUB1. *OTU-domain Ubal-binding Protein-1*
OTUD7B. *Cezanne*

P

PAMP. *Pathogen Associated Molecular Pattern*
PCD. *Programmed Cell Death*
PD-1. *Programmed Cell Death Protein-1*
PFA. *Paraformaldehyde*
PKCθ. *Protein Kinase C theta*
PLCγ1. *Phospholipase C, gamma 1*
PMSF. *Phenylmethanesulfonylfluoride*
PRR. *Pattern Recognition Receptor*
PVDF. *Polyvinylidene Fluoride*

R

RANK. *Receptor Activator Of Nuclear Factor Kappa B*
RHD. *Rel Homolgy Domain*
RIPA. *Radioimmunoprecipitation Assay*
RIPK. *Receptor-interacting Protein Kinase*
RPMI. *Roswell Park Memorial Institute Medium*
RT. *Room Temperature*
RT-qPCR. *Quantitative Reverse Transcription PCR*

S

SDS. *Sodium Dodecyl Sulfate*
SDS-PAGE. *Sodium Dodecyl Sulfate Polyacrylamide Gel Electrophoresis*
SLEC. *short-lived effector cell*
SNP. *Single Nucleotide Polymorphisms*

T

TAB. *TAK-binding Protein*
TAD. *Transactivation Domain*
TAK1. *Transforming Growth Factor Beta-activated Kinase*
TAX1BP1. *TAX1-binding Protein 1*
TBE. *Tris-borate-EDTA*
TBST. *Tris Buffered Saline With Tween*
T_CM. *Central Memory T Cell*
TCR. *T Cell Receptor*
T_eff. *effector T cell*
T_EM. *Effector Memory T Cell*
TEMED. *Tetramethylethylendiamine*
TGFβ. *Transforming Growth Factor Beta*
T_h. *CD4⁺ T Helper Cells*
TLR. *Toll-Like Receptor, Toll-like Receptor*
T_mem. *Memory T Cell*
TNF. *Tumor Necrosis Factor*
TNFAIP3. *Tumor Necrosis Factor Alpha-induced Protein 3*
TNF-R. *Tumor Necrosis Factor Receptor*
TRADD. *TNF-R-associated death-domain*
TRAF6. *TNF-Receptor Associated Factor 6*
T_reg. *Regulatory T Cells*

U

UCH. *Ubiquitin Carboxy-terminal Hydrolase*
USP. *Ubiquitin-specific Protease*

Z

ZAP-70. *Zeta-chain-associated Protein Kinase 70*
ZF. *Zinc Finger*

1. INTRODUCTION

Organisms are in constant exchange with their environment. These interactions can have a profitable or harmful outcome. While nutrition, light and other factors have a beneficial effect; parasites, viruses and bacteria can have a detrimental or even deadly effect on the organism. The key mechanism of a multicellular organism to cope with these pathogens is the immune system. It can distinguish self from non-self antigens and induces a complex and multifaceted response to the latter.

The immune response is broadly regulated by the NF-κB (nuclear factor kappa-light-chain enhancer of activated B cells) transcription family. NF-κB mediates activation, proliferation, cytokine production and survival of the immune cells in response to the surrounding environment. Downregulation of NF-κB, and thereby the immune system, is associated with cancer development or increased risk of infection. However, an overshooting immune response can induce immunopathology, autoimmune disease and allergic reactions.

To maintain the balance between protective and harmful reactions of the immune system, NF-κB has to be tightly regulated by the modulation of upstream signaling events. Ubiquitination is a posttranslational modification regulating signal transduction. Removal of ubiquitin from the substrate by deubiquitinating enzymes, such as A20, can inhibit or redirect signal transduction.

In the course of infection, a tight regulation of the complex network of signal-transducing molecules is crucial. Investigations on regulators in this network contribute not only to our understanding of the immune system but also pave the way for future clinical research and drug development.

1.1 T lymphocytes

The immune system comprises of two parts which closely interact with each other: the innate immune system, generally considered to be the first line of defense, and the specific adaptive immune system comprising of highly specialized cells mediating pathogen elimination as well as the induction of immunological memory. The T lymphocytes are key members of the adaptive immune system. Depending on their surface glycoproteins, they can be further divided into two major subtypes, CD4 (cluster of differentiation 4) or CD8 T lymphocytes: CD4$^+$ T lymphocytes, also named T helper cells, mainly regulate the immune response by releasing cytokines and chemokines to activate or suppress other immune cells. CD8$^+$ T lymphocytes, also called cytotoxic T lymphocytes (CTLs), directly kill infected or damaged cells as well as cancer cells.

1.1.1 T cell development

T lymphocyte progenitors develop from the haematopoietic stem cells in the bone marrow. The progenitor cells then migrate to the cortex of the thymus, the primary lymphoid organ, where the maturation is initiated. The maturation process is divided into three different stages, depending on the expression of CD4 and CD8 surface markers: double-negative, double-positive and single-positive. The T lymphocyte progenitors enter the thymus as double-negative (CD4$^-$CD8$^-$). During this stage the pre-T cell receptor (TCR) is expressed, consisting of a pre-α-chain and a rearranged β-chain. Beta-selection takes place, a process where T cells with non-functional TCRs undergo apoptosis. T cells with a functional pre-TCR receive a weak signal, necessary for survival and enter the double positive stage (CD4$^+$CD8$^+$). During this stage, rearrangement of the α-chain occurs, resulting in the development of a complete αβ TCR (Klein et al., 2016). Thereafter, positive selection takes place, where the thymocytes bind to cortical epithelial cells, which highly express major histocompatibility complex (MHC) class I and II molecules, presenting self-antigens. T cells unable to bind to the MHC molecule undergo apoptosis, while successful binding leads to maturation of the thymocyte into either CD4$^+$ (T helper cells; recognizing MHC class II) or CD8$^+$ T cells (cytotoxic T cells; recognizing MHC class I). During the single-positive stage the thymocytes migrate from the cortex to the medulla where negative selection takes place. Thymocytes with a high affinity for binding self-antigen are considered autoreactive, and, therefore, undergo cell death. Thymocytes with low or weak TCR affinity pass the selection process and are released into the periphery (Germain,

2002). The mature T lymphocytes harbor in the secondary lymphoid organs such as lymph nodes and spleen, where they become activated upon encountering antigens during infection.

1.1.2 T cell receptor

The activation of T lymphocytes is dependent on the presentation of antigen by professional antigen presenting cells (APCs) such as dendritic cells. APCs process and present antigens on MHC molecules. The T cell receptor (TCR), as a T lymphocyte-specific receptor, is responsible for the recognition of antigens presented by the MHC molecule. Interaction of the TCR with the antigen/MHC-complex, leads to T cell activation, induction of cell proliferation, migration to the site of infection and production of effector molecules. While a minority of T lymphocytes express a TCR with γδ-chains, the most common TCR is a heterodimer comprising of the α- and β-subunit, each consisting of a constant region and a variable, antigen binding region (Figure 1). Associated with the TCR is the CD3 co-receptor, which comprises of four chains, a CD3γ chain, a CD3δ chain and two CD3ε chains. Together with the intracellular located ζ-chain, these components form the TCR complex (Choudhuri and van der Merwe, 2007).
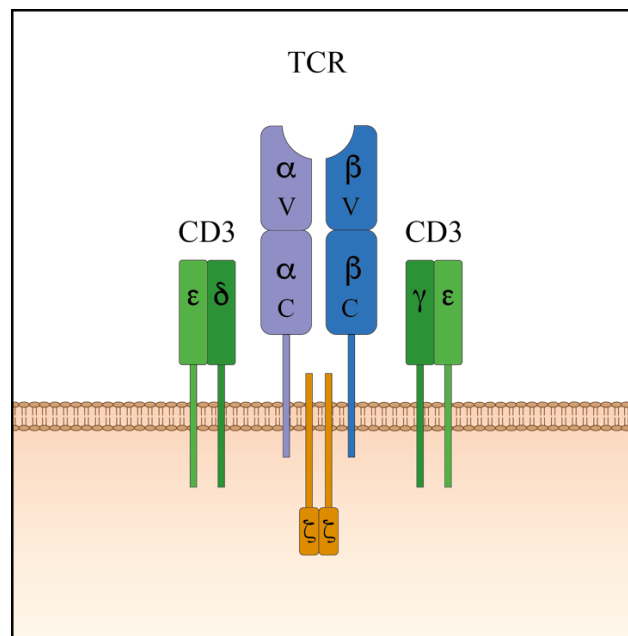
Figure 1: The T cell receptor complex.
The TCR complex comprises of the T cell receptor, the CD3 co-receptor and the ζ-chain. The α- and β-chain of the TCR each consist of two extracellular domains: a constant (C) region and a variable (V) region. The variable region recognizes antigen by binding to the peptide/MHC complex. The co-receptor CD3 consists of the γ-chain, δ-chain and two ε-chains. TCR T cell receptor; CD3 Cluster of differentiation 3.

Each T cell recognizes a different antigen via the variable region in the TCR. This diversity is achieved during T cell development in the thymus by TCR gene rearrangement. Recombination resulting in random antigen-binding sites of the α- and β-TCR chains allowing the recognition of a great variety of antigens.

1.1.3 The T cell network

Initially, a T cell progenitor gives rise to either a γδ- or αβ-T cell in the thymus.
αβ-T cells are then further subdivided into natural killer- (NKT-), regulatory T cells (T_{regs}), $CD4^+$ T helper cells and $CD8^+$ T cells. NKT cells preferably recognize foreign lipids and glycolipids, e.g. from *Mycobacterium tuberculosis* (Chackerian et al., 2002). Malfunction of NKT cells leads to autoimmunity and cancer development. (Berzins et al., 2011)
T_{regs} play a crucial role in the maintenance of immune homeostasis. They prevent inflammation and autoimmune disease by production of anti-inflammatory cytokines like interleukin- (IL-) 10 and transforming growth factor beta (TGFβ) (Vignali et al., 2008).
Upon activation in the periphery, $CD4^+$ T helper cells (T_H) are differentiated based on their cytokine profile into the three main lineages T_h1, T_h2 and T_h17, which perform different functions in immune regulation and infection. T_h1 lineage cells promote the clearance of intracellular pathogens by inducing microbicidal activity of macrophages via IFN-γ secretion (Zhu and Paul, 2009). In addition, T_h1 cells mediate memory $CD8^+$ T cell development in an IL-2-dependent manner (Williams et al., 2006). Malfunctions of T_h1 cells can mediate organ-specific autoimmunity, e.g. insulin-dependent diabetes mellitus or experimental autoimmune encephalomyelitis (EAE) (Trembleau et al., 1999; Zhu and Paul, 2009). T_h2 lineage cells mainly produce IL-4 and IL-10 and defend the host against extracellular parasites, but a dysfunctional T_h2 response can induce asthma and other allergic diseases (Zhu and Paul, 2009). T_h17 lineage cells mediate an immune response against extracellular bacteria and fungi, but on the other hand are inducers of autoimmune diseases like multiple sclerosis, rheumatoid arthritis, inflammatory bowel disease or systemic lupus erythematodes (Bedoya et al., 2013).
Upon infection with intracellular pathogens, such as viruses or certain bacteria e.g. *Listeria monocytogenes*, naïve $CD8^+$ T cells develop into effector CTL and mediate a strong immune response. Dysfunctional $CD8^+$ T cells might induce autoimmune diseases including hepatitis, systemic lupus erythematosus and type-1 diabetes (Blanco et al., 2005; Graham et al., 2011; Ichiki et al., 2005).

1.1.4 Immune response to *Listeria monocytogenes*

Food-borne pathogens are very common and infect worldwide millions of people every year. Listeriosis, caused by the Gram-positive bacterium *Listeria monocytogenes* may lead to mild symptoms including fever, headache, nausea and diarrhea. However, in particular in infants, immunocompromised individuals as well as the elderly, *L. monocytogenes* may cause a life-threatening sepsis, meningitis and encephalitis. During pregnancy, *L. monocytogenes* can be transmitted hematogenously via the placenta resulting in severe complications for the fetus (Hamon et al., 2006).

L. monocytogenes is a widely used model organism to study host-pathogen interactions and has contributed profoundly to our understanding of cellular immune responses (Shen et al., 1998). In a systemic *L. monocytogenes* infection the pathogen disseminates via the blood stream to the liver and the spleen, where it is internalized by macrophages (Pamer, 2004). In the liver, *L. monocytogenes* then transmigrates to hepatocytes, the major replication site. As a facultative intracellular pathogen, *L. monocytogenes* is able to survive and replicate in phagocytic cells, such as macrophages, as well as a wide range of non-phagocytic cells, e.g. epithelial cells and hepatocytes. Inside the host cell, the bacterium replicates and directly spread to neighboring cells, thereby evading antibody neutralization.

Bacterial antigens or pathogen associated molecular patterns (PAMPs), including the cytolytic listeriolysine O and the membrane component peptidoglycane of *L. monocytogenes* are recognized via specific pattern recognition receptors (PRRs) such as Toll-like receptors (TLRs) by innate immune cells (Stavru et al., 2011). The detection of PAMPs leads to an activation of the innate immune cells, recruitment to the site of infection to limit the bacterial growth, induction of cytokine and chemokines production to further recruit leukocytes (Schuppler and Loessner, 2010). Nevertheless, CD8^{+} T cells play a crucial role for the final elimination of *L. monocytogenes* (Pamer, 2004). The classical T cell response can be divided into three phases: (i) expansion phase, (ii) contraction phase and (iii) memory phase (Figure 2). During the expansion phase bacterial antigens are presented via the MHC class I receptor of APCs, which are then recognized by CD8^{+} T cells. Activated CD8^{+} T cells undergo clonal expansion, differentiate into CTLs and migrate to the site of infection where they secrete effector molecules such as granzyme B and perforin, leading to the lysis of infected cells. Furthermore, CTLs produce pro-inflammatory cytokines such as interferon gamma (IFN-γ) and tumor necrosis factor (TNF) which induces chemokine-mediated recruitment of innate immune cell to the site of infection (Stavru et al., 2011).
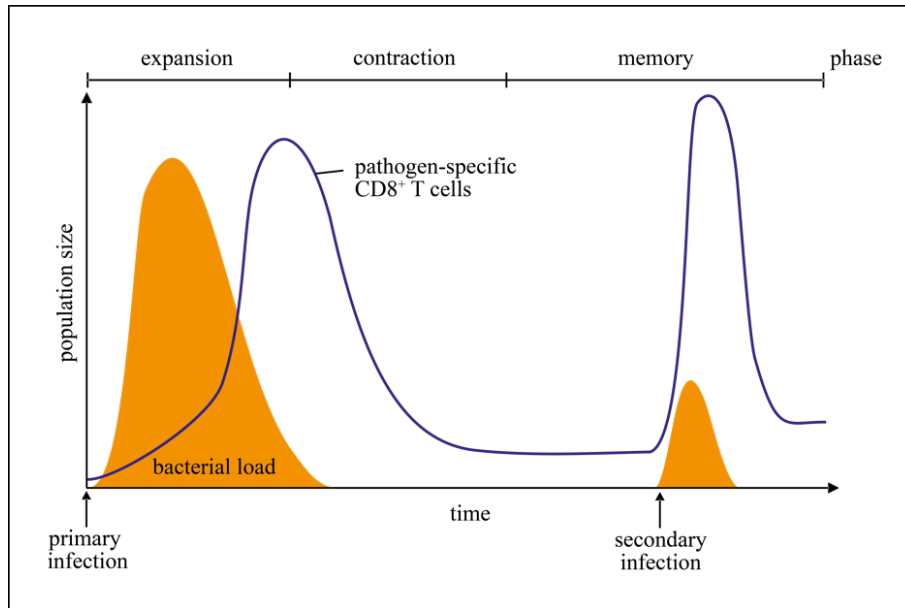
Figure 2: T cell response during primary and secondary bacterial infection.
Infection with the intracellular pathogen *L. monocytogenes* induces a potent CD8$^+$ T cell response. After the contraction phase where most of the pathogen-specific T cells die, a small pool of memory T cells is generated. These memory T cells confer protective immunity against a second infection with the same pathogen. Orange filled curve: bacterial growth; blue curve: number of pathogen-specific CD8$^+$ T cells (adapted and modified from Kaech et al., 2002).

After the elimination of the pathogen, the contraction phase of the pathogen-specific T cell pool is initiated. The contraction is mainly mediated by activation-induced cell death (AICD) and activated cell-autonomous death (ACAD). AICD is a Fas (CD95)-dependent process, initiated upon persistent TCR stimulation. ACAD, also called "death by neglect", occurs due to a lack of survival signals (Krammer et al., 2007; Krueger et al., 2003).

Around 90-95 % of the cells undergo cell death, leaving a small pool of memory T cells (T$_{mem}$) behind (Jameson, 2002; Sprent and Tough, 2001). Many extrinsic and intrinsic factors influencing the formation and function of CD8$^+$ T$_{mem}$ have been identified so far. CD4$^+$ T cells, although not crucial for the clearance of *L. monocytogenes*, are required during the primary response for the generation of a functional CD8$^+$ T$_{mem}$ compartment. Mice lacking CD4$^+$ T cells, have an impaired secondary CD8$^+$ T cell response, characterized by increased bacterial burden as well as reduced CD8$^+$ T$_{mem}$ proliferation and cytokine production (Shedlock and Shen, 2003; Sun and Bevan, 2003).

T$_{mem}$ derive from effector T cells, but, not all effector cells can turn into memory cells. The heterogeneous pool of effector CD8$^+$ T cells can be characterized by their ability to transform into memory T cells. Short-lived effector cells (SLEC) express killer cell lectin like receptor G1 (KLRG-1^{high}) but not IL-7Ra (CD127^{low}) and are not maintained after the infection is cleared.

Memory precursor effector cells (MPEC), however, express CD127, but not KLRG-1 and survive the primary T cell response. Both, MPEC and SLEC, arise from the KLRG-1^{low}CD127^{low} early effector cells (EEC) (Joshi et al., 2007; Zhang and Bevan, 2011). Over time MPECs transition into memory T cells, which can be further divided into two functionally different subsets: CD62L^{high}CD127^{high} central memory T cells (T$_{CM}$) and CD62L^{low}CD127^{high} effector memory T cells (T$_{EM}$) (Huster et al., 2004). T$_{EM}$, which migrate through spleen, blood and non-lymphoid tissue, provide immediate effector function, including cytolytic activity and secretion of cytokines. T$_{CM}$, by migrating through secondary lymphoid organs such as spleen and lymph nodes but not non-lymphoid tissue, provide less effector function, but proliferate and differentiate rapidly to effector cells after antigen recognition (Sallusto et al., 2004).

During the memory phase, a second encounter with *L. monocytogenes* initiates a rapid expansion of memory T cells, leading to an immediate, strong protective immunity and faster bacterial clearance (Figure 2). Many factors contribute to this feature: i) an increased number of pathogen-specific cells, ii) enhanced activation status of CD8$^+$ T$_{mem}$, iii) reduced stimulation threshold and iv) a faster and stronger effector function of the memory T cells (Sallusto et al., 2004; Seder and Ahmed, 2003).

All these processes must be carefully regulated to maintain a balanced immune response. While an overshooting response can cause autoimmune diseases and hyperinflammation, a compromised immune response leads to increased susceptibility to infection and cancer development. Key regulators of the immune system are members of the transcription factor nuclear factor 'kappa-light-chain-enhancer' of activated B-cells (NF-κB) family.

1.2 NF-κB pathway

Cellular processes such as development, proliferation, production of effector molecules and cell survival are strongly dependent on the regulation by members of the NF-κB family (Li et al., 2002). Five members belong to this family: RelA (p65), RelB, c-Rel, NF-κB1 and NF-κB2 (Figure 3A) (Oeckinghaus and Ghosh, 2009).
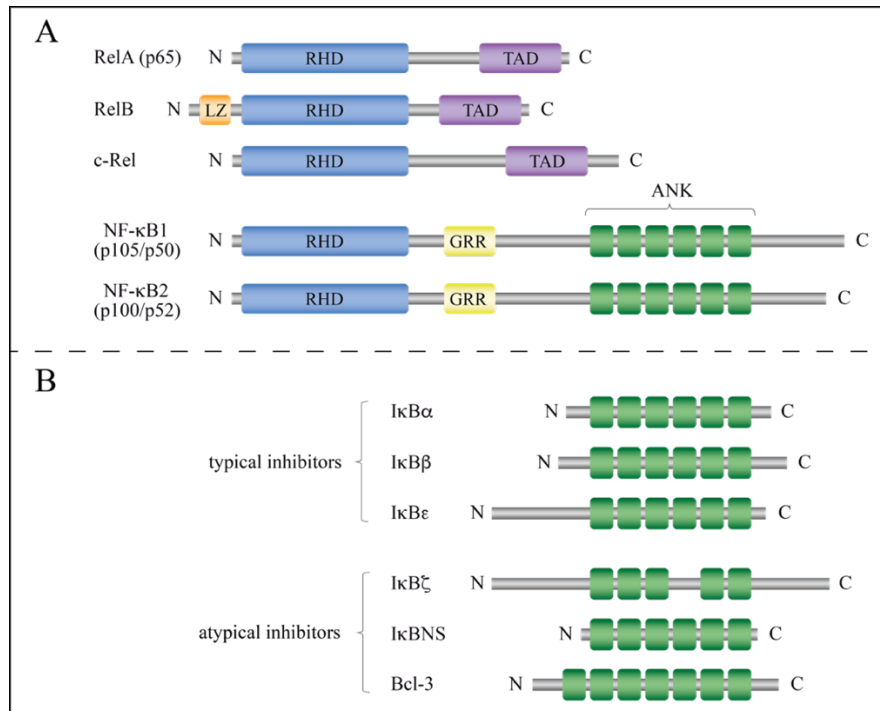
Figure 3: Domain structure of the NF-κB- and IκB- family.
A| The mammalian NF-κB family consists of the members: RelA (p65), RelB, cRel, NF-κB1 (p105/50) and NF-κB2 (p100/p52). All of them share a Rel-homology domain (RHD) at the N-terminal region. In addition, RelA, RelB and c-Rel have a non-homologous transactivation domain (TAD) at the C-terminus. RelB, as the only member, has a leucine-zipper motif (LZ) at the N-terminus region. Instead of a transactivation domain, p105/p50 and p100/p52 share glycine-rich regions (GRR) and ankyrin (ANK) repeats. The precursors p105 and p100 function as inhibitors of NF-κB. After proteasomal degradation the subunits p50 and p52 are released and act as NF-κB transcription factors. **B|** The IκB family contains the typical members IκBα, IκBβ, IκBε and the atypical members IκBζ, IκBNS and Bcl-3. All inhibitors are characterized by their ANK domains (adapted and modified from Ghosh and Hayden, 2008).

All members share a highly conserved domain called Rel homology domain (RHD), required for dimerization, nuclear localization and DNA binding (Ghosh et al., 1998). Furthermore, RelA, RelB and c-Rel possess a transactivation domain (TAD), important for activation of target gene transcription. NF-κB1, also called p50, is derived from the precursor p105, while NF-κB2, also called p52, is derived from the precursor p100 (Oeckinghaus and Ghosh, 2009). Both transcription factors lack a transactivation domain and, therefore, can only initiate transcription by formation of heterodimers with RelA, RelB c-Rel or other factors (Ghosh and Hayden, 2008). In unstimulated cells, the members

of the NF-κB family are sustained inactive in the cytoplasm by interaction with an inhibitor of kappa B (IκB).

Three groups are described in the IκB protein family: the typical inhibitors (IκBα, IκBβ and IκBε), the atypical inhibitors (IκBζ, IκBNS and B cell lymphoma (Bcl) 3) (Figure 3B) and the precursors p105 and p100 which can be cleaved to release p50 or p52, respectively (Figure 3A). All members of the IκB family are characterized by the presence of ankyrin (ANK) repeats, which mediate protein-protein-interactions (Ghosh and Hayden, 2008; Oeckinghaus and Ghosh, 2009).

1.2.1 Canonical and non-canonical NF-κB pathway

NF-κB signaling is commonly divided into two main pathways, the canonical and the non-canonical pathway, inducible by a broad range of different ligand-receptor interactions. The canonical NF-κB pathway (Figure 4A) is activated by antigen receptors, TLRs and cytokine signaling, e.g. via IL-1R or TNF-R (Verstrepen et al., 2008).

The signaling cascades, induced by different stimuli, lead to the phosphorylation and activation of the IκB kinase (IKK) complex, which consists of two catalytical subunits IKKα and IKKβ and the regulatory subunit IKKγ (also known as NF-κB-essential modulator (NEMO)). This complex plays a key role in the activation of NF-κB, as the inhibition of IKK leads to complete blockage of NF-κB activation. The activated IKK complex phosphorylates IκB, initiating ubiquitination and proteasomal degradation of IκB. The NF-κB heterodimer is released and translocates to the nucleus to induce gene transcription (Li et al., 2002).
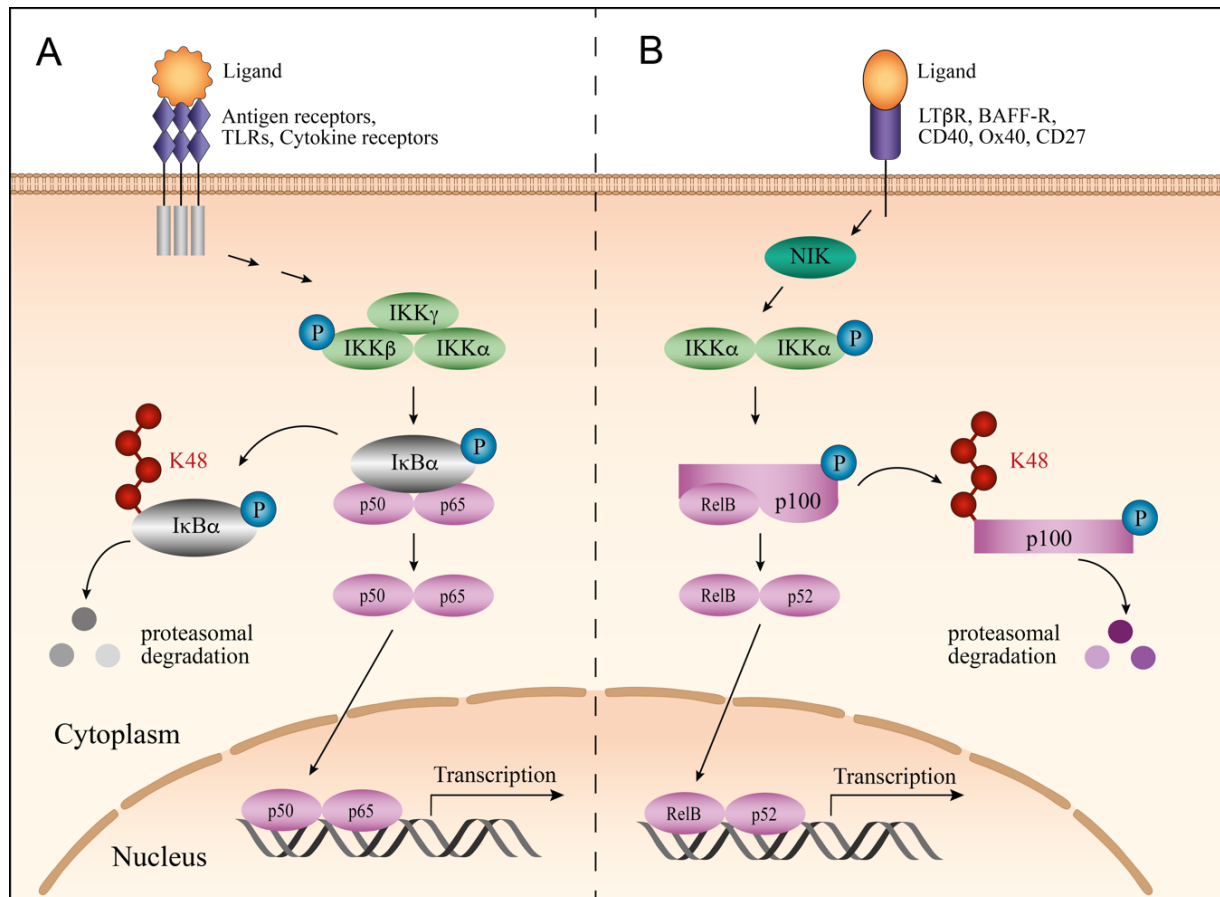
Figure 4: Canonical and non-canonical NF-κB signaling.
Canonical and non-canonical NF-κB pathways are activated by different receptors. **A|** In the canonical NF-κB pathway the IKKβ subunit is activated by phosphorylation. The activated IKK complex then phosphorylates IκB, bound to the NF-κB heterodimer (e.g. p50/p65). Activation of IκB leads to ubiquitination and proteasomal degradation, therefore, releasing the NF-κB transcription factor. NF-κB then translocates to the nucleus and induces transcription of immune regulatory genes.
B| The non-canonical NF-κB pathway is characterized by the activation of NIK, which in turn activates IKKα. IKKα phosphorylates p100 (NF-κB2), leading to ubiquitination and proteasomal degradation, releasing the p52/RelB heterodimer. The NF-κB subunit then translocates to the nucleus and activates transcription of target genes. Red: K48-linked ubiquitin; blue: phosphorylation.
IκB: Inhibitor of kappa B; IKK: IκB kinase; P: Phosphorylation; K48: Lysine-48 linked polyubiquitin chain; NIK: NF-κB inducing kinase; TLR: Toll-like receptor; LTβR: Lymphotoxin beta receptor; BAFF-R: B cell-activating factor receptor. CD: Cluster of differentiation.

The non-canonical NF-κB pathway (Figure 4B) is activated by a variety of receptors, belonging to the tumor necrosis factor (TNF) receptor (TNF-R) superfamily, such as the lymphotoxin-beta-receptor (LTβR), B cell activating receptor (BAFF-R) or CD40. Non-canonical NF-κB activity is regulated independently of IKKβ and IKKγ. The NF-κB inducing kinase (NIK) phosphorylates IKKα, which then in turn activates p100. Activation of p100 leads to its ubiquitination and proteasomal processing, releasing the p52/RelB complex. This heterodimer translocates to the nucleus and induces gene transcription (Sun, 2011). All of the NF-κB dependent signaling pathways share the common principle of ubiquitination as a mode of signal transduction (Harhaj and Dixit, 2010).

1.3 Ubiquitination/Deubiquitination

Ubiquitin, a 76 amino acid small peptide, is covalently attached to lysine (K) residues of substrate molecules (Hershko et al., 1998). Ubiquitin regulates the stability, function or localization of a protein. Ubiquitin molecules bind to the substrate by a process called ubiquitination, which requires three enzymes E1, E2 and E3 (Figure 5) (Pickart and Eddins, 2004).
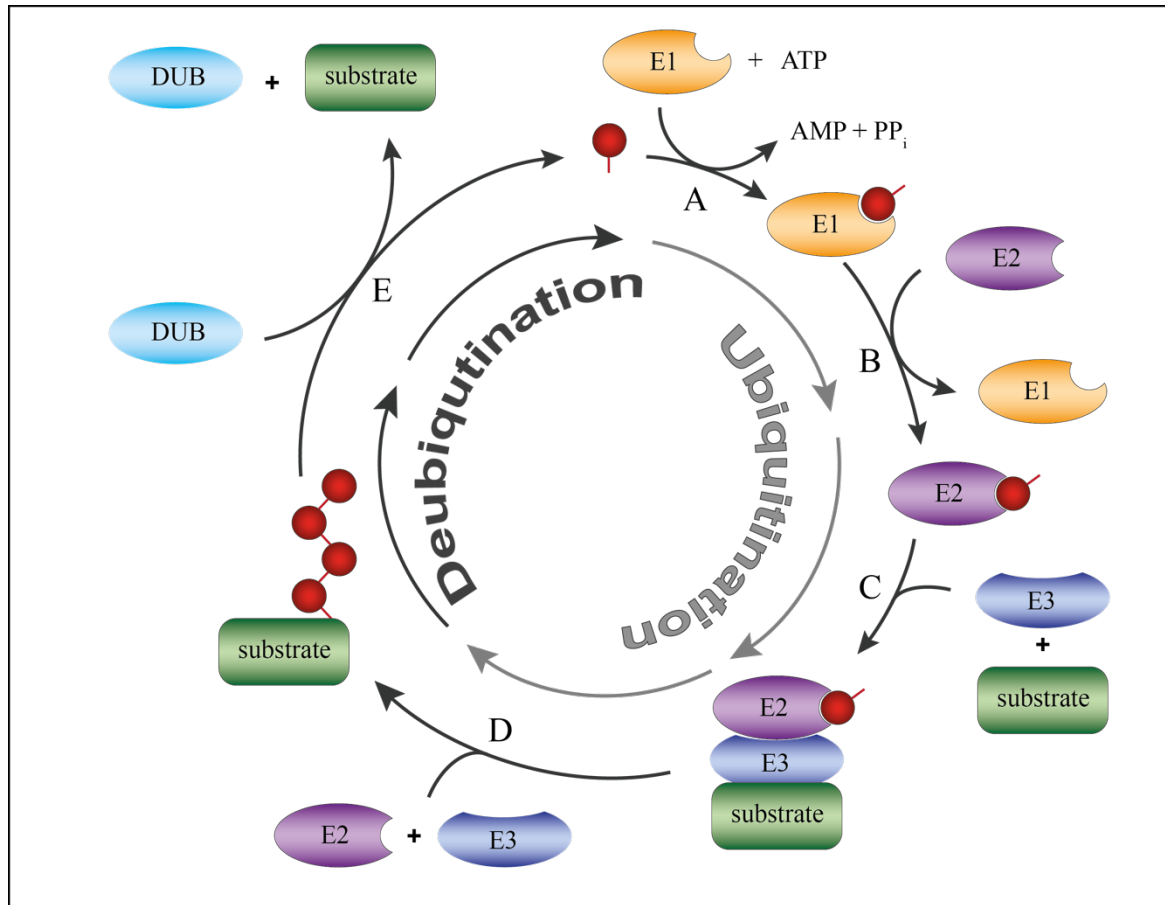
Figure 5: The processes of ubiquitination and deubiquitination.
For the process of ubiquitination, three classes of enzymes (E1, E2 and E3) are required. **A|** The ubiquitin-activating enzyme (E1) activates the ubiquitin molecule, linking E1 with the ubiquitin. **B|** The ubiquitin molecule is transferred to the ubiquitin-conjugating enzyme E2. **C|** E2 conjugates with a substrate-specific ubiquitin ligase (E3). **D|** The E2-E3 complex binds to its target molecule and transfers the ubiquitin to the substrate protein. Polyubiquitin chains are formed by repeating this process multiple times. **E|** The process of ubiquitination is reversible and is mediated by deubiquitinating enzymes (e.g. A20), which remove ubiquitin molecules from the substrate.

The ubiquitin-activating enzyme (E1) activates the C-terminal glycine of the ubiquitin molecule in an ATP (Adenosine triphosphate)-dependent manner and is then linked to a cysteine residue in the active site of E1 (Figure 5A). The ubiquitin is transferred to the ubiquitin-conjugating enzyme E2 through *trans*-acylation (Figure 5B). Finally, E2 conjugates with a substrate-specific ubiquitin ligase (E3), which mediates the transfer of

the ubiquitin to a lysine residue of the targeted substrate (Figure 5C+D). While only two E1s are encoded in the human genome, the specificity increases with at least 38 E2s and between 600- 1000 existing E3s, making the process of ubiquitination highly elaborate and diverse (Ye and Rape, 2009).

A protein may undergo a variety of different ubiquitin modifications, inducing different physiological functions (Figure 6) (Hochstrasser and Amerik, 2004; Malynn and Ma, 2010). Monoubiquitination describes the conjugation of one or more (multiple mono-ubiquitination) ubiquitin molecules to the target lysine (K) residue. This process is mainly involved in endocytosis, DNA repair, protein transport and histone modifications (Kerscher et al., 2006). The ubiquitin molecule itself has seven lysine residues (K6, K11, K27, K29, K33, K48 and K63), which can also be targeted as acceptor sites for the ubiquitination process, leading to the formation of polyubiquitin chains and therefore, to the execution of different cellular processes, such as proteasomal degradation, signal transduction and DNA repair (Adhikari and Chen, 2009; Husnjak and Dikic, 2012).
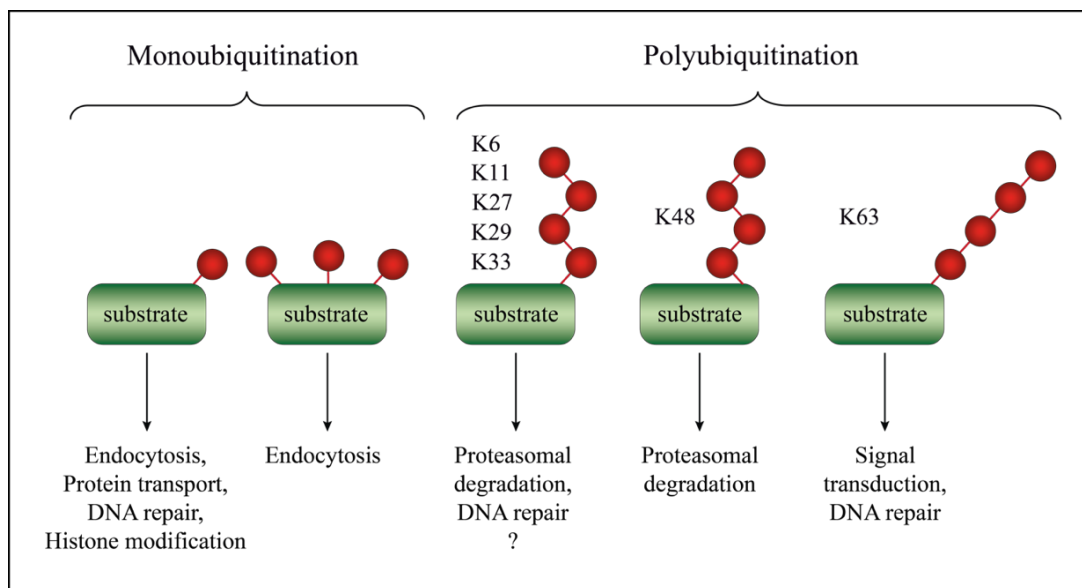
Figure 6: Diversity and cellular function of ubiquitin modifications.
Ubiquitin, an 8.5 kDa small protein, is added to a substrate as a post-translational modification. Different types of ubiquitination can occur. Monoubiquitination is characterized by the addition of one or more (but single) ubiquitin molecules to the target. The linkage of several ubiquitin molecules to one of the internal lysine (K) residues (K6, K11, K27, K29, K33, K48 and K63) leads to polyubiquitination. Different ubiquitin-linkages execute different functions within the cell.

While the function of K6, K11, K27, K29 and K33 polyubiquitin chains is not yet completely understood, K48 and K63-linked ubiquitin are the most intensively studied forms of ubiquitination. Both of them play an important role in the NF-κB signaling pathway. Phosphorylation of IκBα via the IKK complex leads to the induction of the ubiquitination process. K48-linked ubiquitin is added to IκBα, which is then targeted for

degradation via the 26S proteasome, thereby releasing the NF-κB heterodimers p50/p65. Upstream of the IKK complex, K63-linked polyubiquitination of a variety of substrates, such as Receptor-interacting protein kinase 1 (RIPK1), TNF-receptor associated factor 6 (TRAF6) and Mucosa-associated lymphoid tissue lymphoma translocation protein 1 (MALT1), regulates induction of signal transduction (Donnell et al., 2007; Lamothe et al., 2007; Oeckinghaus et al., 2007).

Ubiquitination is a reversible process, adding another level of complexity to this posttranslational modification. Removal of ubiquitin molecules from substrates is mediated by deubiquitinating enzymes like A20 (Figure 5E). Deubiquitination leads to the termination of signal transduction by removal of ubiquitin chains from the target protein. This process requires deubiquitinating enzymes (DUBs). In the human genome, 95 different DUBs are encoded, and can be divided into two classes: cysteine proteases and metalloproteases with JAB1/MPN/Mov34 (JAMMs) as their only member (Nijman et al., 2005). Cysteine proteases can be further divided into four families according to their structural specifications: ubiquitin carboxy-terminal hydrolases (UCHs), ubiquitin-specific proteases (USPs), ovarian tumor proteases (OTUs), Machado-Josephin domain proteases (MJDs). The largest group of DUBs are the USPs with 53 genes identified in the human genome among them the most intensive studied member Cylindromatosis (CYLD). The second largest group, the OTU-family comprises 24 members in the human genome. Among them are several important regulators of NF-κB signaling, such as OTU-domain Ubal-binding protein-1 (Otubain-1 or OTUB1), Cezanne (OTUD7B) and the Tumor necrosis factor alpha-induced protein 3 (TNFAIP3 or A20).

1.4 Immunoregulatory function of A20

A20 was first identified as a TNF-induced gene product in human endothelial cells (Opipari et al., 1990). Subsequently, upregulation of A20 upon a variety of other stimuli has been found in almost all cell types. A20 is induced by the NF-κB pathway. Upon activation, A20 inhibits NF-κB mediated transcription, thereby, acting as a negative feedback regulator in the NF-κB signaling pathway (Harhaj and Dixit, 2010).
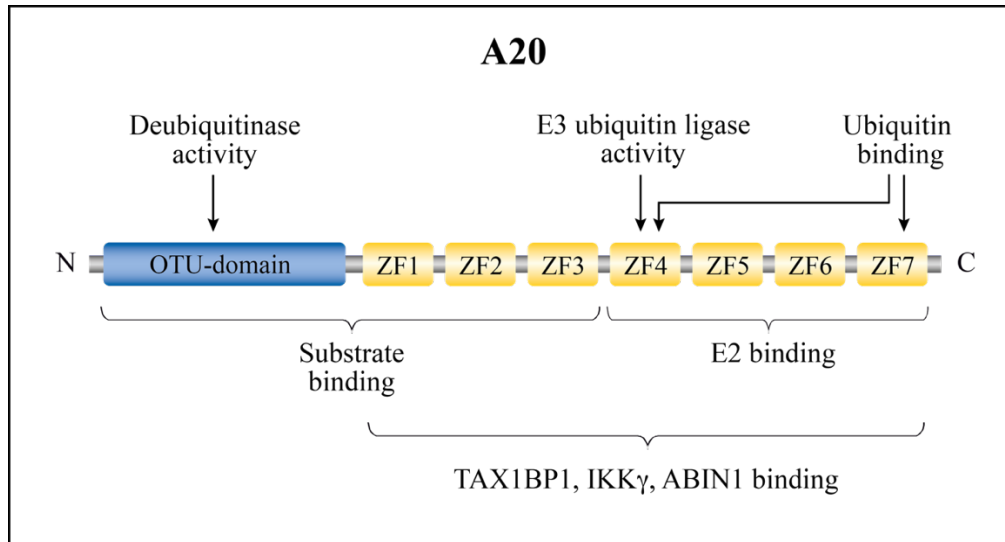
Figure 7: Domain structure of A20 and its biological characteristics.
A20 consists of an N-terminal OTU-domain, which catalyzes the deubiquitinating activity and the seven C-terminal zinc-finger-domains. ZF4 mediates E3 ubiquitin ligase activity. The ubiquitin binding activity is shared by ZF4 and ZF7. OTU: Ovarian tumor; ZF: Zinc finger; TAX1BP1: TAX1 binding protein 1; IKKγ: IκB kinase; ABIN1: A20-binding inhibitor of NF-κB (adapted and modified from Ma and Malynn, 2012).

Its deubiquitinating activity is mediated by the N-terminal OTU-domain (Figure 7), preferentially cleaving K63-linked polyubiquitin from the target protein, thus, leading to the termination of signal transduction. In addition, A20 adds K48-ubiquitin chains to the substrate, targeting it for proteasomal degradation. Furthermore, A20 comprises of seven zinc finger domains (ZFs) at the C-terminal region, each executing different functions like interaction with ubiquitin-binding proteins such as A20-binding inhibitor of NF-κB activation 1 (ABIN1), IKKγ or TAX1-binding protein 1 (TAX1BP1). While substrate binding, e.g. to RIPK1 is mediated by ZF1-3, ZF4 facilitates E3 ubiquitin ligase activity. Furthermore, ZF4 as well as ZF7 display ubiquitin binding activity. Via ZF4-7, A20 binds to E2 enzymes such as UBCH5A (Ma and Malynn, 2012).

Mice deficient for A20 (*Tnfaip3*^{-/-}) die prematurely of cachexia and tissue inflammation due to a hyperactivation of NF-κB (Lee et al., 2000), indicating a crucial role of A20 in immune homeostasis.

In humans, single nucleotide polymorphisms (SNPs) and mutations in the *Tnfaip3* gene locus have been associated with a variety of autoimmune diseases, such as psoriasis, systemic lupus erythematosus, rheumatoid arthritis, celiac disease, type 1 diabetes, as well as lymphomagenesis (Fung et al., 2009; Graham et al., 2008; Honma et al., 2009; Kato et al., 2009; Nair et al., 2009; Schmitz et al., 2009; Thomson et al., 2007; Trynka et al., 2009). Therefore, conditional knock-out mice were generated to study the effects of A20 in different cell populations.

1.4.1 A20 in non-hematopoietic cells

SNPs in the *Tnfaip3* locus are associated with inflammatory bowel disease (IBD) (Barmada et al., 2004). However, mice with A20-deficient intestinal epithelial cells (IECs) do not develop spontaneous IBD but are more susceptible to dextran sulphate sodium (DSS) -induced colitis, associated with apoptosis of IECs. Upon TNF-treatment, these mice suffer from inflammatory bowel disease pathology, characterized by loss of intestinal tissue integrity and apoptosis of enterocytes. This leads to a systemic toxic reaction as a result of infiltrating intestinal bacteria (Vereecke et al., 2010).

Polymorphisms in the human *Tnfaip3* gene have also been associated with psoriasis. In epidermal cells, A20 inhibits NF-κB activation upon stimulation of the ectodysplasin receptor, a member of the TNF-R family. Epidermis-specific deletion of A20 in mice leads to hyperproliferation of keratinocytes, disheveled hair, sebocyte hyperplasia and increased nail growth (Lippens et al., 2011).

Recently, we showed that A20 in astrocytes plays an important role for the inhibition of EAE in mice by suppressing chemokine production and thereby reduces CD4$^+$ T cell recruitment and decreased demyelination (Wang et al., 2013).

1.4.2 A20 in hematopoietic cells

Tnfaip3$^{-/-}$ mice suffer from severe inflammation and die shortly after birth, thus, A20 seems to play an important role in the regulation of the immune system. Conditional knock out mice were generated to study the immune cell type specific function of A20.

A20 in dendritic cells

We (Xuan et al., 2014) and others (Hammer et al., 2011; Kool et al., 2011) generated mouse strains which lack A20 specifically in dendritic cells (DCs). All strains develop splenomegaly and lymphadenopathy. The DCs mature spontaneously, are hyperresponsive to CD40, RANK (Receptor activator of nuclear factor kappa B) and lipopolysaccharide (LPS) stimulation and produce increased amounts of cytokines. However, major differences between the strains were observed. Systemic lupus erythematosus-like symptoms, characterized by the presence of autoantibodies, arthritis and glomerulonephritis occurred in the strain, characterized by Kool et al., (2011). Furthermore, DCs from these mice upregulated antiapoptotic Bcl-2 and Bcl-x. In the strain described by Hammer et al., (2011), IBD-like symptoms were observed,

characterized by enthesitis, colitis and arthritis. The mouse strain, previously generated in our lab, however, develops spontaneous hepatitis, characterized by inflammation of immune cells into the liver (Xuan et al., 2014). Taken together, these data clearly demonstrate the important role of A20 in the regulation of DC function.

<u>A20 in myeloid cells</u>

Mice with A20 deficient myeloid cells (macrophages and granulocytes), were generated to study the role of A20 in rheumatoid arthritis. These mice developed severe spontaneous polyarthritis with production of collagen autoantibodies and increased cytokine concentrations in serum, resembling human RA. Sustained NF-κB activation and cytokine production was observed in LPS-stimulated primary macrophages. The polyarthritis phenotype was TNF-R-independent but IL-6 and MyD88 (myeloid differentiation primary-response gene 88) -dependent. Furthermore, osteoclastogenesis was promoted in myeloid A20-deficient mice (Matmati et al., 2011).

In contrast to the severe autoimmune phenotype, infection of these mice with a lethal dose of influenza A virus resulted in a protective immune response. Macrophages were hyperresponsive to double stranded RNA and influenza A viruses, indicated by increased NF-κB activation as well as cytokine and chemokine production (Maelfait et al., 2012).

<u>A20 in mast cells</u>

Mast cells play an important role in mediating allergic reactions and anaphylaxis. A20 deficiency in mast cells induced an increased pro-inflammatory response upon stimulation with IgE/FcεRI, TLRs, IL-1R and IL-33R, and resulted in aggravated lung inflammation, late phase cutaneous anaphylaxis and collagen-induced arthritis. However, instant degranulation, the release of mediators such as histamines, proteases and heparin, was not regulated by A20 (Heger et al., 2014).

<u>A20 in B Lymphocytes</u>

B lymphocytes as a part of the adaptive immune system play an important role in the pathogen control by production of antibodies. In humans, A20 acts as a tumor suppressor in Hodgkin lymphoma. We (Hövelmeyer et al., 2011) and others (Chu et al., 2011; Tavares et al., 2010) generated mouse strains lacking A20 specifically in B lymphocytes. A20-deficient B cells from all strains exhibited increased responsiveness to stimuli such as LPS and anti-CD40 and increased survival. Furthermore, a mild autoimmune phenotype, but no development of spontaneous B cell lymphomagenesis was observed. Tavares et al. (2010) reported a resistance to Fas-induced apoptosis due to increased expression of

antiapoptotic Bcl-x, resulting in improved B cell survival. Furthermore, these mice had elevated numbers of germinal center B cells and increased levels of autoantibodies. Mouse strains from Chu et al. (2011) and Hövelmeyer et al. (2011) developed inflammation and autoimmunity in aged animals.

<u>A20 in T Lymphocytes</u>

Already under unstimulated conditions A20 is highly expressed in T lymphocytes, suggesting an important function of A20 in T cells. In addition to our mouse strain, two mouse strains with A20-deficient T cells were generated independently. Giordano et al. (2014) described lymphadenopathy and mild organ infiltration in naïve mice, after selective deletion of A20 in mature T cells. Furthermore, A20-deficient CD8+ T cells were highly activated, produced more cytokines and showed improved anti-tumor activity. The second strain, described by Onizawa et al. (2015), developed less severe EAE compared to control mice, due to reduced lymphocyte infiltration. Increased formation of the RIPK1/RIPK3 complex in A20-deficient CD4+ T cells, induced necroptosis of these cells *in vitro* and *in vivo*.

1.4.3 Role of A20 in NF-κB signaling

NF-κB is a major regulator of the innate and adaptive immune system and, thus, plays a crucial role in immune homeostasis and inflammatory responses (Vallabhapurapu and Karin, 2009). As a negative feedback regulator of NF-κB, A20 is involved in different, ubiquitin-dependent, cell type specific signaling pathways in innate immune cells (e.g. TLR signaling, Figure 8B), adaptive immune cells (e.g. TCR signaling, Figure 8A) and general signaling pathways (e.g. cytokine signaling, Figure 8C) (Bhoj and Chen, 2009).

T cell activation is mediated by the TCR recognition of antigen presented on the MHC molecule on APCs. Additionally, the co-stimulation of CD4 or CD8 and CD28 by CD80 or CD86 is necessary for an efficient T cell activation. Upon activation, Lck (lymphocyte-specific protein tyrosine kinase) phosphorylates the CD3ζ-chain and, thereby, enhancing the affinity of ZAP-70 (Zeta-chain-associated protein kinase 70) binding (Wang et al., 2010). The activated form of ZAP-70 initiates the downstream signaling to the phospholipase C, gamma 1 (PLCγ1) and protein kinase C theta (PKCθ), activating the complex consisting of Bcl-10, MALT1 and caspase recruitment domain-containing protein 1 (Carma1). K63-linked ubiquitin is added to MALT1, promoting the recruitment

and activation of the IKK complex (Thome et al., 2010). A20 negatively regulates TCR signaling by removing K63-linked ubiquitin chains from MALT1, thereby inhibiting NF-κB activation (Düwel et al., 2009) (Figure 8A).

Upon TLR activation by their cognate ligands, e.g. LPS, the adaptor protein MyD88 is recruited to the receptor, leading to the association with IRAKs (IL-1 receptor associated kinases). IRAKs mediate the activation of TRAF6, which facilitates the K63-linked ubiquitination and downstream activation of the transforming growth factor β-activated kinase (TAK1) and TAK-binding protein (TAB) complex (Li et al., 2010). A20 terminates TLR signaling by deubiquitination of TRAF6, thereby inhibiting the downstream signaling and NF-κB activation (Boone et al., 2004) (Figure 8B).

The role of A20 as a negative feedback regulator of NF-κB was first described in the TNF-R signaling. Trimerization of the TNF-R facilitates recruitment of the adaptor proteins Fas-associated death-domain (FADD) and TNF-R-associated death-domain (TRADD) to the receptor. TRADD activates RIPK1, which leads to K63-linked ubiquitination by the cellular inhibitor of apoptosis (cIAP). The complex of TAK1, TAB1 and TAB2 is recruited by binding of K63-linked ubiquitin through the ubiquitin binding domains, leading to the activation of TAK1. TAK1 then promotes the activation of the IKK complex by phosphorylation of IKKβ. IKKβ mediates the phosphorylation of IκBα, leading to K48-linked ubiquitination and proteasomal degradation. NF-κB subunits p50 and p65 are released and translocate to the nucleus to initiate transcription. A20 modulates TNF-R signaling by deubiquitinating RIPK1. In addition, A20 can act as an E3 ligase, adding K48-linked ubiquitin to RIPK1, leading to proteasomal degradation and inhibition of signal transduction. Furthermore, it has been shown that A20 promotes the deubiquitination of IKKγ and thereby inhibits activation of NF-κB (Figure 8C) (Mauro et al., 2006). Many more signaling components modulated by A20 have been described in the past years, proposing A20 as a key regulator of the immune response.
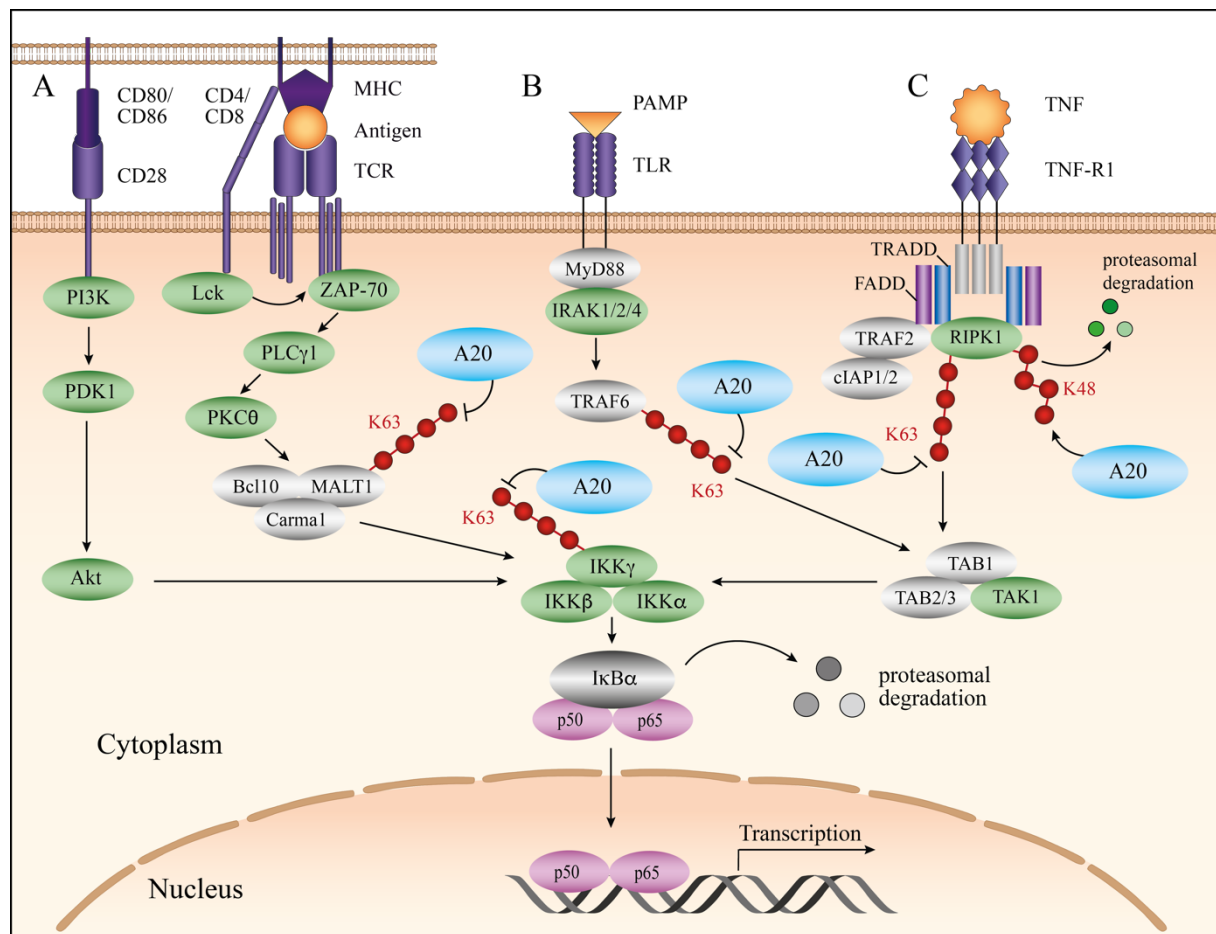
Figure 8: Regulation of the canonical NF-κB pathway by A20.

A20 regulates NF-κB activation via (de-) ubiquitination of different molecules in various signaling pathways. **A|** Simplified model of the TCR signaling with CD28 co-stimulation. A20 deubiquitinates MALT1 and, therefore, inhibits NF-κB signaling. **B|** Simplified model of the TLR signaling, which is important in innate immune cells. Upon binding of the PAMP to the TLR, TRAF6 is activated by K63-linked ubiquitination. A20 inhibits signaling by deubiquitinating TRAF6. **C|** Simplified model of the TNF-R1 signaling. Upon TNF-R trimerization and activation, RIPK1 is recruited and activated by the adaptor proteins FADD and TRADD. RIPK1 is ubiquitinated with K63-linked chains by cIAPs. A20 can inhibit RIPK1 by removing K63-linked and adding K48-linked ubiquitin, leading to proteasomal degradation of RIPK1. Furthermore, A20 deubiquitinates IKKγ, which inhibits activation of IκBα. CD: Cluster of differentiation; MHC: Major histocombatibility complex; TCR: T cell receptor; PI3K: Phosphoinositide 3-kinase; PDK1: Phosphoinositide-dependent kinase-1; Akt: Protein kinase B; Lck: Lymphocyte-specific protein tyrosine kinase); ZAP-70: Zeta-chain-associated protein kinase; PLCγ1: Phospholipase C, gamma 1; PKCθ: Protein kinase C-theta; Bcl-10: B-cell lymphoma 10; MALT1: Mucosa-associated lymphoid tissue lymphoma translocation protein 1; Carma1: Caspase recruitment domain-containing protein 11; K63: Lysine-63-linked polyubiquitin chain; PAMP: pathogen associated molecular pattern; TLR: Toll-like receptor; MyD88: Myeloid differentiation primary response 88; TNF: Tumor necrosis factor; TNF-R1: TNF receptor 1; TRAF: TNF receptor-associated factor; TRADD: TNF-R-associated death-domain; FADD: Fas-associated death-domain; cIAP: cellular inhibitor of apoptosis; RIPK1: Receptor-interacting serine/threonine-protein kinase 1; TAK1: Transforming growth factor β-activated kinase; TAB: TAK-binding protein; IκB: Inhibitor of kappa B; IKK: IκB kinase.

1.4.4 Role of A20 in cell death

Damaged or infected cells as well as effector T cells during the contraction phase are eliminated by programmed cell death (PCD). Apoptosis and necroptosis are important mechanisms of PCD with distinct morphological and biochemical features. Apoptosis, a caspase-dependent cell death mode, is characterized by nuclear condensation, DNA fragmentation, cell shrinkage and membrane blebbing. Induction of necroptosis, a caspase-independent and RIPK3-dependent cell death mode, leads to cytoplasmic and nuclear swelling as well as membrane rupture (Henry et al., 2013; Pietkiewicz et al., 2015). Both PCDs are inducible by death receptors. TNF-R and CD95 (also known as Fas) are well characterized members of the death receptor family. Activation of these receptors by their cognate ligands can lead to cell survival signals or the initiation of PCD (Figure 9).

TNF-R signaling induces NF-κB activation by complex I formation consisting of TRAF2, TRADD, cIAP and RIPK1. CIAP mediates K63-linked ubiquitination of RIPK1, which subsequently leads to the activation of IKKγ and NF-κB and the induction of survival signals (Figure 9). Disruption of complex I via deubiquitination of RIPK1 leads to formation of the TRADD-dependent complex IIa, consisting of TRADD, FADD and caspase-8. In this complex, caspase-8 is activated, which in turn leads to the downstream activation of caspase-3 and finally the induction of apoptosis. Conditions such as cIAP depletion or inhibition of either TAK1 or IKKγ induces complex IIb (or ripoptosome) formation. The ripoptosome consists of RIPK1, RIPK3, FADD and caspase-8. The long isoform of FLICE-like inhibitory proteins (FLIP$_L$) inactivates RIPK1 and RIPK3, therefore leading to the activation of caspase-8 and the induction of apoptosis. Inhibition as well as failed recruitment of caspase-8 or FLIP$_L$, though, leads to necrosome formation, consisting of RIPK1, RIPK3 and MLKL (mixed lineage kinase domain-like protein). Via oligomerization, MLKL creates a supramolecule protein complex at the cell membrane, leading to the induction of necroptosis (Conrad et al., 2016; Pasparakis and Vandenabeele, 2015; Vanden Berghe et al., 2014).

Ligation of CD95 with CD95L induces DISC (death inducing signaling complex) formation, composed of the receptor, FADD and caspase-8. Depending on the presence or absence of cIAP, DISC formation can lead to RIPK1-dependent or -independent apoptosis, respectively. Similar to TNF-R signaling, inhibition of caspase-8 leads to necrosome formation, and the induction of necroptosis (Pasparakis and Vandenabeele, 2015). Furthermore, at low concentrations CD95L has a co-stimulatory effect on T cells and augments activation and proliferation (Kreuz et al., 2004; Paulsen and Janssen, 2011; Wajant et al., 2003).
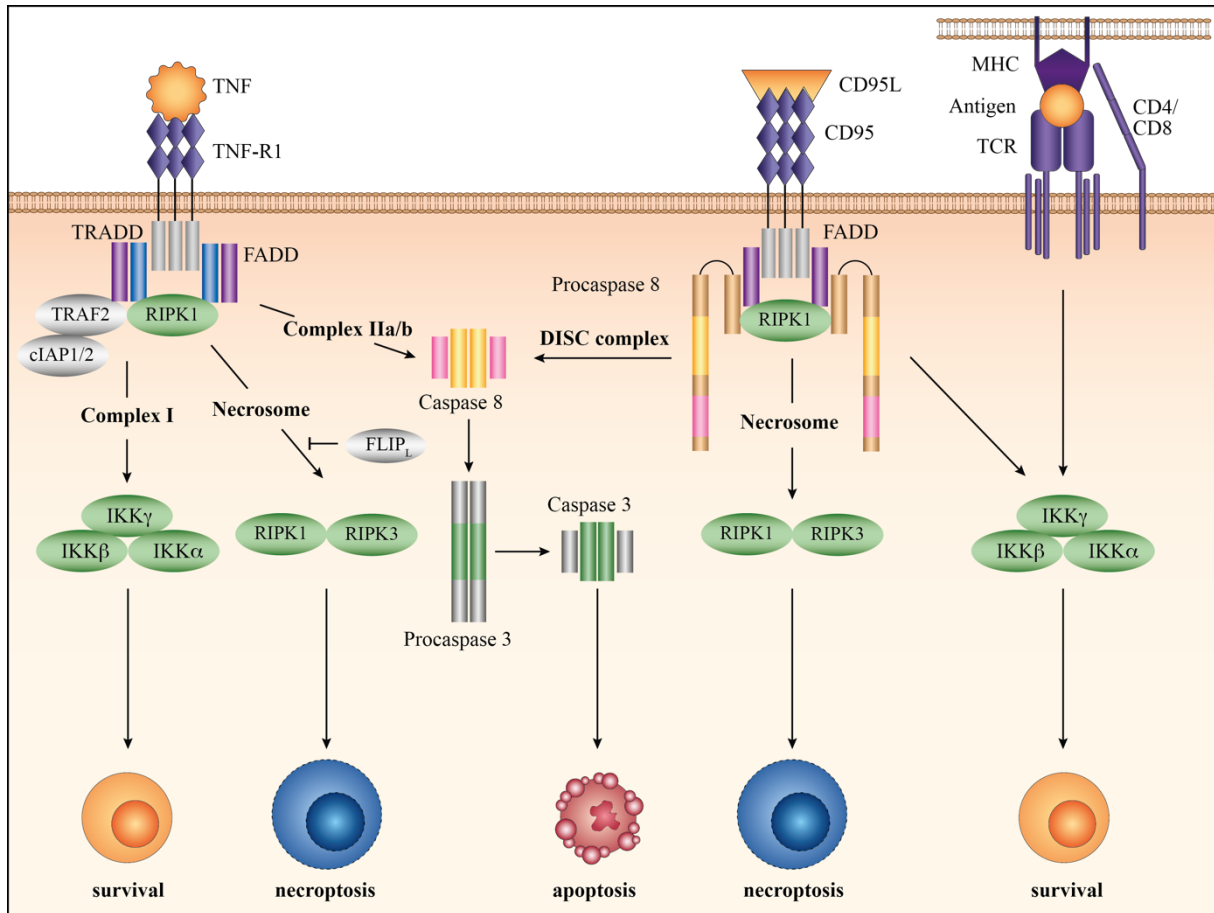
Figure 9: Cell death and survival signals.
Posttranslational modifications of RIPK1 influences the outcome of death receptor signaling to either survival/NF-κB activation, apoptosis or necroptosis. Activation of the TNF-R, TRADD binds to the receptor. TRADD then leads to the recruitment of FADD and RIPK1. RIPK1 is then ubiquitinated by cIAP, leading to survival signals via NF-κB activation. Deubiquitination of RIPK1 or inhibition of cIAP, however, promotes cell death. When caspase-8 is recruited and oligomerization takes place, further caspases (e.g. caspase-3) are activated, leading to the initiation of apoptosis. The second mode of cell death, necroptosis, can be initiated by the induction of RIPK3, leading to the RIPK1/RIPK3 complex, or the so called necrosome formation. TNF: Tumor necrosis factor; TNF-R1: TNF receptor 1; TRADD: TNF-R-associated death-domain; FADD: Fas-associated death-domain; cIAP: cellular inhibitor of apoptosis; RIPK: Receptor-interacting serine/threonine-protein kinase; TRAF: TNF receptor-associated factor; IKK: Inhibitor of kappa B kinase. CD: Cluster of differentiation; CD95L: CD95 ligand; MHC: Major histocompatibility complex; TCR: T cell receptor.

A20 as a regulator of apoptosis

A20 has both, anti- and pro-apoptotic functions. The anti-apoptotic function of A20 was first described in the TNF-R signaling pathway of human breast carcinoma cell lines (Opipari et al., 1992). Since then many studies confirmed an anti-apoptotic effect of A20 in different cell types and stimulating conditions. In LPS-induced hepatitis, A20 protects hepatocytes from cell death (Arvelo et al., 2002). Furthermore, A20 protected endothelial cells from CD40- as well as death receptor (TNF-R and CD95)-induced and NK cell-mediated cell death (Daniel et al., 2004; Longo et al., 2003). In mice, A20-deficient intestinal epithelial cells were highly susceptible to TNF-mediated apoptosis and DSS-induced colitis, resulting in the breakdown of the intestinal barrier and systemic inflammation (Vereecke et al., 2010).

Nevertheless, several studies reported a pro-apoptotic function of A20. Smooth muscle cells have been shown to be prone to cytokine- and CD95-mediated cell death in the presence of A20 in a nictric oxide-dependent manner (Patel et al., 2006). Several studies have shown the pro-apoptotic role of A20 in leukocytes. A20-deficient DC's are resistant to apoptosis due to upregulation of the prosurvival proteins Bcl-2 and Bcl-x (Kool et al., 2011). Tavares et al. (2010) found a resistance to apoptosis of A20-deficient B cells in response to CD95 activation. In addition, a pro-apoptotic function of A20 was observed in mast cells, where survival was promoted and proliferation was increased in A20-deficient mast cells (Heger et al., 2014).

A20 as a regulator of necrosis/necroptosis

A20 has been shown to protect endothelial cells from complement-mediated necrosis (Daniel et al., 2004). In HeLa cells, A20 promoted oxidative stress induced necrosis by inhibiting NF-κB-mediated cell survival (Storz et al., 2005). Furthermore, Onizawa et al. (2015) could recently show that A20 restricted RIPK3-dependent necroptosis in CD4^{+} T cells by deubiquitinating RIPK3, thereby inhibiting RIPK1/RIPK3 necrosome formation.

During the past decade, A20 has been studied extensively in various cell types under different stimulating conditions. However, the role of A20 during bacterial infection is still undetermined. Here, we show for the first time the dual function of A20 *in vivo* upon *L. monocytogenes* infection.

1.5 Aims

To gain more insight into the T cell specific function of A20, we addressed the following questions:

<u>Role of A20 in T cell development and activation</u>

Mice with a deletion of A20 in innate immune cells as well as B cells are prone to developing autoimmune diseases even under naive conditions, therefore a characterization of the CD4-Cre A20$^{fl/fl}$ mice is crucial to determine possible effects of the A20 deletion in T cells on T cell development in thymus and peripheral organs such as spleen, liver and lymph nodes. A20$^{fl/fl}$ mice were used as control mice. To determine possible off-target effects of the Cre-recombinase, CD4-Cre A20$^{wt/wt}$ mice were tested as well. T cells from naïve mice were isolated and stimulated *in vitro* to study the T cell activation.

<u>Regulation of the pathogen-specific CD8$^+$ T cell response by A20</u>

T cells play an important role in the clearance of pathogens. To study the effect of A20 in T cells during immune response, CD4-Cre A20$^{fl/fl}$ mice and A20$^{fl/fl}$ control mice were infected with wildtype *L. monocytogenes* (*L. monocytogenes* WT). Colony forming units (CFUs) were determined from spleen and liver at day 3, 7 and 14 p.i. Genetically modified *L. monocytogenes* expressing ovalbumin (*L. monocytogenes* OVA) were used to detect antigen-specific T cells in mice. *Ex vivo* restimulation with ovalbumin-specific peptide was performed to analyze effector function of antigen-specific T cells.

<u>Characterization of the function of A20 in memory CD8$^+$ T cell development and protection against secondary infection</u>

T cells are not only important for the final elimination of an infection, they also induce a potent memory response upon reinfection with the same pathogen. Therefore, we infected CD4-Cre A20$^{fl/fl}$ mice and A20$^{fl/fl}$ control mice with a low dose of *L. monocytogenes* and after 50 days reinfected them with a higher dose of the same pathogen. Three days later, spleen and liver were isolated and CFUs were determined. In addition, memory T cell response was analyzed by flow cytometry.

<u>Role of A20 in CD8$^+$ T cell death</u>

Upon the final elimination of an infection, the contraction phase is induced, in which around 90 % of the pathogen-specific T cells undergo cell death. Depending on stimulation conditions and the cell type A20 can act as a pro- as well as an anti-apoptotic molecule. Therefore, the role of A20 during T cell contraction phase remains to be investigated.

2. MATERIALS AND METHODS

2.1 Materials

2.1.1 Chemicals and buffers

Table 1: Chemicals and buffers

Description	Company
Agarose	Biozym (Hessisch Oldendorf, Germany)
Ammonium chloride (NH_4Cl)	Carl Roth (Karlsruhe, Germany)
Ammonium persulfate (APS)	Carl Roth (Karlsruhe, Germany)
Bovine serum albumine (BSA)	PAA Laboratories GmbH (Pasching, Austria)
Brefeldin A	BioLegend (San Diego, USA)
Dimethylsulfoxide (DMSO)	Sigma-Aldrich (Steinheim, Germany)
Dithiothreitol (DTT)	Invitrogen by Life Technologies (Darmstadt, Germany)
Dulbecco's Phosphate-Buffered Saline (DPBS)	Gibco by Life Technologies (Darmstadt, Germany)
Ethanol (70 %, 100 %)	Fischer (Saarbrücken, Germany)
Ethylenediaminetetraacetic acid (EDTA)	Sigma-Aldrich (Steinheim, Germany)
Glycine	Carl Roth (Karlsruhe, Germany)
Heparin (5000 U/ml)	Biochrom AG (Berlin, Germany)
IKK Inhibitor VII	Calbiochem (San Diego, USA)
Isoflurane (Forene)	Baxter (Unterschleißheim, Germany)
Magnesium chloride ($MgCl_2$)	Qiagen (Hilden, Germany)
Methanol	J.T. Baker (Deventer, Netherlands)
Paraformaldehyde (PFA)	Carl Roth (Karlsruhe, Germany)
Percoll	GE Healthcare (Uppsala, Sweden)
Phenylmethanesulfonylfluoride (PMSF)	Cell Signaling Technology (Danvers, USA)
Potassium hydrogene carbonate ($KHCO_3$)	Merck (Darmstadt, Germany)
Powdered milk	Carl Roth (Karlsruhe, Germany)
RIPA Buffer (10X)	Cell Signaling Technology (Danvers, USA)
Rotiphorese Gel 30 (Acrylamide)	Carl Roth (Karlsruhe, Germany)
Sodium chloride (NaCl)	Carl Roth (Karlsruhe, Germany)
Sodium dodecyl sulfate (SDS)	Carl Roth (Karlsruhe, Germany)
Tetramethylethylendiamine (TEMED)	Sigma-Aldrich (Steinheim, Germany)
Tris base, Tris HCl	Carl Roth (Karlsruhe, Germany)
Trypan blue	Sigma-Aldrich (Steinheim, Germany)
Tween 20	Sigma-Aldrich (Steinheim, Germany)
Z-VAD-FMK (Caspase Inhibitor)	Merck, Darmstadt, Germany

2.1.2 Bacterial culture

L. monocytogenes wildtype EGD (*L. monocytogenes* WT) and ovalbumin-expressing *L. monocytogenes* (*L. monocytogenes* OVA) were used for infection. Bacteria were cultured in brain heart infusion (BHI) broth (Merck, Darmstadt, Germany). For cultivation of *L. monocytogenes* OVA, 5 µg/ml erythromycin (Sigma-Aldrich, Steinheim, Germany) was added to the broth.

2.1.3 Reagents for cell culture

Table 2: Media for cell culture

Description	Company
Hank's Balanced Salt Solution (HBSS)	Gibco by Life Technologies (Darmstadt, Germany)
Roswell Park Memorial Institute (RPMI) 1640	Gibco by Life Technologies (Darmstadt, Germany)

Table 3: Supplementation reagents for cell culture media

Description	Company
Fetal calf serum (FCS**)**	Gibco by Life Technologies (Darmstadt, Germany)
(4-(2-Hydroxyethyl)-1-piperazine-ethanesulfonic acid (HEPES)	Biochrom AG (Berlin, Germany)
Non-essential amino acids (NEAA) (100X)	Gibco by Life Technologies (Darmstadt, Germany)
Penicillin/Streptomycin (100X)	Gibco by Life Technologies (Darmstadt, Germany)
Sodium pyruvate (100X)	Gibco by Life Technologies (Darmstadt, Germany)
L-Glutamine	Gibco by Life Technologies (Darmstadt, Germany)
β-Mercaptoethanol (50 mM)	Gibco by Life Technologies (Darmstadt, Germany)

Cell culture plates and pipettes were purchased from Greiner Bio-One (Frickenhausen, Germany). Counting of cells was performed with trypan blue (Sigma-Aldrich, Steinheim, Germany) in a Neubauer counting chamber (Paul Marienfeld GmbH & Co. KG, Lauda-Königshofen, Germany).

2.1.4 Reagents for molecular biology

Table 4: Reagents for molecular biology

Description	Company
dNTPs (100 mM)	Invitrogen by Life Technologies (Darmstadt, Germany)
First Strand Buffer (5X)	Invitrogen by Life Technologies (Darmstadt, Germany)
HotStarTaq DNA Polymerase	Qiagen (Hilden, Germany)
KAPA PROBE FAST Universal	PEQLAB (Erlangen, Germany)
Oligo(dT)$_{12\text{-}18}$ Primer	Invitrogen by Life Technologies (Darmstadt, Germany)
PCR Buffer (10X)	Qiagen (Hilden, Germany)
PCR Primer	Eurofins MWG Operon (Ebersberg, Germany)
SuperScript II Reverse Transcriptase	Invitrogen by Life Technologies (Darmstadt, Germany)
TaqMan Probes	Applied Biosystems by Life Technologies (Darmstadt, Germany)

Table 5: Primer for conventional PCR

Primer	Sequence (5'→3')	Amplicon Size
CD4-Cre sense CD4-Cre anti-sense	5'-TCT CTG TTG CTG GCA GTT TCT CCA-3' 5'-TCA AGG CCA GAC TAG GCT GCC TAT-3'	450 bp
A20 sense A20 anti-sense	5'-AGT CTG GGA CTG GAT GTA GC-3' 5'-CTGGCTAAGGCCTTGATACC-3'	300 bp
HPRT sense HPRT anti-sense	5'-GCT GGT GAA AAG GAC-3' 5'-CCA GTT TCA CTA ATG-3'	see below

Amplicon size of A20$^{\text{wt/wt}}$ = 300 bp; amplicon size of A20$^{\text{fl/fl}}$ = 410 bp

Amplicon size of HPRT (Hypoxanthine guanine phosphoribosyl transferase) of genomic

DNA = 945 bp; amplicon size of HPRT of cDNA = 145 bp

All primers were obtained from Eurofins MWG Operon (Ebersberg, Germany).

Table 6: TaqMan probes

Primer	Assay ID	Amplicon Length
A20	Mm00437121_m1	76
CD95	Mm01204974_m1	76
HPRT	Mm01545399_m1	81

All primers were obtained from Applied Biosystems by Life Technologies (Darmstadt,

Germany)

2.1.5 Reagents for proteomics

Table 7: Reagents used for proteomics

Description	Company
Lane Marker Reducing Sample Buffer (5X)	Thermo Fisher Scientific (Waltham, USA)
GammaBind G Sepharose Beads	GE Healthcare Bio-Sciences (Uppsala, Sweden)
PageRulerPrestained Protein Ladder (10-180 kDa)	Thermo Fisher Scientific (Waltham, USA)
PhosSTOP	Roche Diagnostics (Mannheim, Germany)
Protease Inhibitor Cocktail (25X)	Sigma-Aldrich (Steinheim, Germany)
Protein Assay Dye Reagent Concentrate	Bio-Rad (California, USA)

2.1.6 Antibodies

Table 8: Primary antibodies used for Western blotting

Description	Specification	Company
Anti-A20	A-12	Santa Cruz biotechnology (Heidelberg, Germany)
Anti-Caspase-3	polyclonal	Cell Signaling Technology (Danvers, USA)
Anti-Caspase-8	polyclonal	Cell Signaling Technology (Danvers, USA)
Anti-GAPDH	D16H11	Cell Signaling Technology (Danvers, USA)
Anti-phospho-ERK1/2	Thr202/Tyr204 (197G2)	Cell Signaling Technology (Danvers, USA)
Anti-phospho-IκBα	Ser32/36 (5A5)	Cell Signaling Technology (Danvers, USA)
Anti-phospho-p38	Thr180/Tyr182	Cell Signaling Technology (Danvers, USA)
Anti-RIPK1	D94C12	Cell Signaling Technology (Danvers, USA)
Anti-RIPK3	polyclonal	Abcam (Cambridge, UK)

Table 9: Secondary antibodies used for Western blotting

Description	Clone	Company
Swine Anti-Rabbit Immunoglobulins/HRP	Polyclonal	Dako (Glostrup, Denmark)
Rabbit Anti-Mouse Immunoglobulins/HRP	Polyclonal	Dako (Glostrup, Denmark)

Table 10: Antibodies used for flow cytometry

Description	Conjugated fluorochrome	Clone	Company
Anti-Caspase-3, cleaved	Alexa Fluor 647	D3E9	Cell Signaling Technology (Danvers, USA)
Anti-CD3ε	FITC	145-2C11	eBioscience by affymetrix (San Diego, USA)
Anti-CD3ε	Pe/Cy7	145-2C11	BioLegend (San Diego, USA)
Anti-CD4	Brilliant Violet 421	GK1.5	BioLegend (San Diego, USA)
Anti-CD8	Brilliant Violet 510	53-6.7	BioLegend (San Diego, USA)
Anti-CD11b	PE	M1/70	eBioscience by affymetrix (San Diego, USA)
Anti-CD11c	APC	N418	BioLegend (San Diego, USA)
Anti-CD16/32	-	93	BioLegend (San Diego, USA)
Anti-CD19	PE	MB19-1	eBioscience by affymetrix (San Diego, USA)
Anti-CD25	APC	PC61.5	eBioscience by affymetrix (San Diego, USA)
Anti-CD44	FITC	IM7	BD Biosciences (San Jose, USA)
Anti-CD44	Pe/Cy7	IM7	BioLegend (San Diego, USA)
Anti-CD45	PerCP	30-F11	BioLegend (San Diego, USA)
Anti-CD45R/B220	Brilliant Violet 421	RA3-6B	BD Biosciences (San Jose, USA)
Anti-CD62L	APC	MEL-14	BioLegend (San Diego, USA)
Anti-CD62L	PerCP/Cy5.5	MEL-14	BioLegend (San Diego, USA)
Anti-CD69	APC	H1.2F3	BioLegend (San Diego, USA)
Anti-CD95	APC	15A7	eBioscience by affymetrix (San Diego, USA)
Anti-CD127	APC	A7R34	eBioscience by affymetrix (San Diego, USA)
Anti-F4/80	Brilliant Violet 421	BM8	BioLegend (San Diego, USA)
Anti-Granzyme B	PE	NGZB	eBioscience by affymetrix (San Diego, USA)
Anti-IFN-γ	PerCP/Cy5.5	XMG1.2	BioLegend (San Diego, USA)
Anti-KLRG-1	Brilliant Violet 421	2F1	BD Biosciences (San Jose, USA)
Anti-Ly-6C	APC	HK1.4	eBioscience by affymetrix (San Diego, USA)
Anti-Ly-6G	FITC	1A8	BioLegend (San Diego, USA)
Anti-NK 1.1	PE	PK136	BD Biosciences (San Jose, USA)
Anti-PD-1	APC eFluor 780	J43	eBioscience by affymetrix (San Diego, USA)

Cells were stained with Fixable Viability Dye eFluor 506 or eFluor 780 (eBioscience by affymetrix, USA) prior to fixation to exclude dead cells.

For detection of *Listeria*-specific CD8^{+} T cells, PE-conjugated H2-Kb SIINFEKL pentamer from ProImmune (Oxford, UK) was used. This pentamer binds to CD8^{+} T cells specific for the epitope 257-264 of the ovalbumin antigen expressed on *L. monocytogenes* OVA.

Table 11: antibodies for T cell stimulation

Description	Clone	Company
Anti-CD3ε	145-2C11	BioLegend (San Diego, USA)
Anti-CD28	37.51	BioLegend (San Diego, USA)

2.1.7 Reagents used for apoptosis detection

Table 12: Reagents used for apoptosis detection

Description	Specification	Company
7-amino-actinomycin D (7-AAD**)**	DNA-binding, fluorescent dye	eBioscience by affymetrix (San Diego, USA)
Annexin V	Phosphatidylserine-binding proteins	eBioscience by affymetrix (San Diego, USA)
CellEvent Caspase-3/7 Green	DEVD-peptide conjugated to a nucleic acid binding dye	Molecular probes by Life Technologies (Darmstadt, Germany)

2.1.8 Consumables

Table 13: Consumables used

Description	Company
6 well cell culture plates 12 well cell culture plates 96 well culture plates (round bottom)	Greiner Bio-One (Frickenhausen, Germany)
Cell strainer (70 µm, 40 µm)	Falcon (Durham, USA)
Combitips advanced (10 ml)	Eppendorf (Hamburg, Germany)
Cuvettes	Sarstedt AG & Co. (Nümbrecht, Germany)
Filter Paper 583 Gel Dryer	Bio-Rad (California, USA)
Needles (26G)	B. Braun Melsungen AG (Melsungen, Germany)
Petri dishes	Sarstedt AG & Co. (Nümbrecht, Germany)
Polyvinylidene fluoride (PVDF) membrane	Roche Diagnostics (Mannheim, Germany)

Serological Pipette (5 ml, 10 ml, 25 ml)	Greiner Bio-One (Frickenhausen, Germany)
Syringes (2 ml)	BD Biosciences (San Jose, USA)
Tubes	
0.2 ml, 1.5 ml, 2.0 ml	Eppendorf (Hamburg, Germany)
5 ml round bottom tube	Falcon (Durham, USA)
15 ml, 50 ml	Greiner Bio-One (Frickenhausen, Germany)

2.1.9 Peptides

Table 14: Peptides used for *ex vivo* restimulation

Name	Description	Sequence	Company
OVA$_{323-339}$	H-2Kb-restricted OVA MHC class I epitope	H-ISQAVHAAHAEINEAGR-OH	JPT Peptide Technologies GmbH (Berlin, Germany)
OVA$_{257-264}$	I-Ad-restricted OVA MHC class II epitode	H-SIINFEKL-OH	JPT Peptide Technologies GmbH (Berlin, Germany)

2.1.10 Kits

Table 15: Kits used

Description	Company
Annexin V Apoptosis Detection Kit	eBioscience by affymetrix (San Diego, USA)
Cytometric Bead Array Mouse Th1/Th2/Th17 (CBA)	BD Biosciences (San Jose, Germany)
EasySep Mouse CD4+ T Cell Isolation Kit	STEMCELL Technologies (Cologne, Germany)
EasySep Mouse CD8+ T Cell Isolation Kit	STEMCELL Technologies (Cologne, Germany)
FoxP3/Transcription Factor Staining Buffer Set	eBioscience by affymetrix (San Diego, USA)
Intracellular Fixation &Permeabilization Buffer Set	eBioscience by affymetrix (San Diego, USA)
KAPA Mouse Genotyping Kit	KAPA Biosystems (Boston, USA)
Pierce ECL 2 Western Blotting Substrate	Thermo Fisher Scientific (Waltham, USA)
RNeasy Mini Kit	Qiagen (Hilden, Germany)

2.1.11 Instruments

Table 16: Instruments used

Description	Company
Agagel Midi-wide Biometra	AnalytikJena (Jena, Germany)
AlphaImager Gel Imaging System	Alpha Innotech (San Leandro, USA)
Bacterial Incubator	Memmert (Schwabach, Germany)
Biometra Standard Power Pack P25	AnalytikJena (Jena, Germany)
Bio Photometer	Eppendorf (Hamburg, Germany)
BD FACS Canto™ II Flow Cytometer	BD Biosciences (San Jose, Germany)
Centrifuge ROTANTA 460R	Hettich (Beverly, USA)
Centrifuge Mikro 22R	Hettich (Beverly, USA)
Chemo Cam Luminescent Image Analysis system	INTAS (Göttingen, Germany)
CO_2 Incubator	Heraeus (Hanau, Germany)
EasySep Magnet	STEMCELL Technologies (Cologne, Germany)
Electrophoresis chamber	Bio-Rad (California, USA)
Flowsight Imaging Flow Cytometer	Merck Millipore (Darmstadt, Germany)
Incubator shaker GFL 3032	Gesellschaft für Labortechnik (Burgwedel, Germany)
Laboratory balance	Sartorius (Göttingen, Germany)
Laminar flow hood	Heraeus (Hanau, Germany)
LightCycler 480 II	Roche Diagnostics (Mannheim, Germany)
Microscope Olympus-CX 41	Olympus (Hamburg, Germany)
MiniColdLab	Pharmacia Biosystems (Sweden)
Multichannel pipette	Eppendorf (Hamburg, Germany)
Multipette plus	Eppendorf (Hamburg, Germany)
NanoDrop ND-1000 Spectrophotometer	Thermo Fisher Scientific (Waltham, USA)
Neubauer Chamber (improved)	LO Laboroptik (Lancing, UK)
pH meter	Schott (Mainz, Germany)
Pipette	Eppendorf (Hamburg, Germany)
Pipette aid	Eppendorf (Hamburg, Germany)
PowerPac HC	Bio-Rad (California, USA)
Semi Dry Blotter	PEQLAB (Erlangen, Germany)

Tissue grinder	Thermo Fisher Scientific (Waltham, USA)
Thermocycler	PEQLAB (Erlangen, Germany)
Thermomixer	Eppendorf (Hamburg, Germany)
Tube Roller SRT9	Bibby Scientific (Staffordshire, UK)
Vortex Genius 3	IKA (Staufen, Germany)

2.1.12 Mouse strains

To study the T cell specific function of A20, conditional A20-knock-out mice were generated. LoxP sites were inserted, flanking exon 3 of the *Tnfaip3* allele, generating A20$^{fl/fl}$ mice. For specific deletion of A20 in T cells, C57BL/6 A20$^{fl/fl}$ mice were crossed to C57BL/6 CD4-Cre, resulting in CD4-Cre A20$^{fl/fl}$ mice with a loss of A20 protein in cells expressing CD4. Efficiency of the deletion was confirmed by PCR, RT-qPCR and Western blot analysis. CD4-Cre A20$^{wt/wt}$ mice were used for the basic characterization to determine possible Cre-specific effects.

Animal care and experimental procedure was performed according to the German Animal Welfare Act (Deutsches Tierschutzgesetz) and approved by state authorities (Landesverwaltungsamt Sachsen-Anhalt, Germany; file number: 42502-2-994). All efforts were made to minimize suffering; surgery was performed after euthanization of the animals.

2.2 Methods

2.2.1 Genotyping of mouse strains

Genotyping of mice was performed by obtaining a tissue sample from the tail tip. Genomic DNA was isolated using the KAPA Mouse Genotyping Kit according to manufacturer's protocol. PCR was performed using the program described below. PCR products were run on a 1.5 % agarose gel (from Biozym, Hessisch Oldendorf, Germany) in 1X TBE (Tris-borate-EDTA) buffer.

TBE buffer (10X), pH 8.3		
		Distilled water
100	mM	Boric acid
100	mM	TRIS base
2.5	mM	EDTA

PCR reaction mix		
1	X	Genotyping mix (2X)
25	mM	$MgCl_2$
1	µM	Primer s
1	µM	Primer as
1.0	µl	Template
		distilled water (to a final volume of 25 µl)

PCR program			
Step	Temperature	Time	Cycle
Initial denaturation	95 °C	3 min	1x
Denaturation	95 °C	15 sec	
Annealing	60 °C	15 sec	35x
Extension	72 °C	15 sec	
Final Extension	72 °C	10 min	1x

2.2.2 Cultivation of *Listeria monocytogenes*

To maintain *L. monocytogenes* WT and OVA were grown from frozen stocks over night in BHI broth. For the cultivation of *L. monocytogenes* OVA, 5 µg/ml erythromycin was added to the broth. On the following day, a fresh log-phase culture was prepared from the overnight culture. Glycerol was added to the 1 h culture to a final concentration of 40 % and aliquots were stored at -80 °C.

2.2.3 Infection of mice with *Listeria monocytogenes* and determination of colony forming units

CD4-Cre A20$^{fl/fl}$ mice and A20$^{fl/fl}$ control mice were intravenously (i.v.) infected with either *L. monocytogenes* WT or recombinant *L. monocytogenes* OVA. A fresh log-phase culture was prepared from an overnight culture and optical densities were determined. Infection dose was adjusted according to a standard growth curve to 1×10^4 *L. monocytogenes* WT or 5×10^4 *L. monocytogenes* OVA for primary infection and 1×10^6 for secondary infection in 200 µl DPBS, respectively. The bacterial dose was confirmed by colony counting after plating an inoculum on BHI agar and incubating it for 24 h at 37 °C.

To analyze the bacterial burden in spleen and liver of infected mice, CFUs were determined. CD4-Cre A20$^{fl/fl}$ mice and A20$^{fl/fl}$ control mice were anesthetized with isoflurane and liver and spleen were isolated after perfusion with 0.9 % NaCl. With sterile tissue grinders the organs were homogenized and serial dilutions with DPBS were plated on BHI agar plates and incubated at 37 °C for 24 h. Colonies were counted macroscopically with a counting grid.

2.2.4 Serum isolation and leukocyte isolation from organs

Animals were anesthetized with isoflurane and the heart was punctured with a 26 gauge needle on a 1 ml syringe to extract the blood. Heparin was added to the blood to prevent clotting. The blood samples were centrifuged at $10,000 \times$ g for 5 min and the serum was collected and stored at -80 °C until further processed.

For organ isolation, mice were perfused with 0.9 % NaCl solution to remove intravascular leukocytes. Liver, spleen, thymus and lymph nodes were obtained and stored in HBSS supplemented with 3 % FCS. The organs were passed through a 70 µm cell strainer and centrifuged at $300 \times$ g for 6 min at 4 °C. The cell pellet was resuspended in ACK lysis

buffer (described on page 35) and incubated for 10 min at 4 °C for erythrocyte lysis. Afterwards, cells were washed once with HBSS supplemented with 3 % FCS. The supernatant was discarded and the cells from spleen, lymph nodes and thymus were resuspended in HBSS + 3 % FCS. The cell suspension was passed through a 40 µm cell strainer and number of living cells was determined by diluting a sample with trypan blue microscopical counting in a Neubauer chamber.

ACK lysis buffer		
155	mM	NH$_4$Cl
10	mM	KHCO$_3$
0.12	mM	EDTA

For leukocyte isolation from the liver, cells were resuspended after erythrocyte lysis in 15 ml of 80 % Percoll (described below). Equal volume of 40 % Percoll was slowly layered on top. The gradient was then centrifuged at 2,000 × g for 20 min at 2 °C without rotor brakes. The top layer, containing dead cells, was removed and the interphase ring, containing hepatic leukocytes, was transferred to a new tube and washed once and resuspended in HBSS supplemented with 3 % FCS.

Percoll stock (per liver)		
25	ml	Percoll
2.7	ml	NaCl (1.5 M)

80 % Percoll (per liver)		
15	ml	Percoll stock
3.75	ml	HBSS + 3 % FCS

40 % Percoll (per liver)		
7.5	ml	Percoll stock
11.25	ml	HBSS + 3 % FCS

2.2.5 Determination of alanine aminotransferase from serum

In collaboration with Dr. Katrin Borucki from the Institute of Clinical Chemistry, University Hospital Magdeburg, alanine aminotransferase (ALT) levels from serum of naïve mice were analyzed to determine liver damage, by incubation with pyridoxal phosphate at 37 °C and measurement on a Cobas Modular platform (Roche, Mannheim, Germany) according to the International Federation of Clinical Chemistry.

2.2.6 T cell isolation

For *in vitro* T cell experiments, spleen and lymph nodes from uninfected CD4-Cre A20^fl/fl and A20^fl/fl control mice were removed and single cell suspension was obtained as described in 2.2.4. After counting the cells, the suspension was adjusted to a concentration of 1×10^8 cells/ml in T cell isolation buffer (described below). The isolation was performed with EasySep™ CD4+ or CD8+ T cell Isolation Kits according to the manufacturer's instruction. The isolated T cells were washed once and the pellet was resuspended in T cell stimulation medium (described below). Purity of the isolated fraction was measured by flow cytometry and varied between 90-95 %.

T cell isolation buffer		
		DPBS
2	%	FCS
1	mM	EDTA

T cell stimulation medium		
		RPMI1640 + L-Glutamine
10	%	FCS
1	X	NEAA (100X)
1	X	Sodium Pyruvate (100X)
1	X	Penicillin/Streptomycin (100X)
5	mM	HEPES
50	μM	β-ME

2.2.7 Flow Cytometry

2.2.7.1 Staining of surface antigens

Cells (as prepared in 2.4.4) were transferred to a 5 ml round bottom tube and washed once with FACS buffer (DPBS + 3 % FCS) and centrifuged at 300 × g for 5 min at 4 °C. Unspecific binding sites were blocked by adding 1 µg of anti-CD16/CD32 for 10 min at 4 °C. Without washing fluorochrome-conjugated antibodies (listed in Table 10) were added to a total volume of 100 µl in FACS buffer and incubated in the dark for 20 min at 4 °C. Prior to fixation, cells were washed with protein-free DPBS and incubated with Fixable Viability Dye for 30 min at 4 °C in the dark to label dead cells. Cells were washed with FACS buffer and fixed with 1 % paraformaldehyde (PFA) for 20 min at 4 °C in the dark. PFA was removed by washing and cells were resuspended in FACS buffer.

2.2.7.2 Staining of intracellular antigens

Prior to staining of intracellular antigens, cells were restimulated with peptides (listed in Table 14) for 4 h in T cell stimulation medium (described before) at 37 °C, 5 % CO_2 and 60 % of water vapor. After 1 h of stimulation, 1X Brefeldin A and Monensin was added to the cells to block secretion of the intracellular molecules. Staining of cytoplasmic proteins was performed using the Intracellular Fixation & Permeabilization Buffer Set. After surface staining, IC Fixation Buffer was added to the cells and incubated for 20 min at room temperature (RT) in the dark. Afterwards, cells were washed two times with 1X Permeabilization buffer. The fluorochrome-conjugated antibody was added and incubated for 20 min at RT in the dark. Cells were then washed two times with 1X Permeabilization buffer and resuspended in FACS buffer.

2.2.7.3 Detection of antigen-specific CD8+ T cells

For detection and characterization of antigen-specific CD8+ T cells, CD4-Cre A20$^{fl/fl}$ mice and A20$^{fl/fl}$ control mice were infected with *L. monocytogenes* OVA. Leukocytes from spleen and liver were isolated as described in 2.4.4. after different time points post infection. Cells were transferred to a 5 ml round bottom tube, washed once with FACS buffer and resuspended in the residual volume. 10 µl of the H2-Kb SIINFEKL pentamer per 1×10^6 cells was added. The cells were incubated for 10 min in the dark at 37 °C, followed by a washing step with FACS buffer before continuing with the extracellular staining.

2.2.7.4 Cytometric Bead Array

Cytokine levels in serum and supernatant were analyzed by flow cytometry using the Cytometric Bead Array (CBA). The standard dilution and the bead mixture was prepared according to manufacturer's protocol. 50 µl of the Capture beads and 50 µl of Th1/Th2/Th17 PE detection reagent was added to all samples and the standard. Samples were incubated for 2 h at RT in the dark. Wash buffer was added and the samples were centrifuged at 200 × g for 5 min at RT. Supernatant was discarded and the pellet was resuspended in wash buffer. Samples were measured on a BD FACSCanto II and analyzed using FCAP Array Software (BD Biosciences, USA).

2.2.7.5 Carboxyfluoresceindiacetatesuccinimidyl ester (CFSE) labeling

CFSE was used to determine the proliferative activity of T cells *in vitro*. After purification of T cells (described in 2.2.6), cells were resuspended in 1 ml DPBS. 1 ml of a 5 µM CFSE solution was added to the cells and mixed thoroughly. After incubation for 15 min at RT in the dark, T cell stimulation medium was added to the cells to quench the CFSE staining. The cells were then centrifuged at 300 × g for 6 min at 4 °C and resuspended in fresh medium.

2.2.7.6 *In vitro* T cell proliferation and activation

For *in vitro* T cell activation, a 96-well round bottom plate was coated with 1-10 µg/ml anti-CD3. The plate was incubated for 90 min at 37 °C and afterwards washed with DPBS to remove unbound antibody. CD8$^+$ T cells were purified as described in 2.2.6, and labeled with CFSE. 2×10^5 cells were added per well in a total volume of 200 µl supplemented with soluble 2-5 µg/ml anti-CD28. The T cells were cultured at 37 °C, 5 % CO_2 and 60 % of water vapor for 3 days in T cell stimulation medium (described in 2.2.6). For detection of T cell activation, extracellular activation markers were stained and measured via flow cytometry. Cytokine production was determined from supernatant with CBA (see 2.2.7.4).

2.2.7.7 Activation-induced cell death (AICD)

For activation induced cell death, 1×10^6 cells were incubated in a 24-well plate coated with 10 µg/ml anti-CD3 and 2 µg/ml anti-CD28. T cell stimulation medium was supplemented with 20 ng/ml of recombinant IL-2 (Peprotech, USA). T cells were incubated at 37 °C, 5 % CO_2 and 60 % of water vapor. After 2 days, cells were transferred to new wells without anti-CD3/CD28 stimulation and were expanded with 20 ng/ml IL-2 for three days. Thereafter, T cell blasts were restimulated for 6 h with 10 µg/ml plate-bound anti-CD3.

2.2.7.8 Detection of cell death

Annexin V and 7-AAD

Annexin V and 7-AAD staining was performed using the Annexin V Apoptosis Detection Kit. Annexin V binds to phosphatidylserine, which, in dying cells, translocates from the cytoplasm to the extracellular region of the cell membrane and can then be detected by antibody staining. 7-AAD, a fluorescent marker which intercalates with double-stranded DNA when the cell membrane is not intact was used to detect differences between early and late cell death events. After surface staining, the cells were washed once in DPBS, then once in 1X Binding Buffer. Cells were resuspended in 1X Binding Buffer and 5 µl of fluorochrome-conjugated Annexin V was added per 1×10^6 cells. After 10 min incubation at RT, the cells were washed with 1X Binding Buffer and resuspended in 200 µl of 1X Binding Buffer. 5 µl of 7-AAD Viability Staining Solution was added. Cells were analyzed by flow cytometry within 4 h.

Detection of caspase-3/7 activity

For measurement of caspase-3/7 activity with flow cytometry, 2 µl of CellEvent Caspase-3/7 Green was added to 1×10^6 cells after surface staining. Without washing, cells were analyzed by flow cytometry after 30 min incubation on ice, protected from light.

Imaging Flow Cytometry (IFC)

After *in vitro* TCR stimulation for 72 h, T cells were fixed in 3 % formaldehyde for 10 min at RT and permeabilized with 90 % ice-cold methanol for 30 min on ice. Thereafter, cells were washed two times with incubation buffer (PBS + 0.5 % BSA). Cells were stained for 1 h in the dark at RT with an antibody against caspase-3 cleaved at Asp175 and conjugated to AlexaFluor 647.

For determining cell death mode upon CD95 stimulation *in vitro*, T cells from naïve mice were isolated and stimulated for 3 h with 500 ng/ml recombinant CD95L after pre-treatment with or without the pan-caspase inhibitor z-VAD-FMK.

For *ex vivo* analysis of pathogen-specific CD8+ T cells, animals were infected with *L. monocytogenes* OVA. On day 7 and 11 spleens were isolated and stained for cell death analysis. IFC was performed on FlowSight Amnis Imaging Flow Cytometer (EMD Millipore) in collaboration with Prof. Inna Lavrik, Department of Translational Inflammation Research, Otto von Guericke University Magdeburg.

2.2.8 Two-step quantitative reverse transcription PCR (RT-qPCR)

To investigate the A20 deletion efficiency, CD4+ and CD8+ T cells were isolated as described before (see 2.2.6). CD8+ T cells from CD4-Cre A20$^{fl/fl}$ mice and A20$^{fl/fl}$ control mice were isolated and stimulated with anti-CD3 and anti-CD28 for 0 h, 6 h and 24 h in the presence or absence of IKK-Inhibitor VII to determine the expression and regulation of CD95. Isolation of mRNA was performed with the RNeasy Mini Kit according to manufacturer's instruction. RNA concentration and purity was measured with a NanoDrop Spectrophotometer. Equal amounts of RNA in a total volume of 50 µl were used for cDNA synthesis.

Denaturing and annealing		
		RNA
1	µg	Oligo(dT) Primer
1	mM	dNTPs

The samples were incubated at 65 °C for 5 min with Oligo(dT) primer and dNTPs and thereafter cooled on ice.

cDNA synthesis		
1	X	First-Strand Buffer
0.1	M	DTT
250	U	SuperScript™ II RT

For cDNA synthesis, SuperScript reverse transcriptase with First-Strand buffer and DTT was added to the samples. After an incubation at 42 °C for 50 min the reaction was inactivated by heating the samples to 70 °C for 10 min.

PCR for the HPRT gene with an intron-spanning primer was performed to detect contaminations with genomic DNA.

PCR reaction mix		
1	X	PCR buffer (10X)
200	µM	dNTPs
0.4	µM	HPRT Primer s
0.4	µM	HPRT Primer as
0.6	U	HotStarTaq DNA Polymerase
1.5	µl	cDNA
		distilled water (to a final volume of 25 µl)

PCR program			
Step	Temperature	Time	Cycle
Initial denaturation	95 °C	15 min	1x
Denaturation	94 °C	45 sec	
Annealing	53 °C	45 sec	38x
Extension	72 °C	45 sec	
Final Extension	72 °C	7 min	1x

The amplicon for HPRT cDNA is detectable at 145 bp. Contamination with genomic DNA results in a band at 984 bp.

The qPCR was performed, when no contamination of the cDNA was detectable. For qPCR the KAPA Probe Fast Universal Kit (peqlab, Erlangen, Germany) was used.

qPCR reaction mix		
1	X	KAPA Probe Fast qPCR Master Mix (2X)
1	X	TaqMan Gene Expression Assays
2	µl	cDNA
		distilled water (to a final volume of 20 µl)

The qPCR reaction was performed in the Lightcycler 480 system (Roche, Mannheim, Germany). The mRNA expression of A20 and CD95 in T cells of CD4-Cre A20$^{fl/fl}$ mice and A20$^{fl/fl}$ mice was determined from the ratio between the target genes (A20 and CD95) and the reference gene (HPRT) with the $\Delta\Delta$ cycle threshold method (Livak and Schmittgen, 2001).

2.2.9 Protein isolation and Western Blot

Isolated and stimulated T cells were lysed with radioimmunoprecipitation assay (RIPA) lysis buffer (described below) for 30 min on ice. Afterwards, lysates were centrifuged for 15 min at 13,000 × g. The supernatant was transferred to a new tube and protein concentration was measured using Bradford assay according to manufacturer's instruction.

RIPA lysis buffer		
1	X	RIPA buffer (10X)
1	mM	PMSF
1	X	PhosSTOP (10X)
1	X	Protease Inhibitor Cocktail (25X)

1X lane marker reducing sample buffer was added and the samples were incubated for 5 min at 99 °C to denature proteins. Equal amounts of proteins were separated on 10-12 % gels via SDS-PAGE (sodium dodecyl sulfate polyacrylamide gel electrophoresis).

Reagents	10 % resolving gel	12 % resolving gel	5 % stacking gel
distilled water	40 %	33 %	68 %
Acrylamide (30 %)	33 %	40 %	17 %
Tris (pH 8.8)	0.4 M	0.4 M	0.17 M
SDS	0.1 %	0.1 %	0.1 %
APS	0.1 %	0.1 %	0.1 %
TEMED	0.04 %	0.04 %	0.1 %

Gel running buffer (pH 8.3)		
	distilled water	
25	mM	Tris
0.1	%	SDS
200	mM	Glycine

For Western blotting, the proteins were transferred on a polyvinylidene fluoride (PVDF) membrane at 0.11 A for 1-2 h with the semi-dry transfer technique. Thereafter, the membrane was incubated for 1 h at RT with blocking buffer (5 % BSA or 1 % BSA with 1 % milk, according to antibody specifications). Antibodies were diluted 1:1,000 in blocking buffer (as described in the manufacturer's instructions) and incubated overnight at 4 °C. The membrane was washed three times each 15 min with Tris buffered saline with Tween (TBST; described below). Secondary antibody, diluted 1:1000 in blocking buffer, was added for 1 h at RT. The membrane was washed three times for 15 min with TBST and the blot was developed with Pierce ECL Plus Western Blotting Substrate kit, according to manufacturer's manual.

Transfer buffer (pH 8.4)		
	distilled water	
25	mM	Tris
1	%	SDS
20	mM	Glycine
20	%	Methanol

TBST (pH 7.4)		
	distilled water	
20	mM	Tris
140	mM	NaCl
0.1	%	Tween 20

2.2.10 Immunoprecipitation

Proteins from unstimulated and anti-CD3/CD28-stimulated CD8$^+$ T cells were isolated as described before (2.2.6). 400 μg of protein per time point were pre-incubated with Sepharose beads for 30 min at 4 °C with agitation to block unspecific binding. Thereafter, samples were centrifuged for 10 min at 10,000 × g. Supernatants were transferred to a new tube and incubated with anti-RIPK1 antibody in a 1:100 dilution over night at 4 °C on a rocker. Sepharose beads were added to the samples to capture the immune-complex and incubated over night at 4 °C on a rocker. To collect the immunoprecipitate, the samples were centrifuged for 30 sec at 3,000 × g and the supernatant was removed carefully. The beads were washed three times with PBS to remove unspecific binding. After the last washing step, beads were resuspended in 1X lane marker reducing sample buffer and incubated at 99 °C for 3 min. The beads were removed by centrifugation and western blot analysis was performed as described above (2.2.9).

2.2.11 Software

For Western Blot development, Intas Chemo Cam Luminescent Image Analysis system (INTAS Science Imaging Instruments, Göttingen, Germany) was used.
Flow cytometry was performed on BD Fluorescent activated cell sorter (FACS) Canto II using BD FACSDiva Software (BD Biosciences, San Jose, USA). Aquired data were analyzed with FlowJo vX software (Tree Star, Ashland, USA). Data from Cytometric Bead Array was analyzed with FCAP Array v3.0 Software (Soft Flow Inc., St. Louis Park, USA). Statistical analysis was performed using GraphPad Prism 5 (GraphPad Software, San Diego, USA)

2.2.12 Statistics

Statistical significance was determined with two-tailed Student's t test, nonparametric Mann-Whitney U test or multiple comparison, as indicated in the figure legends, using GraphPad Prism 5 software. P values < 0.05 were considered significant. All experiments were performed at least twice.

3. RESULTS

3.1 Role of A20 in T cell development and activation

3.1.1 Generation of CD4-Cre A20$^{fl/fl}$ mice

Exon 3 of the *Tnfaip3* gene from mouse embryonic stem cells was flanked with loxP sites to generate A20$^{fl/fl}$ mice. The neomycin resistance cassette, a positive selection marker flanked by FRT (flippase recognition target) sites, was removed by flippase-mediated recombination and stem cells with the successful targeted *Tnfaip3* gene were used to generate A20$^{fl/fl}$ mice. A20$^{fl/fl}$ mice were bred with CD4-Cre mice, expressing the Cre-recombinase under control of the CD4 promotor. The Cre-recombinase targets loxP sites of cells expressing CD4, leading to the excision of exon 3. The deletion causes a frameshift during the translational process, thus, inactivating A20.
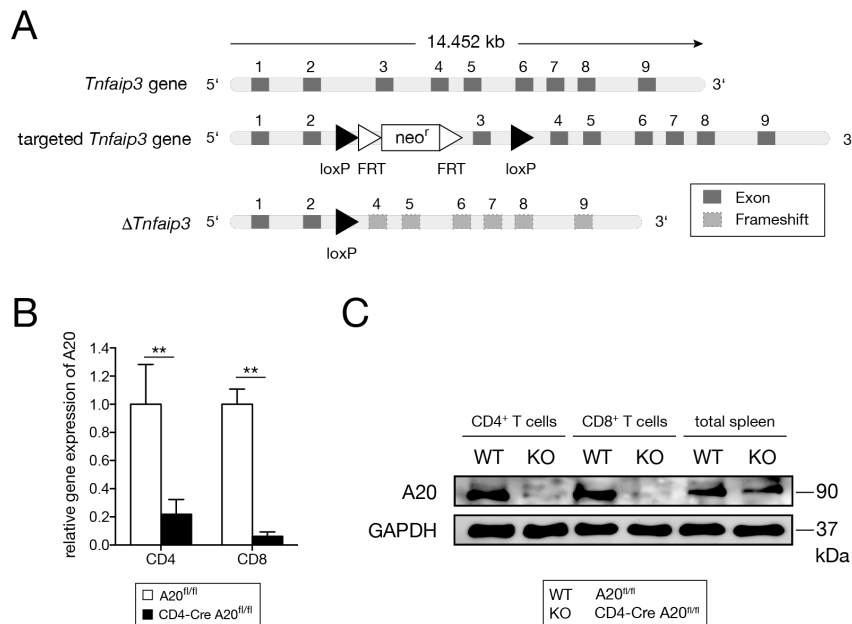
Figure 10: Successful deletion of A20 in T cells.
CD4-Cre A20$^{fl/fl}$ mice were generated to delete A20 specifically in T cells. Spleens and lymph nodes were isolated from CD4-Cre A20$^{fl/fl}$ and A20$^{fl/fl}$ control mice for mRNA and protein isolation to determine A20 expression. **A|** Schematic representation of targeting the exon 3 of the *Tnfaip3* gene to obtain A20$^{fl/fl}$ mice. **B|** Relative gene expression of A20 in CD4$^+$ and CD8$^+$ T cells. **C|** Proteins were isolated from unstimulated CD4$^+$ and CD8$^+$ T cells, as well as splenocytes. Western blot analysis was performed and stained for A20 and the loading control GAPDH. Black triangle: loxP sites; white triangles: flippase recognition target (FRT) sites; Neo^r: Neomycin resistance cassette; WT: A20$^{fl/fl}$; KO: CD4-Cre A20$^{fl/fl}$. A representative of 3 independent experiments is shown. Error bars indicate +SEM. Student's *t*-test, ** $p < 0.01$.

To determine the efficiency of the deletion, CD4$^+$ and CD8$^+$ T cells were isolated from spleen and lymph nodes of CD4-Cre A20$^{fl/fl}$ and A20$^{fl/fl}$ control mice. MRNA and Proteins were isolated to perform RT-qPCR (Figure 10B) and Western blot analysis (Figure 10C), which confirmed the successful deletion of A20 in T cells.

3.1.2 T cell development

Thymus of naïve 8-week-old CD4-Cre A20$^{fl/fl}$ mice and A20$^{fl/fl}$ as well as CD4-Cre A20$^{wt/wt}$ control mice were isolated to determine a possible influence of A20 on T cell development. Figure 11A shows the gating strategy of the flow cytometric analysis. Cells were gated on FSC-A/SSC-A to remove debris, FSC-A/FSC-H to eliminate doublets and life/dead staining was performed to gate on living cells.
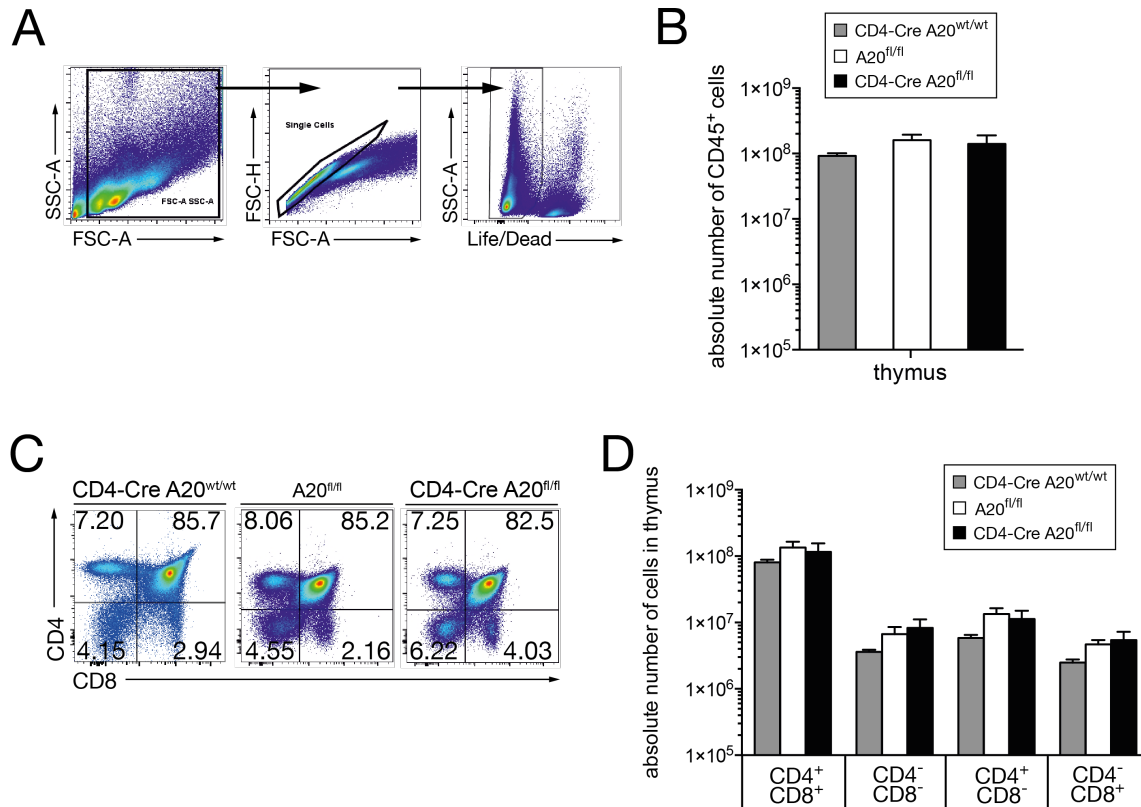
Figure 11: T cell development is not impaired in CD4-Cre A20$^{fl/fl}$ mice.
Thymus of 8-week-old naïve CD4-Cre A20$^{fl/fl}$ mice, as well as A20$^{fl/fl}$ and CD4-Cre A20$^{wt/wt}$ control mice, was isolated and analyzed by flow cytometry to study the stages of T cell development. **A|** General gating strategy. After debris removal, selection of single cells and living cells, cells were gated on markers shown. **B|** Absolute number of leukocytes in thymus. **C|** Representative dot plot of T cells in thymus. **D|** Absolute number of double positive (CD4$^+$CD8$^+$), double negative (CD4$^-$CD8$^-$) and single positive (CD4$^+$CD8$^-$ and CD4$^-$CD8$^+$) T cells. A representative of 3 independent experiments is shown. 3-4 mice per group were used. Error bars indicate +SEM. Student's t-test.

The absolute number of leukocytes did not differ between CD4-Cre A20$^{fl/fl}$ mice and the control groups (Figure 11B). Staining of T cells revealed no significant differences in the relative (Figure 11C) or absolute number (Figure 11D) of double positive (CD4$^+$CD8$^+$), single positive (CD4$^+$CD8$^-$ and CD4$^-$CD8$^+$) and double negative (CD4$^-$CD8$^-$) T cells.

3.1.3 Leukocyte populations in lymph nodes and spleen

Deletion of A20 in immune cells is associated with autoimmune diseases (Chu et al., 2011; Hammer et al., 2011; Hövelmeyer et al., 2011; Kool et al., 2011; Matmati et al., 2011; Tavares et al., 2010; Xuan et al., 2014). Therefore we analyzed the secondary lymphoid organs spleen and lymph nodes from 8-week-old naïve CD4-Cre A20$^{fl/fl}$ mice as well as A20$^{fl/fl}$ and CD4-Cre A20$^{wt/wt}$ control mice. Cells were isolated and characterized by flow cytometry for the composition of leukocyte populations.
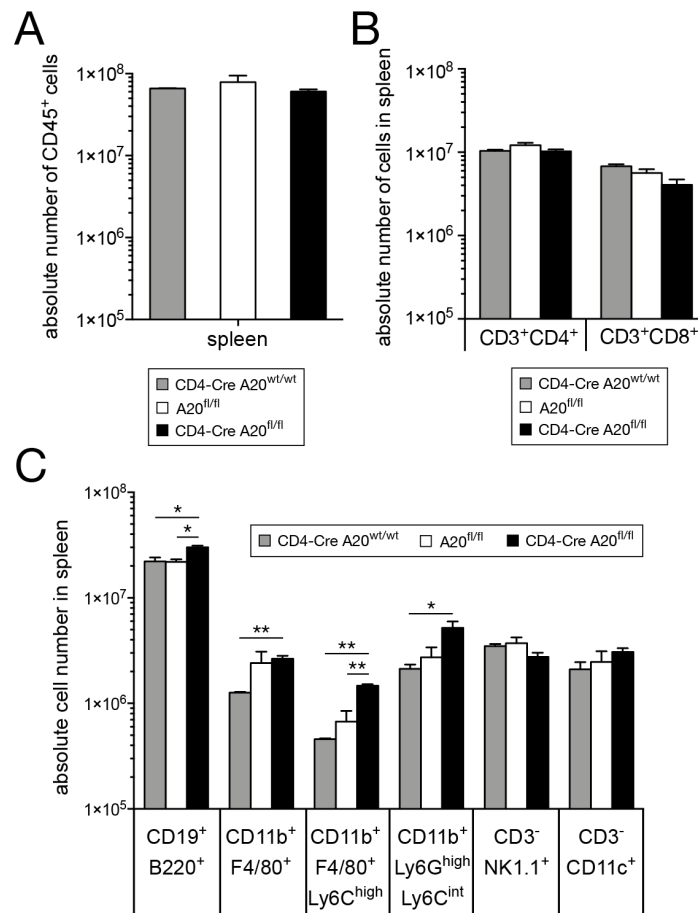
Figure 12: Leukocyte numbers in spleen of CD4-Cre A20$^{fl/fl}$ mice.
Spleens of 8-week-old naïve mice were isolated and splenocyte populations were analyzed by flow cytometry. **A|** Absolute number of leukocytes in spleen. **B|** Absolute number of B cells (CD19$^+$B220$^+$), macrophages (F4/80$^+$CD11b$^+$), monocytes (F4/80$^+$CD11b$^+$Ly6C^{high}), neutrophils (CD11b$^+$Ly6C^{int}Ly6G^{high}), NK cells (NK1.1$^+$CD3$^-$) and dendritic cells (CD11c$^+$CD3$^-$). **C|** Representative dot plots and **D|** Absolute number of CD4$^+$ and CD8$^+$ T cells in spleen. A representative of 3 independent experiments is shown, with 3-4 mice per group. Error bars indicate +SEM. Student's t-test, * p< 0.05; ** p<0.01.

Absolute numbers of leukocytes were similar in spleens of all groups (Figure 12A). Analysis of the T cell compartment revealed no significant differences for both, CD4$^+$ and CD8$^+$ T cells, in spleens of CD4-Cre A20$^{fl/fl}$ mice (Figure 12B). However, increased numbers of B cells (CD19$^+$B220$^+$), macrophages (F4/80$^+$CD11b$^+$), monocytes (F4/80$^+$CD11b$^+$Ly6C^{high})

and neutrophils (CD11b$^+$Ly6C^{int}Ly6G^{high}) were detected in CD4-Cre A20$^{fl/fl}$ mice, whereas numbers of NK cells (NK1.1$^+$CD3$^-$) and dendritic cells (CD11c$^+$CD3$^-$) were equal in all groups (Figure 12C).
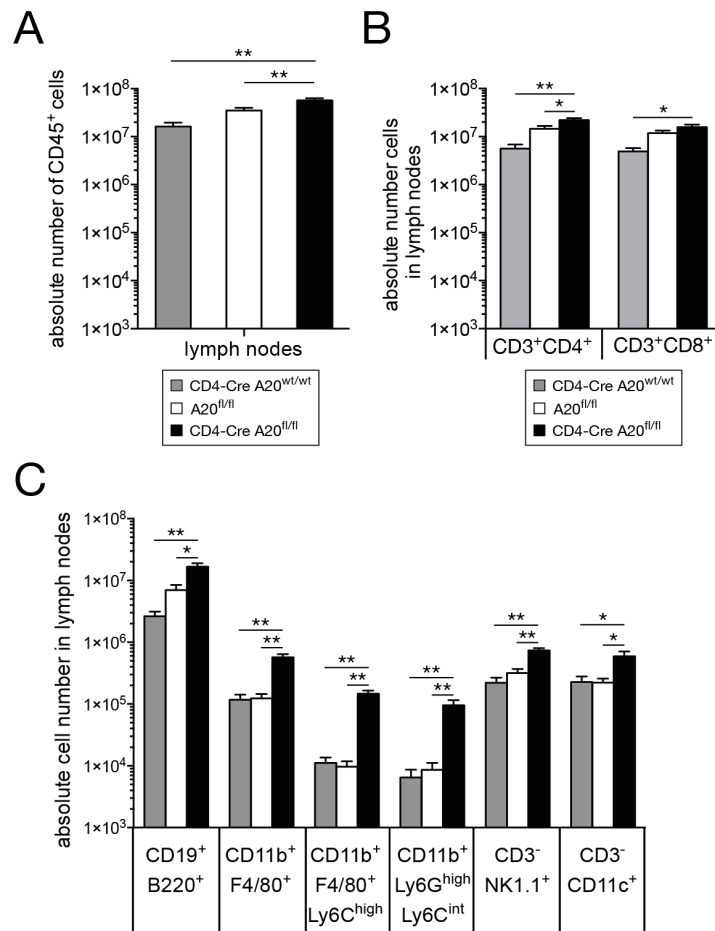
Figure 13: Leukocyte numbers in lymph nodes of CD4-Cre A20$^{fl/fl}$ mice.
Lymph nodes of 8-week-old naïve mice were isolated and leukocyte populations were analyzed by flow cytometry. **B|** Absolute number of B cells (CD19$^+$B220$^+$), macrophages (F4/80$^+$CD11b$^+$), monocytes (F4/80$^+$CD11b$^+$Ly6C^{high}), neutrophils (CD11b$^+$Ly6C^{int}Ly6G^{high}), NK cells (NK1.1$^+$CD3$^-$) and dendritic cells (CD11c$^+$CD3$^-$). **C|** Representative dot plots and **D|** Absolute number of CD4$^+$ and CD8$^+$ T cells in lymph nodes. A representative of 3 independent experiments is shown, with 3-4 mice per group. Error bars indicate +SEM. Student's t-test, * p< 0.05; ** p<0.01.

Absolute numbers of leukocytes in lymph nodes were significantly increased in CD4-Cre A20$^{fl/fl}$ mice compared to both control groups (Figure 13A), thus, explaining the increase of absolute numbers of CD4$^+$ and CD8$^+$ T cells (Figure 13B), as well as B cells, macrophages, monocytes, neutrophils, NK cells and dendritic cells (Figure 13C) in lymph nodes of CD4-Cre A20$^{fl/fl}$ mice.

Leukocyte subpopulations of 24-week-old mice from all groups remained unchanged as compared to 8-week-old mice.

3.1.4 Serum cytokine levels of CD4-Cre A20$^{fl/fl}$ mice

Cytokine profile from serum of 8-week-old and 24-week-old mice was determined by CBA to detect inflammatory responses (Figure 14A-G).
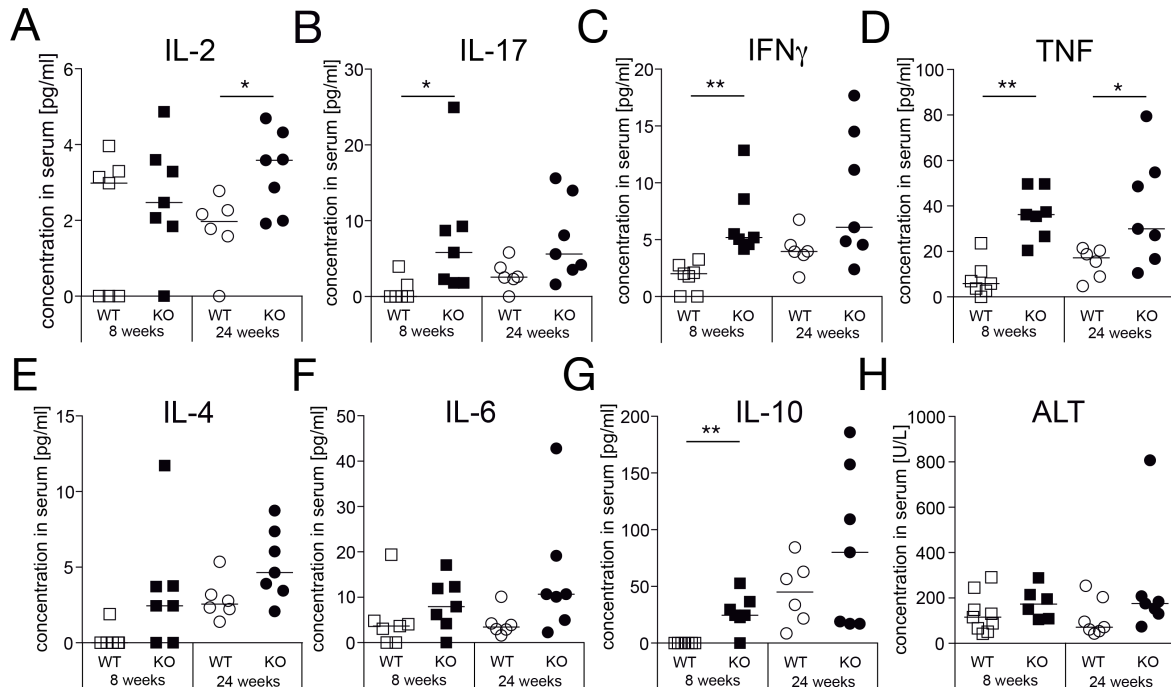
Figure 14: Serum analysis of 8-week and 24-week old mice
A| IL-2, **B|** IL-17, **C|** IFN-γ, **D|** TNF, **E|** IL-4, **F|** IL-6 and **G|** IL-10 in serum of young (8-week old) and aged (24-week-old) mice. **H|** Alanine transaminase (ALT) concentration in serum. Data are compiled of 2 independent experiments with 3-4 animals per group and experiment. Line indicates median. WT: A20$^{fl/fl}$; KO: CD4-Cre A20$^{fl/fl}$. Student's *t*-test, * p< 0.05; ** p<0.01.

Analysis of cytokines in serum revealed significantly increased concentrations of pro-inflammatory IL-17, IFN-γ and TNF in serum of 8-week-old CD4-Cre A20$^{fl/fl}$ mice (Figure 14B,C,D and G) and a minor increase of anti-inflammatory IL-4 and IL-10 (Figure 14E,G). In aged CD4-Cre A20$^{fl/fl}$ mice no increase of pro-inflammatory cytokines compared to 8-week-old mice was observed. Anti-inflamatory IL-4 and IL-10 were increased in serum of both genotypes. Giordano et al. have reported that mature T-Cre A20$^{fl/fl}$ mice, which lack A20 specifically in peripheral T cells, develop a spontaneous mild hepatitis with increased levels of ALT. Therefore, we determined serum alanine transaminase (ALT) levels in CD4-Cre A20$^{fl/fl}$ and A20$^{fl/fl}$ mice. However, ALT levels were similar in all groups, illustrating normal liver function (Figure 14H).

3.1.5 Increased activation and proliferation of A20-deficient CD8⁺ T cells *in vitro*

A20 is an important negative regulator of NF-κB activation, therefore we investigated the role of A20 in T cells on a cellular level *in vitro*. Considering the important role of CD8⁺ T cells in listeriosis, we studied the activation and proliferation of A20-sufficient and A20-deficient CD8⁺ T cells *in vitro*.
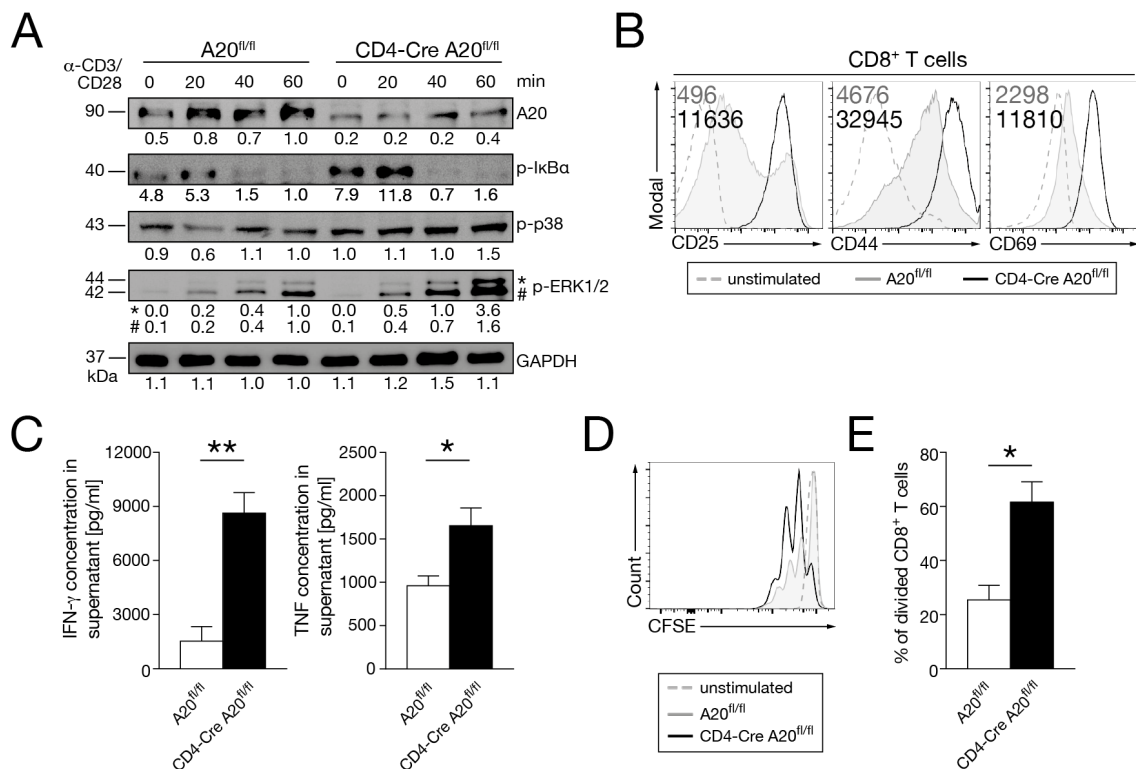
Figure 15: Increased activation and proliferation of A20-deficient CD8⁺ T cells in vitro.
CD8⁺ T cells from naïve mice were isolated and cultivated in the presence of 1 µg/ml plate-bound α-CD3 and 2 µg/ml soluble α-CD28 for 3 days, respectively. **A|** Proteins from T cells were isolated after stimulation with α-CD3/CD28 for 0, 10, 30 or 60 min. Western blot analysis was performed on total cell lysate for A20, p-IκBα, p-p38, p-ERK and GAPDH. **B|** Flow cytometric analysis of activation markers CD25, CD44 and CD69 by CD8⁺ T cells, respectively. Grey numbers indicate MFI of A20-sufficient CD8⁺ T cells and black numbers indicate MFI of A20-deficient CD8⁺ T cells. **C|** Concentration of IFN-γ and TNF in the supernatant of stimulated CD8⁺ T cells was determined by CBA. **D|** Cells were labeled with CFSE and proliferative activity of CD8⁺ T cells was determined by flow cytometry. **E|** Frequency of divided cells after stimulation. A representative of 2 independent experiments is shown, with 3 mice per group. Error bars indicate +SEM. Student's *t*-test, * p< 0.05; ** p< 0.01.

Stimulation of the TCR with anti-CD3 in combination with anti-CD28 resulted in an upregulation of A20 in control CD8$^+$ T cells (Figure 15A). Consistent with previous reports of A20 as a negative regulator of NF-κB, TCR stimulation of A20-deficient cells induced stronger activation of NF-κB but also MAPK signaling pathways indicated by increased phosphorylation of IκBα, p38 and ERK.

After stimulation for 72 h with anti-CD3 and anti-CD28, expression of T cell activation markers was measured (Figure 15B). A20-deficient CD8$^+$ T cells (black histograms) showed increased expression of CD25, CD44 and CD69 compared to A20-sufficient CD8$^+$ T cells (grey-filled histograms). Analysis of cytokines revealed increased levels of IFN-γ and TNF in the supernatant of A20-deficient CD8$^+$ T cells. For measuring proliferative activity, cells were stained with CFSE and then stimulated with low amounts of anti-CD3 and anti-CD28. Decrease in CFSE intensity determines proliferation of cells. A20-deficient CD8$^+$ T cells (black histogram) proliferated significantly stronger than A20-sufficient CD8$^+$ T cells (grey-filled histogram) (Figure 15D+E). Similar results for activation, cytokine production and proliferation were observed in CD4$^+$ T cells (data not shown). In conclusion, A20 plays an important role in TCR signaling and T cell activation.

3.2 Regulation of T cell responses by A20 upon infection with *L. monocytogenes*

To investigate the T cell-specific role of A20 *in vivo*, we infected the mice with L. monocytogenes, which induces a strong CD8$^+$ T cells response in the infected host. The experimental design of the infection model is shown in Figure 16A. On day 0, CD4-Cre A20$^{fl/fl}$ and A20$^{fl/fl}$ control mice were infected with a non-lethal dose of *L. monocytogenes* WT or ovalbumin-expressing *L. monocytogenes* (*L. monocytogenes* OVA), respectively. Spleens were isolated and analyzed at the indicated time points. On day 50 p.i., mice were reinfected with a high dose of *L. monocytogenes* WT or *L. monocytogenes* OVA, respectively and three days later, spleens were isolated and analyzed to determine memory T cell response.
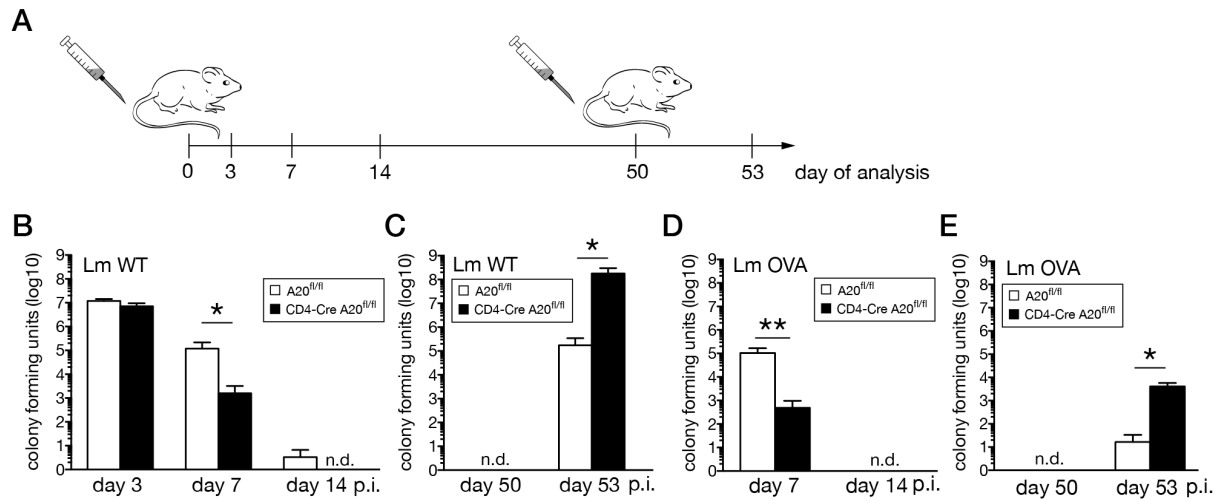
Figure 16: Infection of CD4-Cre A20$^{fl/fl}$ and A20$^{fl/fl}$ mice with *L. monocytogenes*.
CD4-Cre A20$^{fl/fl}$ and A20$^{fl/fl}$ control mice were infected with a non-lethal dose of *L. monocytogenes* WT or OVA. After 50 days, mice were reinfected with a high dose of *L. monocytogenes* WT or OVA, respectively. **A|** Experimental design of the study. Spleens were analyzed at the indicated time points. **B-E|** CFUs in spleen were determined **B+C|** after infection with *L. monocytogenes* WT **B|** on day 3, 7 and 14 p.i. and **C|** on day 50 and 3 days after reinfection, as well as **D+E|** after infection with *L. monocytogenes* OVA **D|** on day 7 and 14 p.i. and **E|** on day 50 and 3 days after reinfection. Data are compiled of 3 independent experiments with 3-4 mice per group. Data are represented as mean +SEM. Mann Whitney test, * p< 0.05; ** p< 0.01; n.d.: not detectable; Lm WT: *L. monocytogenes* WT; Lm OVA: *L. monocytogenes* OVA.

At day 3 p.i., before the onset of the T cell response, no significant differences in CFU were observed. However, at the peak of the T cell response at day 7 p.i., the bacterial burden in CD4-Cre A20$^{fl/fl}$ mice was nearly 100-fold reduced compared to A20$^{fl/fl}$ control mice (Figure 16B). Furthermore, CD4-Cre A20$^{fl/fl}$ mice were able to clear the *L. monocytogenes* WT infection faster than the control mice.

On day 50 p.i., no bacteria were detectable in mice of both genotypes. However, upon reinfection, the pathogen load in spleen of CD4-Cre A20$^{fl/fl}$ mice was more than 1,000-fold higher than in spleen of A20$^{fl/fl}$ control mice (Figure 16C). Similar results were obtained after infection with *L. monocytogenes* OVA (Figure 16D and E)

For the detection of pathogen-specific CD8$^+$ T cells, mice were infected with *L. monocytogenes* OVA and splenocytes were stained with the fluorochrome-labeled H2-Kb SIINFEKL pentamer at different time points. The pentamer binds to CD8$^+$ T cells which recognize the OVA$_{257-264}$ peptide of the ovalbumin protein, therefore, specifically binding *L. monocytogenes* OVA-specific CD8$^+$ T cells. Ovalbumin-specific cells were detected by flow cytometry on days 0, 7, 21, 50 and day 53 (three days after reinfection) p.i. A strong increase of the relative (Figure 17A) and absolute numbers (Figure 17B) of *L. monocytogenes* OVA-specific CD8$^+$ T cells were detectable in CD4-Cre A20$^{fl/fl}$ mice at day 7 p.i.. After pathogen clearance at day 21 and 50 p.i., numbers of H2-Kb SIINFEKL-specific CD8$^+$ T cells were reduced in both strains. Three days after reinfection,

L. monocytogenes OVA-specific CD8$^+$ T cells strongly expanded in A20$^{fl/fl}$ control mice. The number of pathogen-specific CD8$^+$ T cells in CD4-Cre A20$^{fl/fl}$ mice, however, was even weaker compared to the peak of the primary response (Figure 17B).

To determine the effector function of pathogen-specific CD8$^+$ T cells, we measured IFN-γ and granzyme B production of CD8$^+$ T cells via flow cytometry. During the peak of the CD8$^+$ T cell response at day 7 p.i., the relative and absolute numbers of IFN-γ-producing OVA-specific CD8$^+$ T cells were significantly increased in CD4-Cre A20$^{fl/fl}$ mice, consistent with the increased cytokine production *in vitro* (Figure 15). In addition, we observed that pathogen-specific A20-deficient CD8$^+$ T cells produced more IFN-γ (Figure 17E+F) and granzyme B (Figure 17G+H) compared to A20-sufficient cells.

During the T cell contraction phase, we detected a decline of IFN-γ- and granzyme B-producing cells at day 21 and 50 p.i. in both genotypes (Figure 17C and D). However, in CD4-Cre A20$^{fl/fl}$ mice, the reduction was significantly stronger. Interestingly, not only the number of cells but also the amount of IFN-γ was drastically reduced in A20-deficient CD8$^+$ T cells beyond the peak of the infection, while in A20-sufficient CD8$^+$ T cells the amount of IFN-γ produced remained the same up to day 50 p.i (Figure 17E+F).

Three days after reinfection (day 53 p.i.), relative and absolute numbers of IFN-γ-producing CD8$^+$ T cells strongly increased in A20$^{fl/fl}$ control mice (Figure 17C and D), similar to the expansion of H2-Kb SIINFEKL-specific CD8$^+$ T cells (Figure 17A+B). In addition, granzyme B was strongly upregulated in A20-sufficient CD8$^+$ T cells (Figure 17G+H). In sharp contrast, only a minor increase of *L. monocytogenes* OVA-specific IFN-γ and granzyme B-producing CD8$^+$ T cells was observed in CD4-Cre A20$^{fl/fl}$ mice (Figure 17C-F), similar to the weak expansion of H2-Kb SIINFEKL-specific CD8$^+$ T cells (Figure 17A+B). Interestingly, not only fewer cells produced IFN-γ in CD4-Cre A20$^{fl/fl}$ mice, but these cells also produced significantly less IFN-γ compared to A20$^{fl/fl}$ control mice (Figure 17E+F).
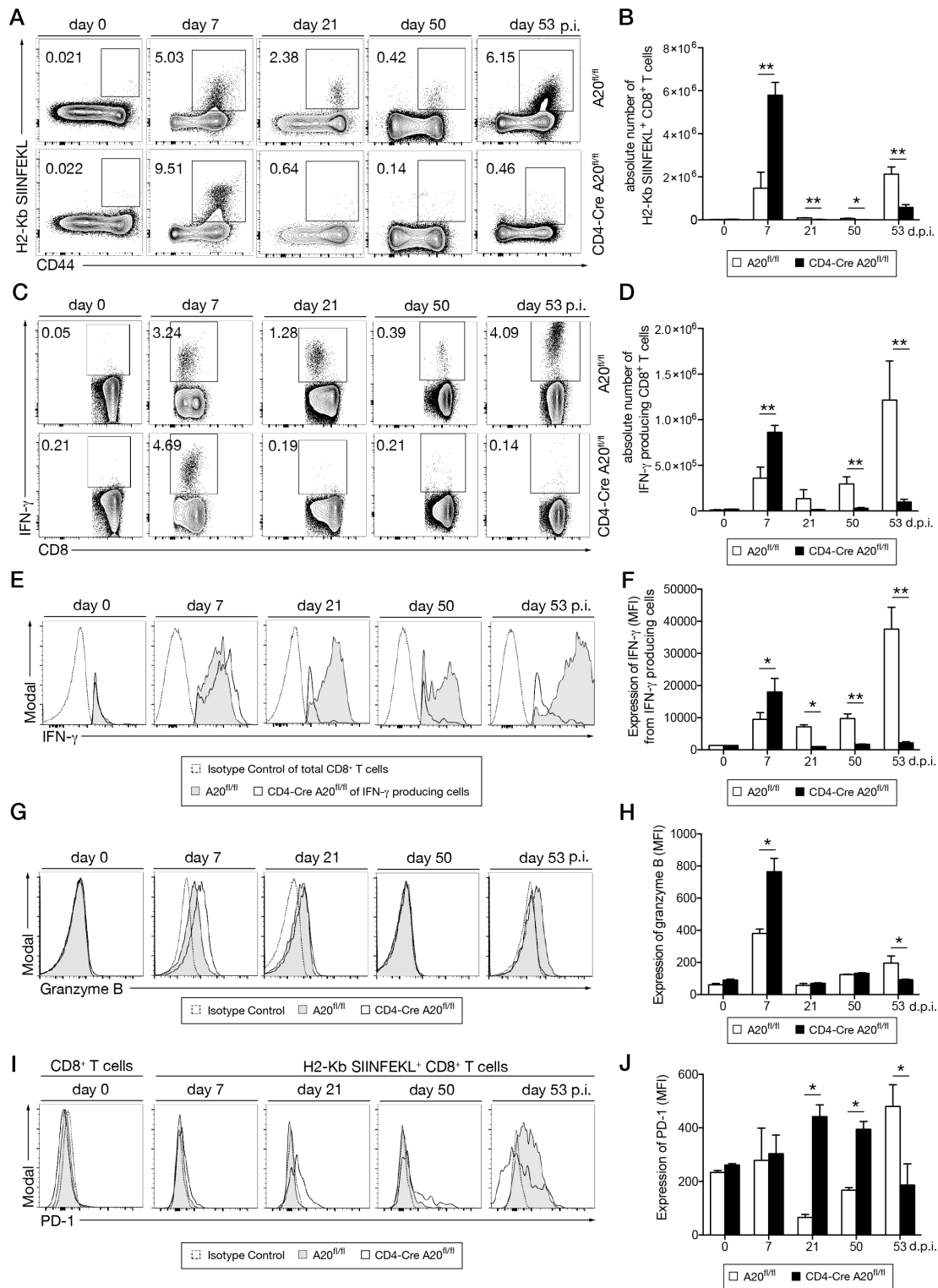
Figure 17: Effector function of A20-deficient CD8+ T cells

CD4-Cre A20^fl/fl and A20^fl/fl control mice were infected with *L. monocytogenes* OVA and flow cytometric analysis was performed from splenocytes at day 0, 7, 21, 50 and 53 p.i. **A|** Representative dot plots with relative numbers and **B|** absolute number of H2-Kb SIINFEKL pentamer+ CD8+ T cells. **C|** Representative dot plots with relative numbers and **D|** absolute number of IFN-γ producing CD8+ T cells after *ex vivo* restimulation with SIINFEKL-peptide for 4 h in the presence of Brefeldin A. **E|** Histogram and **F|** MFI of IFN-γ gated on IFN-γ producing CD8+ T cells. **G|** Histogram and **H|** MFI of granzyme B-producing CD8+ T cells after *ex vivo* restimulation with SIINFEKL-peptide for 4 h in the presence of Brefeldin A. **I|** Histogram and **J|** MFI of PD-1 expression on H2-Kb SIINFEKL pentamer+ CD8+ T cells. A representative of 3 independent experiments is shown with 3 mice per group. Error bars indicate +SEM. Student's *t*-test, * p< 0.05.

54

Since A20-deficient CD8^{+} T cells seemed to develop a functional defect in cytokine production, we further studied the expression of the co-inhibitory receptor PD-1 which is upregulated on activated and functionally impaired CD8^{+} T cells. In fact, we observed a significant increase of PD-1 expression on A20-deficient *L. monocytogenes* OVA-specific CD8^{+} T cells after the peak of infection at day 21 and 50 p.i., while in A20^{fl/fl} control mice a downregulation of PD-1 was observed. In acute listeriosis (day 7 p.i.) and upon reinfection (day 53 p.i.), PD-1 was upregulated on A20-suffcient pathogen-specific CD8^{+} T cells which is consistent with PD-1 expression on activated T cells. On A20-deficient H2-Kb SIINFEKL-specific CD8^{+} T cells, PD-1 was first upregulated in the acute phase, and remained at high levels until day 50 p.i. Upon reinfection a downregulation was observed, which confirmed impaired activation of A20-deficient CD8^{+} T cells.

In summary, these data indicate, that A20 critically regulates and coordinates distinct phases of the pathogen-specific CD8^{+} T cell response.
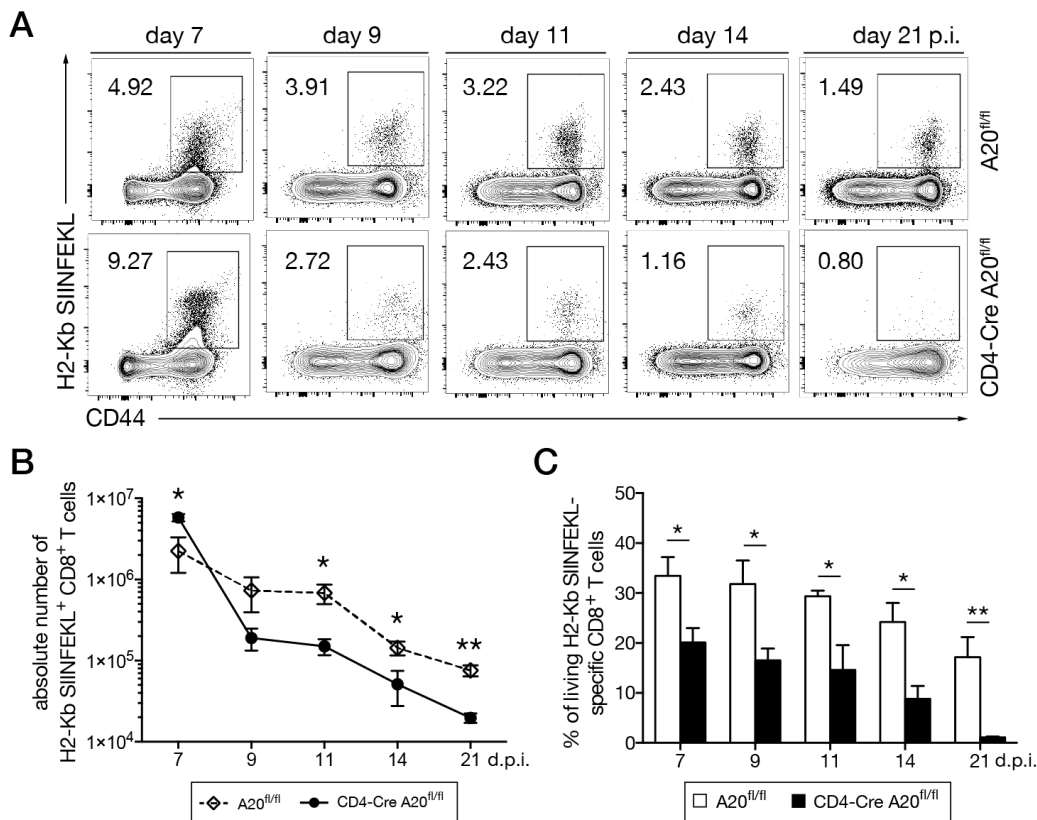
Figure 18: Detailed kinetic of H2-Kb SIINFEKL-specific CD8^{+} T cells.
CD4-Cre A20^{fl/fl} and A20^{fl/fl} control mice were infected with *L. monocytogenes* OVA and spleens were analyzed at the indicated time points. **A|** Representative dot plots and **B|** absolute numbers of H2-Kb SIINFEKL pentamer^{+} CD8^{+} T cells on day 7, 9, 11, 14 and 21 p.i. **C|** Relative numbers of living H2-Kb SIINFEKL-specific CD8^{+} T cells was determined by annexin V and 7-AAD staining. Double negative cells were considered living. Data compiled from two independent experiments with 3-4 mice per group and experiment. Error bars indicate +SEM. Student's *t*-test, * p< 0.05; ** p< 0.01.

CD4-Cre A20$^{fl/fl}$ mice developed an improved early primary CD8$^+$ T cell response but failed to induce a pathogen-specific memory T cell response. Therefore, we performed a detailed kinetic of *L. monocytogenes* OVA-specific CD8$^+$ T cells. From day 7, the peak of the T cell response, to day 21, when the loss of pathogen-specific CD8$^+$ T cells became evident (Figure 17).

Again at day 7 p.i. relative (Figure 18A) and absolute (Figure 18B) numbers of pathogen-specific CD8$^+$ T cells were increased in CD4-Cre A20$^{fl/fl}$ mice. At day 9 p.i., after the peak of the T cell response, numbers of *L. monocytogenes* OVA-specific CD8$^+$ T cells decreased in both strains. However, the decline was even stronger in CD4-Cre A20$^{fl/fl}$ mice as compared to A20$^{fl/fl}$ control mice. Thus already at day 9 p.i., the number of pathogen-specific CD8$^+$ T cells was decreased in CD4-Cre A20$^{fl/fl}$ mice. Thereafter, *L. monocytogenes* OVA-specific CD8$^+$ T cells declined with similar kinetic in both strains up to day 21 p.i., but remained at lower levels in CD4-Cre A20$^{fl/fl}$ mice and decreased even stronger towards day 21 p.i.

The rapid decline of A20-deficient pathogen-specific CD8$^+$ T cells suggests that A20 regulates cell death events. Therefore, we performed a kinetic of the number of living (annexin$^-$/7-AAD$^-$) *L. monocytogenes* OVA-specific CD8$^+$ T cells. Starting at the peak of T cell response at day 7 p.i., already a reduced frequency of living cells was observed in CD4-Cre A20$^{fl/fl}$ mice compared to control mice (Figure 18C). The relative number of living A20-sufficient cells was maintained at similar levels and reduced only slightly at day 21 p.i., whereas the number of living A20-deficient *L. monocytogenes* OVA-specific CD8$^+$ T cells reduced significantly over time. At day 21 p.i. a 13-fold decrease of living cells was detected in spleens of CD4-Cre A20$^{fl/fl}$ mice, while A20-sufficient pathogen-specific CD8$^+$ T cells decreased only 1.4-fold from day 7 to day 21 p.i.

3.3 Regulation of memory CD8⁺ T cell formation by A20

Early after infection, antigen-stimulated CD8⁺ T cells can be, according to their expression of KLRG-1 and the α-subunit of the IL-7R (CD127), divided into short-lived effector cells (SLEC; KLRG-1$^+$CD127$^-$) and memory precursor effector cells (MPEC; KLRG-1$^-$CD127$^+$). To investigate if CD8⁺ T$_{mem}$ formation is impaired in A20-deficient T cells, we analyzed the relative and absolute numbers of SLEC and MPEC subpopulations within the *L. monocytogenes* OVA-specific CD8⁺ T cell compartment (Figure 19).

Figure 19: MPEC survival is impaired in CD4-Cre A20$^{fl/fl}$ mice.
CD4-Cre A20$^{fl/fl}$ and A20$^{fl/fl}$ control mice were infected with *L. monocytogenes* OVA and spleens were analyzed at day 7, 9, 11, 14 and 21 p.i. Cells were gated on H2-Kb SIINFEKL pentamer⁺ CD8⁺ T cells. **A|** Representative dot plots with relative numbers and **B-C|** Kinetics with absolute numbers of **B|** pathogen-specific SLEC (KLRG-1$^+$CD127$^-$) and **C|** pathogen-specific MPEC CD8⁺ T cells (KLRG-1$^-$CD127$^+$). SLEC: short-lived effector cells; MPEC: memory precursor effector cells. A representative of two independent experiments is shown with 3-4 mice per group. Error bars indicate +SEM. Student's *t*-test, * p< 0.05; ** p< 0.01.

At day 7 p.i. similar relative numbers of SLEC and MPEC were observed in both groups of mice (Figure 19A-C). During the course of the contraction phase, an enrichment of MPECs was observed in the *L. monocytogenes* OVA-specific CD8⁺ T cell population of A20$^{fl/fl}$ mice, whereas in CD4-Cre A20$^{fl/fl}$ mice similar numbers of both SLEC and MPEC were detectable at day 21 p.i. (Figure 19A). The kinetic of absolute numbers revealed that in both groups *L. monocytogenes* OVA-specific SLEC decreased at a similar rate, however, less cells survived in CD4-Cre A20$^{fl/fl}$ mice. Absolute numbers of MPEC remained stable

in A20$^{fl/fl}$ mice, while there was a significant reduction in CD4-Cre A20$^{fl/fl}$ mice indicating that A20 regulates survival of memory-precursor CD8$^+$ T cells.

Next, we studied the maintenance of the T$_{mem}$ sub-populations T$_{EM}$ and T$_{CM}$ as well as effector T cells (T$_{eff}$) at day 50 p.i. and 3 days after reinfection at day 53.
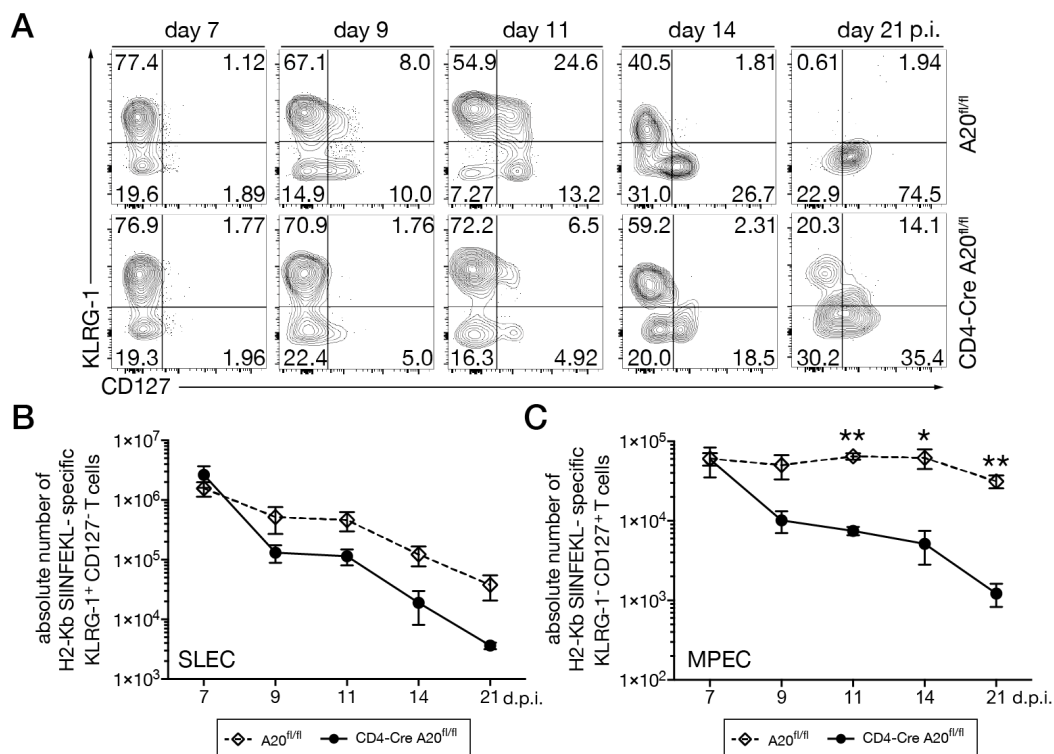

Figure 20: Impaired memory T cell response in CD4-Cre A20$^{fl/fl}$ mice.
CD4-Cre A20$^{fl/fl}$ and A20$^{fl/fl}$ control mice were infected with *L. monocytogenes* OVA and spleens were analyzed at day 50 p.i. For memory T cell response, mice were reinfected at day 50 p.i. and spleens were analyzed three days later (day 53 p.i.). Cells were gated on H2-Kb SIINFEKL pentamer$^+$ CD8$^+$ T cells. **A|** Representative dot plots with relative numbers and **B-D|** absolute numbers of pathogen-specific **B|** T$_{eff}$ CD8$^+$ T cells (CD62L$^-$CD127$^-$), **C|** T$_{EM}$ CD8$^+$ T cells (CD62L$^-$CD127$^+$) and **D|** T$_{CM}$ CD8$^+$ T cells (CD62L$^+$CD127$^+$). A representative of two independent experiments is shown with 3-4 mice per group. Error bars indicate +SEM. Student's *t*-test, * p< 0.05; ** p< 0.01.

At day 50 and 53 p.i. relative numbers of *L. monocytogenes* OVA-specific T$_{CM}$ were increased in CD4-Cre A20$^{fl/fl}$ mice, while numbers of T$_{EM}$ were drastically reduced (Figure 20A). Absolute numbers of *L. monocytogenes* OVA-specific T$_{EM}$, T$_{CM}$ and T$_{eff}$ were significantly reduced at day 50 p.i. in CD4-Cre A20$^{fl/fl}$ mice compared to A20$^{fl/fl}$ control mice. Upon reinfection, T$_{eff}$, T$_{EM}$ and T$_{CM}$ expanded strongly in control animals, but only marginally in CD4-Cre A20$^{fl/fl}$ mice (Figure 20B-D).

An effective memory T cell response is dependent on several extrinsic and intrinsic factors. Especially CD4$^+$ T cells are detrimental for the formation and function of CD8$^+$ T$_{mem}$ in listeriosis. Therefore, we further investigated if A20 is controlling CD8$^+$ T$_{mem}$ development indirectly, by regulating CD4$^+$ T cell responses.

Of note, IFN-γ and IL-2-production of CD4$^+$ T cells in CD4-Cre A20$^{fl/fl}$ mice was normal, compared to A20$^{fl/fl}$ control mice (Figure 21A+B). Upon reinfection, cytokine-producing CD4$^+$ T cells expanded similarly in both groups indicating that CD4$^+$ T cell responses were normal in CD4-Cre A20$^{fl/fl}$ mice (Figure 21C+D). Therefore, the impaired CD8$^+$ T$_{mem}$ response in CD4-Cre A20$^{fl/fl}$ mice might not be caused by a defective CD4$^+$ T cell response, but rather due to CD8$^+$ T cell intrinsic regulations.
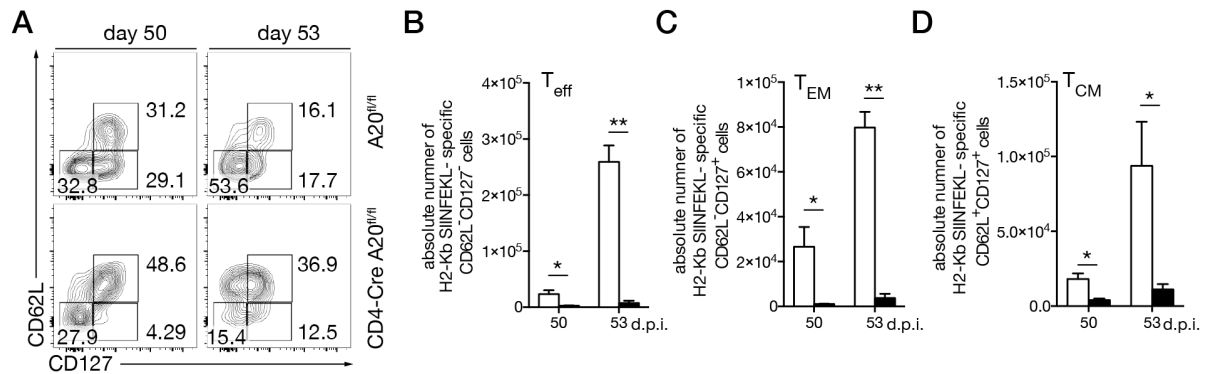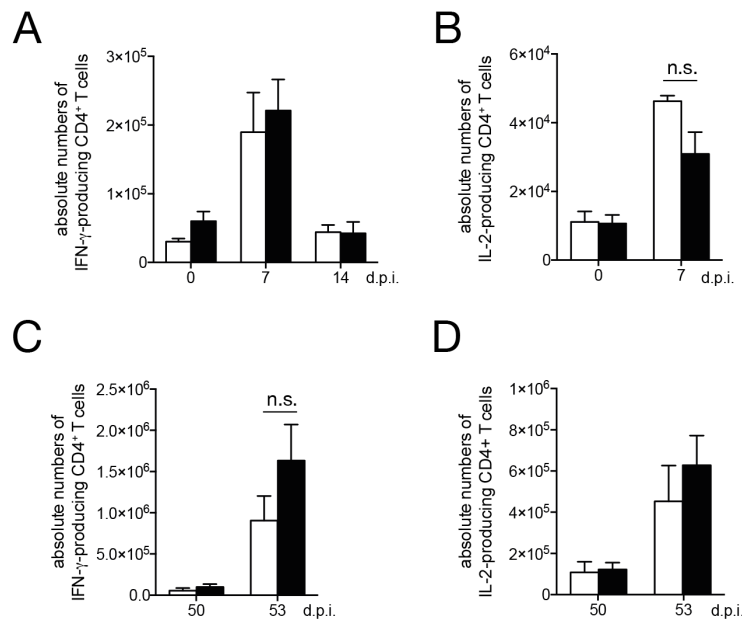
Figure 21: CD4+ T cell response is normal in CD4-Cre A20fl/fl mice.
CD4-Cre A20fl/fl and A20fl/fl control mice were infected with *L. monocytogenes* OVA and spleens were analyzed at different timepoints p.i. For memory T cell response, mice were reinfected at day 50 p.i. and spleens were analyzed three days later (day 53 p.i.). Splenocytes were restimulated with OVACD4-peptide in the presence of brefeldin A for 4 h. Cytokines were measured by flow cytometry. **A|** Absolute number of IFN-γ-producing CD4+ T cells in primary response. **B|** Absolute number of IL-2-producing CD4+ T cells in primary response. **C|** Absolute number of IFN-γ-producing CD4+ T cells in secondary response. **D|** Absolute number of IL-2-producing CD4+ T cells in secondary response. A representative of two independent experiments is shown with 3-4 mice per group. Error bars indicate +SEM. Student's *t*-test, n.s. not significant.

Taken together, A20 regulates the survival of *L. monocytogenes* OVA-specific CD8+ T cell subsets. Furthermore, A20-deficiency disrupted T$_{mem}$ formation and re-expansion, which, however, was not due to a defective CD4+ T cell response.

Since we observed a massive decrease in pathogen-specific memory precursor cells, we further focused on the role of A20 in cell death of CD8+ T cells during the contraction phase of primary CD8+ T cell response.

3.4 Regulation of CD8$^+$ T cell death by A20

3.4.1 A20 limits apoptosis and necroptosis in activated CD8$^+$ T cells *in vivo*

Considering the accelerated loss of pathogen-specific CD8$^+$ T cells in CD4-Cre A20$^{fl/fl}$ mice, we further determined whether A20 inhibits cell death pathways in T cells. Cell death and sensitivity to cell death induction can be determined via several factors: i) morphological changes of cells, ii) activation of effector caspases or necrosome formation, iii) detection of effector caspase activity and iv) upregulation of death receptor CD95.

To analyze morphological changes in dying cells IFC analysis was performed *ex vivo* as well as *in vitro*. Figure 22A illustrates the gating strategy and Figure 22B-E shows representative pictures of morphological changes in dying cells.

First, only cells inside the focus range were selected by gating on the Gradient RMS in the bright field channel. Single cells were selected from aspect ratio and area and were further gated on CD3$^+$ CD8$^+$ cells. From this population, H2-Kb SIINFEKL pentamer$^+$ cells were selected and separated into healthy (7-AAD$^-$/annexin V$^-$), early apoptotic (7-AAD$^-$/annexin V$^+$) and late apoptotic/necroptotic (7-AAD$^+$/annexin V$^+$). While healthy cells had a normal, round morphology, early apoptotic cells showed already signs of membrane blebbing and shrunken cell size (Figure 22B-C). Double positive cells were further divided by sharpness/contrast and intensity of the 7-AAD staining. Late apoptotic cells are characterized by a high contrast morphology and a low intensity threshold, as the 7-AAD signal is strong but located only in a small area of the cell due to chromatin condensation (Figure 22D). Furthermore, apoptosis is defined by nuclear condensation, cell shrinkage and membrane blebbing, clearly indicated in Figure 22D. Necroptotic cells, however, are characterized by a low contrast morphology and high intensity threshold due to cytoplasmic and nuclear swelling (Figure 22E).
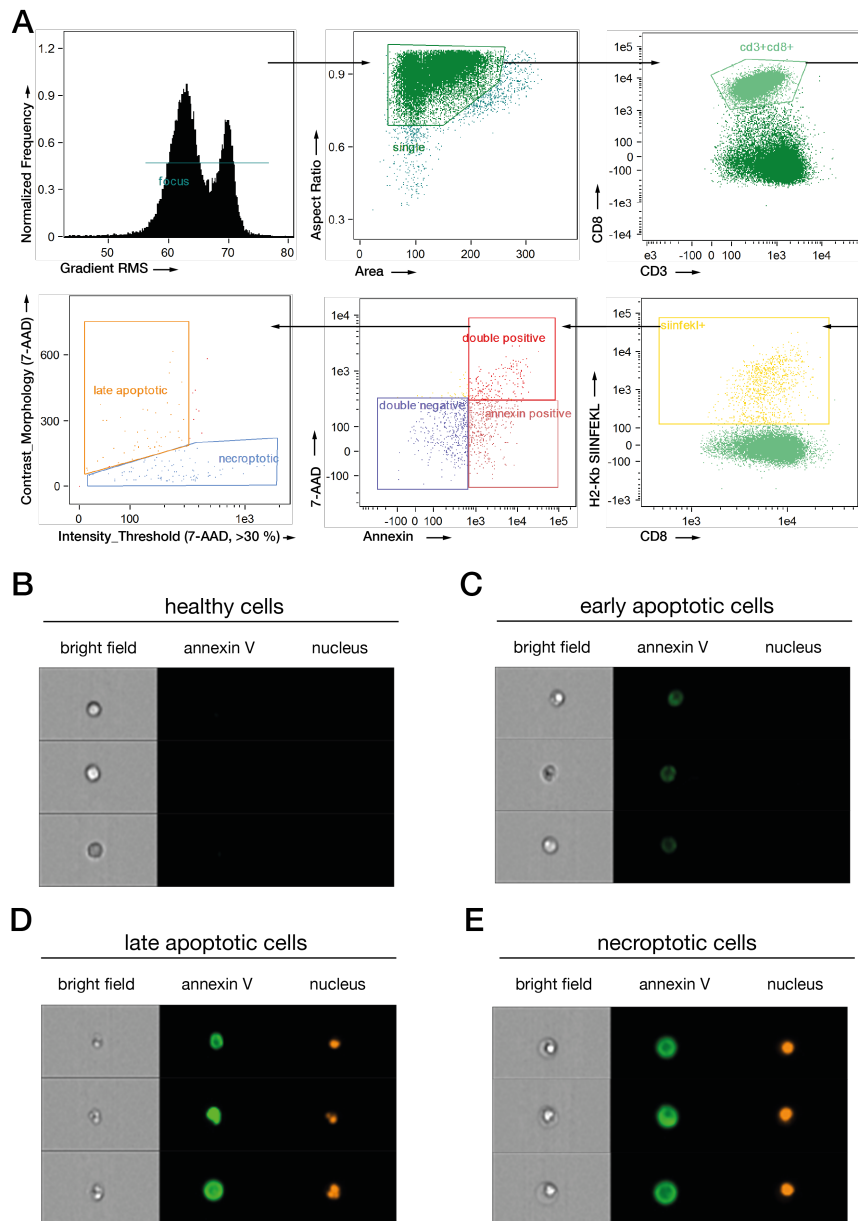
Figure 22: Gating strategy and morphological differences in the IFC analysis of pathogen-specific CD8+ T cells *ex vivo*.

CD4-Cre A20^fl/fl and A20^fl/fl control mice were infected with *L. monocytogenes* OVA and splenocytes were isolated and stained for H2-Kb SIINFEKL pentamer+ CD8+ T cells as well as cell death indicators annexin V and 7-AAD. **A|** Gating strategy for IFC analysis. **B-E|** Representative pictures of cells in different stages of cell death. **B|** Healthy cells, annexin V+ and 7-AAD⁻. **C|** Early apoptotic cells, annexin V+ and 7-AAD⁻. **D|** Late apoptotic cells, annexin V+ and 7-AAD+ with condensed chromatin, indicated by small areas of high 7-AAD intensity. **E|** Necroptotic cells, annexin V+ and 7-AAD+. Nucleus: 7-AAD

To identify, which cell death pathways are affected by A20 in T cells *in vivo*, we determined if *L. monocytogenes* OVA-specific CD8+ T cells undergo apoptosis or necroptosis by IFC. Since no antibodies are available for staining of necroptotic cells for conventional flow cytometry, IFC was used to determine the morphology of single cells, therefore, allowing the differentiation between apoptosis and necroptosis (Pietkiewicz et al., 2015).

61

IFC analysis of *L. monocytogenes* OVA-specific CD8⁺ T cells was performed at day 7 p.i. and during the contraction phase at day 11 p.i. Cells were gated as described in Figure 22. Relative numbers of healthy, early and late apoptotic as well as necroptotic H2-Kb SIINFEKL pentamer⁺ cells were determined (Figure 23).
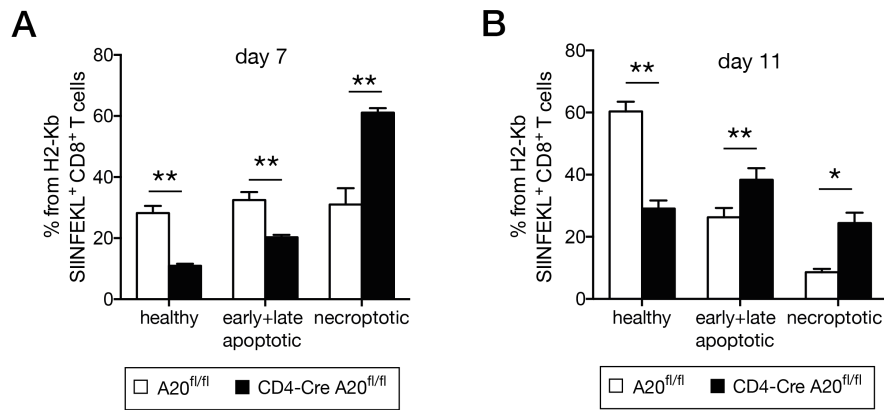
Figure 23: Morphological analysis of cell death *in vivo*.
CD4-Cre A20$^{fl/fl}$ and A20$^{fl/fl}$ control mice were infected with *L. monocytogenes* OVA and splenocytes were isolated at **A|** day 7 p.i. or **B|** day 11 p.i. At both time points, cells were stained with anti-annexin V and 7-AAD. IFC analysis of *L. monocytogenes* OVA-specific CD8⁺ T cells was performed to determine healthy, early and late apoptotic and necroptotic morphology. A representative of two independent experiments is shown with 3-4 mice per group. Error bars indicate +SEM. Student's *t*-test, * p< 0.05; ** p< 0.01.

At day 7 p.i. the relative number of healthy, apoptotic and necroptotic cells was equally distributed (between 28.2 % and 32.5 %) in A20$^{fl/fl}$ control mice. In CD4-Cre A20$^{fl/fl}$ significantly increased numbers of necroptotic cells (61.1 % ± 1.49 %) had been retrieved from CD4-Cre A20$^{fl/fl}$ mice (Figure 23A).

At day 11 p.i. we detected a change in the distribution pattern of apoptotic versus necroptotic cells in both groups. The relative number of healthy cells increased in both strains, but was maintained 2-fold higher in A20-sufficient *L. monocytogenes* OVA-specific CD8⁺ T cells. Necroptotic cells were reduced dramatically in both groups, but were still higher in A20-deficient mice.

No change was observed in the relative number of apoptotic cells in A20$^{fl/fl}$ control mice compared to day 7, but a 2-fold increase in CD4-Cre A20$^{fl/fl}$ mice was observed from day 7 to day 11 p.i., thus, leading to a significant increase as compared to control T cells (Figure 23B).

3.4.2 A20 limits apoptosis and necroptosis in activated CD8$^+$ T cells *in vitro*

In addition, we performed IFC analysis after CD8$^+$ T cell isolation and *in vitro* restimulation. Approximately 80 % of healthy CD8$^+$ T cells in both groups were isolated from spleens and lymph nodes prior to stimulation (Figure 24). However, already a slight increase of necroptotic morphology was observed in A20-deficient cells. After 72 h of stimulation, the relative number of living cells reduced to 36 % (± 8.09 %) in A20-sufficient CD8$^+$ T cells and 8.0 % (± 2.23 %) in A20-deficient cells, while the frequency of necroptotic and apoptotic cells was increased in A20-deficient CD8$^+$ T cells.
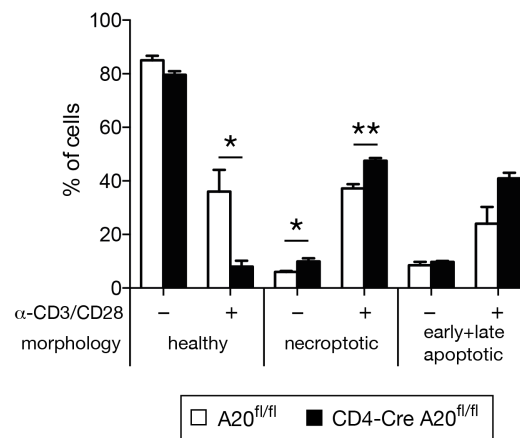
Figure 24: Morphological analysis of cell death *in vitro*.
CD8$^+$ T cells were purified from spleen and lymph nodes and stimulated with anti-CD3/CD28 for 72 h (+) or were left untreated (-). IFC was performed after annexin V and 7-AAD staining to determine cell death morphology. A representative of 2 independent experiments is shown with n = 3. Error bars indicate +SEM. Student's *t*-test, * p< 0.05; ** p< 0.01.

In conclusion, morphological analysis revealed that apoptosis as well as necroptosis are induced during the contraction phase of pathogen-specific CD8$^+$ T cells *in vivo* and upon TCR stimulation *in vitro*, and both seemed to be regulated by A20.

3.4.3 Regulation of cell death pathways in A20-deficient CD8$^+$ T cells *in vitro*

On a molecular level, apoptosis and necroptosis can be distinguished by upregulation and activation of different signaling components. For the induction of apoptosis activation of effector caspases such as caspase-3 and -7 is distinctive, whereas necrosome formation is characterized by the recruitment of RIPK3 to RIPK1.

To further analyze how A20 augments cell death *in vitro* upon TCR-stimulation, CD8⁺ T cells were stimulated with anti-CD3/CD28 or TNF, respectively, and the cleavage of procaspase-3 and -8 was analyzed by western blotting (Figure 25A).
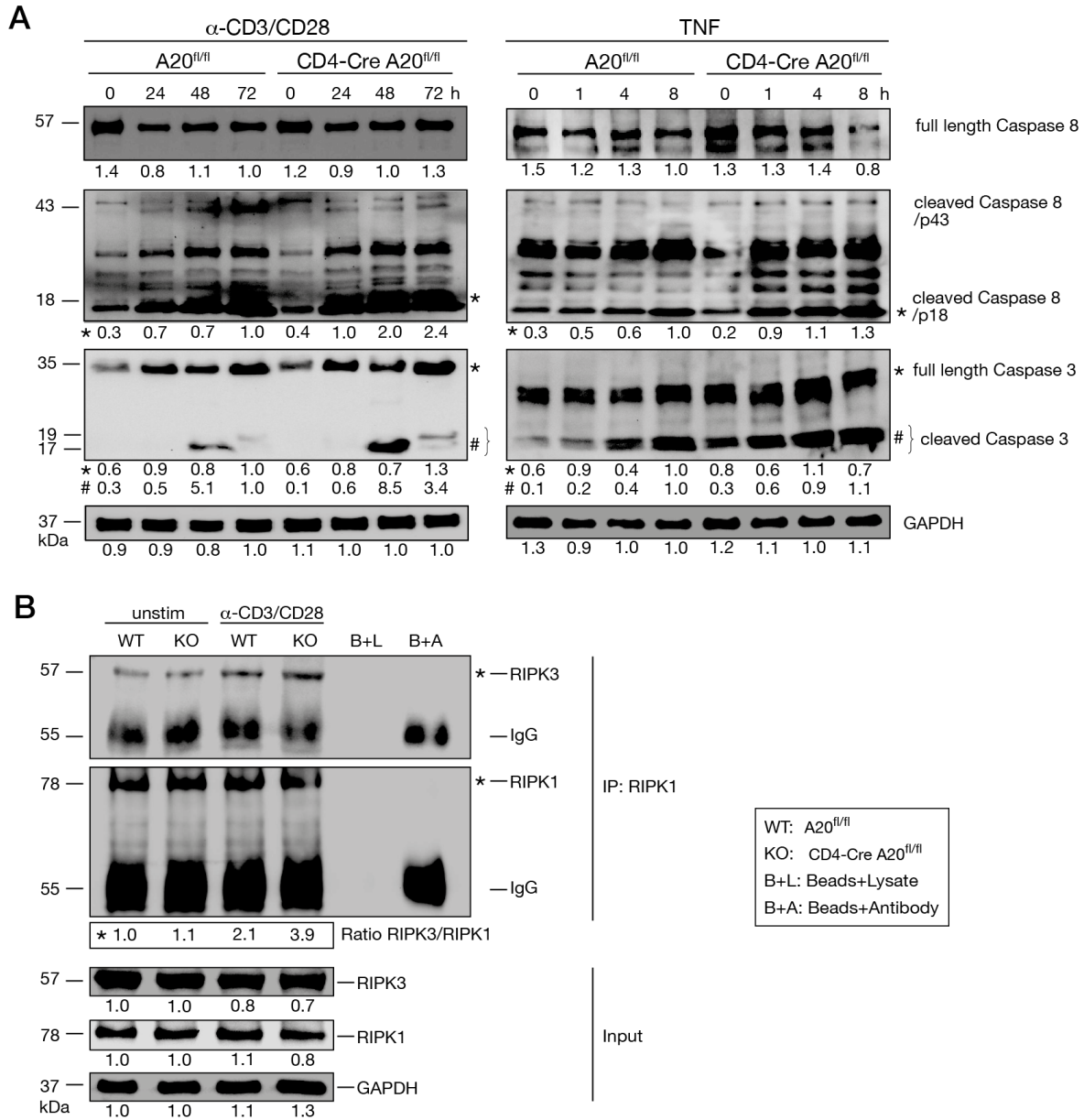
Figure 25: Increased caspase cleavage and necrosome formation in A20-deficient CD8⁺ T cells.

CD8⁺ T cells were purified and stimulated with anti-CD3/CD28. **A|** Proteins were isolated at the indicated timepoints after stimulation and western blot analysis was performed on total cell lysates for caspase-8, caspase-3 and the loading control GAPDH. **B|** CD8⁺ T cells were stimulated for 48 h with anti-CD3/CD28 or left untreated. Proteins were isolated and immunoprecipitated with anti-RIPK1. Immunoprecipitates were stained for RIPK1 and RIPK3. B+L: beads with lysate loading control; B+A: beads with antibody loading control. Representative results one of two independent experiments are shown.

Upon TCR stimulation, as well as TNF stimulation the expression of full length caspase-8 reduced, while caspase-8 cleavage products p43 and p18 increased in A20-sufficient and A20-deficient cells. However, caspase-8 cleavage occurred earlier and was increased in A20-deficient CD8+ T cells.

Effector caspases such as caspase-3 execute apoptosis by hydrolyzing peptide bonds of cellular proteins and, thus, are key molecules for identifying apoptotic cell death. After 48 h of TCR stimulation and upon TNF stimulation, cleavage of full length caspase-3 was observed, an important indicator of apoptosis. In A20-deficient CD8+ T cells cleavage of caspase-3 was strongly induced compared to A20-sufficient cells, indicating that A20 is involved in the regulation of apoptosis in CD8+ T cells.

We further analyzed the necroptotic pathway by studying necrosome formation before and after TCR stimulation (Figure 25B). RIPK1 was immunoprecipitated from total cell lysates and stained for RIPK1 and RIPK3. In unstimulated cells small amounts of RIPK3 were associated with RIPK1. Upon TCR stimulation, RIPK1/RIPK3 complex formation was observed in both groups, but was strongly increased in A20-deficient CD8+ T cells. Thus, A20 inhibits both, necrosome formation and apoptosis of activated CD8+ T cells.

Effector caspase activity is an important tool in determining cell death. Thus, capsase-3/7 activity was measured using a DEVD-substrate in anti-CD3/CD28-stimulated CD8+ T cells (Figure 26). The fluorochrome-labeled DEVD-peptide is cleaved by active effector caspase-3 and -7. Thus, fluorochrome is released, binds to the DNA and emits a fluorescent signal, which is detectable by flow cytometry. Thus, the MFI of the DEVD-substrate is equivalent to caspase-3/7 activity.
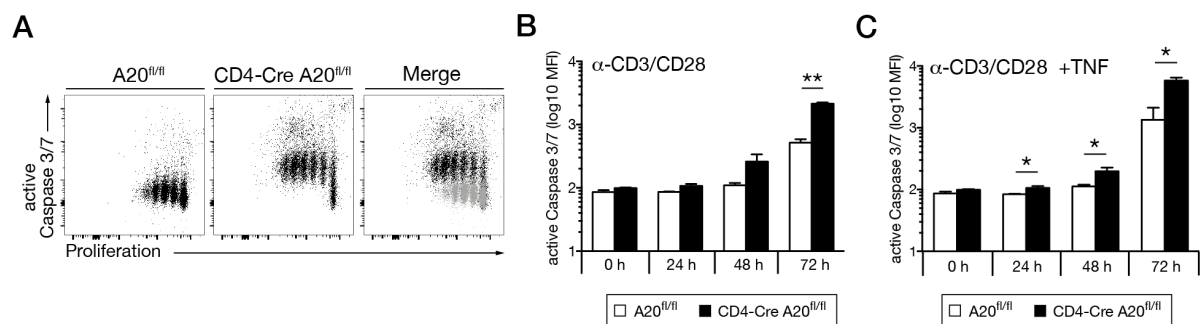
Figure 26: Increased caspase-3/7 activity in A20-deficient CD8+ T cells
CD8+ T cells were purified and stimulated with anti-CD3/CD28. **A|** Proliferation as indicated by the CFSE dilution and DEVD-substrate cleavage by active caspase-3/7 was determined for A20-sufficient CD8+ T cells (left), A20-deficient CD8+ T cells (center) and an overlay of both (right; grey A20-sufficient cells; black A20-deficient cells). **B-C|** DEVD-substrate was used to measure caspase-3/7 activity via flow cytometry. **B|** Stimulation with anti-CD3/CD28 only. **C|** Stimulation with anti-CD3/CD28 and TNF. A representative of two independent experiments is shown with three mice per group. Error bars indicate +SEM. Student's *t*-test, * p< 0.05; ** p< 0.01.

As comparable to Figure 15E, A20-deficient CD8^{+} T cells again proliferated stronger but concurrently upregulated caspase-3/7 activity (Figure 26A). In contrast, proliferating A20-competent cells maintained a low caspase-3/7 activity.

Upon anti-CD3/CD28-stimulation, caspase-3/7 activity increased in A20-sufficient and -deficient cells, but 72 h after stimulation A20-deficient CD8^{+} T cells had significantly augmented caspase-3/7 activity (Figure 26B). When TNF was added, significant differences were already detectable 24 h after stimulation. Thus, A20-deficient CD8^{+} T cell are more sensitive to cell death *in vitro*.

3.4.4 Increased sensitivity of A20-deficient CD8^{+} T cells to CD95-induced cell death

Caspase-3/7 activity was also determined *in vivo* by isolating splenocytes from infected mice starting at the peak of the T cell response at day 7 and until the end of the contraction phase at day 21 (Figure 27A). Already at day 7 p.i., an increased caspase-3/7 activity was detected in *L. monocytogenes* OVA-specific CD8^{+} T cells from CD4-Cre A20^{fl/fl} mice, indicating increased apoptosis. During the course of infection, caspase-3/7 activity was only slightly upregulated in A20-sufficient pathogen-specific CD8^{+} T cells with a peak activity at day 14 p.i. However, caspase-3/7 activity increased strongly from day 9 to day 11 in A20-deficient in *L. monocytogenes* OVA-specific CD8^{+} T cells and was maintained at high levels until day 21 p.i.

The contraction phase of pathogen-specific CD8^{+} T cells is mediated by activation-induced cell death (AICD) and activated cell autonomous death (ACAD) to maintain lymphocyte homeostasis. AICD is a CD95-dependent process, and therefore we analyzed CD95 expression on *L. monocytogenes* OVA-specific CD8^{+} T cells *in vivo* (Figure 27B).

Already at day 7 p.i., expression of CD95 was almost 3-fold increased on A20-deficient *L. monocytogenes* OVA-specific CD8^{+} T cells. During the contraction phase, CD95 expression increased in both groups but remained significantly higher in CD4-Cre A20^{fl/fl} mice at all time points.
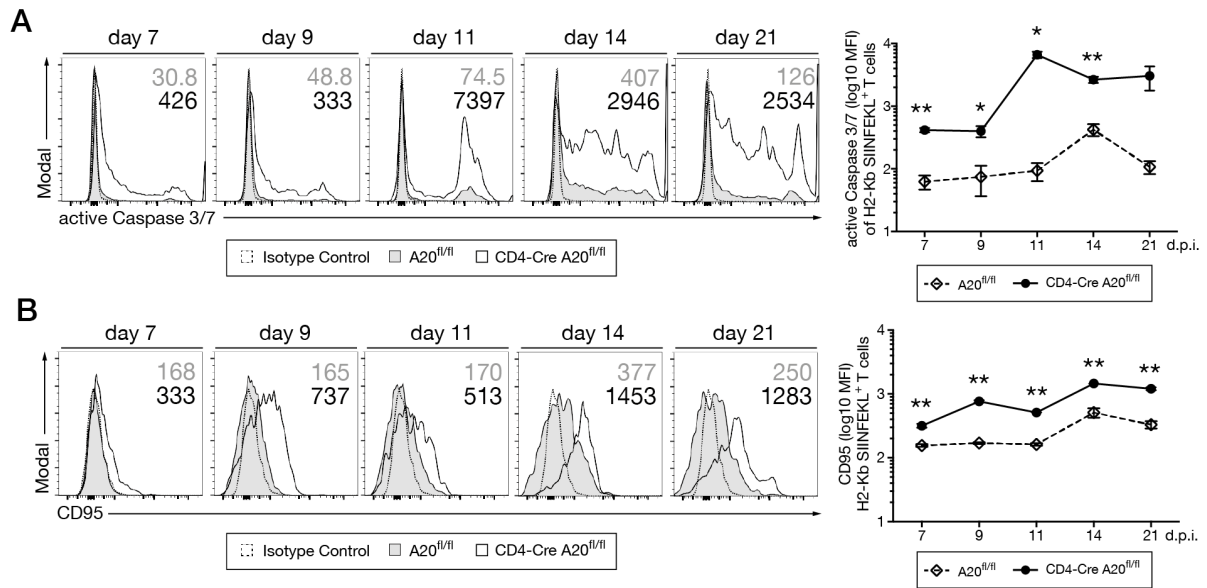
Figure 27: Increased caspase-3/7 activity and CD95 expression *in vivo*.
Splenocytes from infected animals were isolated at day 7, 9, 11, 14 and 21 p.i. Flow cytometric analysis was performed and cells were gated on H2-Kb SIINFEKL pentamer^{+} CD8^{+} T cells. **A|** DEVD-substrate was used to determine caspase-3/7 activity of *L. monocytogenes* OVA-specific CD8^{+} T cells. Grey numbers and histograms represent MFI of caspase-3/7 activity in A20 fl/fl mice, black numbers and histograms represent MFI of caspase-3/7 activity in CD4-Cre A20fl/fl mice. **B|** CD95 expression of *L. monocytogenes* OVA-specific CD8^{+} T cells was determined. Representative histograms and graphs of the MFI are displayed. Grey numbers determine MFI of CD95 expression in A20 fl/fl mice, black numbers represent MFI of CD95 expression in CD4-Cre A20fl/fl mice. A representative of two independent experiments is shown with 3-4 mice per group. Error bars indicate +SEM. Student's *t*-test, * $p < 0.05$; ** $p < 0.01$.

In addition, *in vitro* stimulation of CD8^{+} T cells with anti-CD3/CD28 induced a significant upregulation of CD95 in A20-deficient cells (Figure 28A). Furthermore, when CD95L was supplemented to the TCR stimulation, caspase-3/7 activity significantly increased already after 24 h in A20-deficient cells (Figure 28B).

To determine, if CD95 signaling induced stronger apoptosis in the absence of A20, CD8^{+} T cells from both genotypes were treated with Z-VAD-FMK, a pan-caspase inhibitor, prior to CD95L stimulation (Figure 28C). In the absence of the caspase inhibitor, CD95L treatment resulted in significantly stronger reduction of living A20-deficient cells compared to A20-sufficient cells. Addition of Z-VAD-FMK improved the viability of CD8^{+} T cells from both groups, however, the frequency of living A20-deficient cells was still significantly reduced, strongly indicating that other cell death pathways, e.g. necroptosis, are augmented in the absence of A20.

Expression of CD95 is induced upon NF-κB activation (Chan et al., 1999) and since CD95 was strongly upregulated in A20-deficient cells *in vitro* and *in vivo*, A20 may indirectly regulate CD95 expression by inhibition of NF-κB signaling. To test this hypothesis, CD95 mRNA levels in CD8^{+} T cells were determined upon *in vitro* TCR stimulation in the presence or absence of an IKK-inhibitor (Figure 28D). Anti-CD3/CD28 stimulation

induced a significantly stronger upregulation of CD95 mRNA in A20-deficient CD8^{+} T cells, compared to control cells. Importantly, inhibition of NF-κB activation by an IKK-inhibitor reduced levels of CD95 mRNA and abolished the difference between both groups, suggesting a critical role of A20 in the inhibition of CD95 expression.
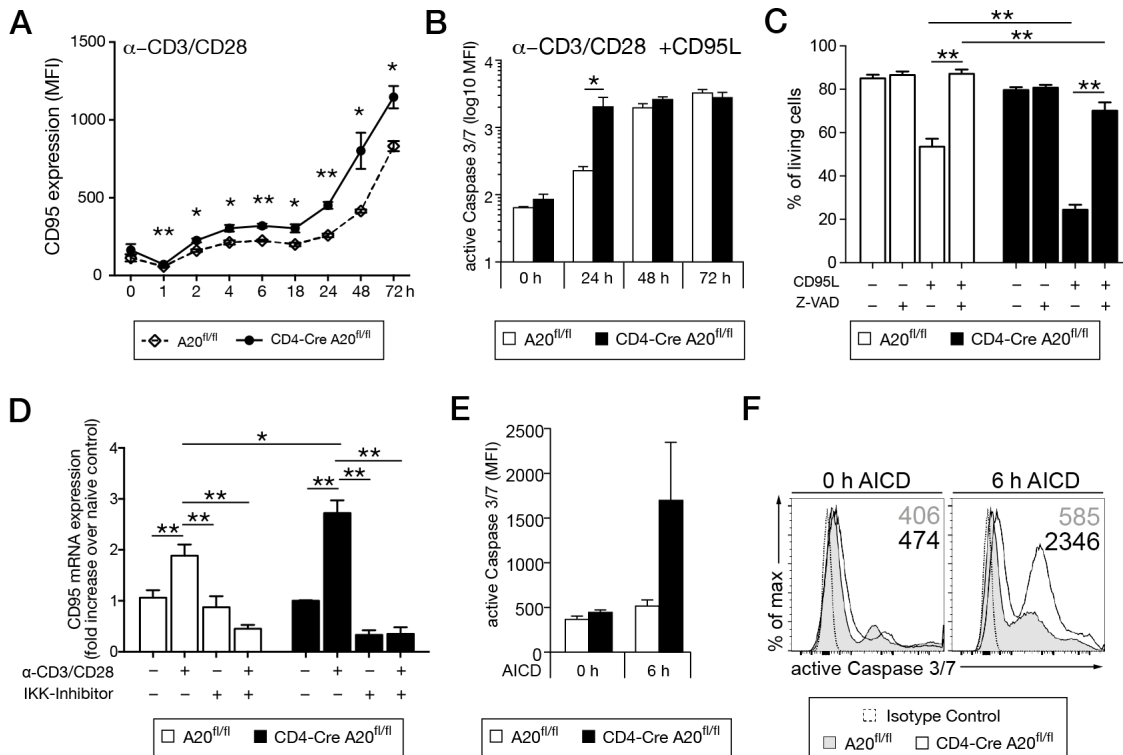
Figure 28: A20-deficient CD8^{+} T cells are sensitive to CD95 stimulation *in vitro*.
A20-sufficient and –deficient CD8^{+} T cells were purified. **A|** Cells were stimulated with anti-CD3/CD28 for up to 72 h and a kinetic of the CD95 expression was determined. **B|** Caspase-3/7 activity was measured upon stimulation with CD95L in addition to anti-CD3/CD28. **C|** Frequency of living cells was determined after CD8^{+} T cells were stimulated with recombinant CD95L for 2 h. Inhibition of apoptosis was performed by adding Z-VAD-FMK prior to the stimulation. (+) treatment, (-) no treatment. **D|** T cells were stimulated with anti-CD3/CD28 and treated with IKK-inhibitor or were left untreated. Afterwards, levels of CD95 mRNA were determined by RT-qPCR. (+) treatment, (-) untreated cells. **E|** Caspase-3/7 activity was determined before and after AICD by adding DEVD-substrate. Grey numbers and histograms: MFI of caspase-3/7 activity from A20-sufficient CD8^{+} T cells. Black numbers and histograms: MFI of caspase-3/7 activity from A20-sufficient CD8^{+} T cells. A representative of two independent experiments is shown with 3 mice per group. Error bars indicate +SEM. C-D Tukey's multiple comparison test; A-B and E Student's *t*-test, * p< 0.05; ** p< 0.01.

In vivo, AICD mediates cell death after the peak of the T cell response upon infection. This process can be initiated *in vitro* by restimulation of activated and expanded T cells. As shown in Figure 28E+F, restimulation of A20-deficient CD8^{+} T cells induced a much stronger caspase-3/7 activity compared to A20-sufficient cells. Taken together, these data define the inhibitory role of A20 in CD95-mediated cell death of CD8^{+} T cells

4. DISCUSSION

4.1 Characterization of CD4-Cre A20$^{fl/fl}$ mice

Since its discovery in 1990 (Opipari et al., 1990), A20 has been identified as a key regulator of inflammation and immune response in different cells and tissues with a broad range of cell type specific functions, defining its complex role in the immune system.

A20-deficient mice die shortly after birth due to severe inflammation and cachexia, pointing out that A20 is an important mediator of immune homeostasis. Tissue-specific deletion of A20 is commonly associated with autoimmunity, similar to polymorphisms in the human *Tnfaip3* gene. Dysregulation of A20 in humans is implicated in a wide range of autoimmune diseases such as SLE and rheumatoid arthritis due to the constitutive activation of the NF-κB pathway. In addition, reduced A20 expression has been associated with increased oncogenic potential. Downregulation of A20 in T cell-lymphoma and T cell non-Hodgkin-lymphoma patients have been reported (Wang et al., 2014). In patients with cutaneous T cell lymphoma, also called Sézary syndrome which is characterized by erythroderma, lymphadenopathy, hepatosplenomegaly and skin lesions, a deletion of the *Tnfaip3* gene was detected (Braun et al., 2011).

To study the function of A20 in T cells, we successfully generated conditional knock out mice with a specific deletion of A20 in CD4$^+$ and CD8$^+$ T cells. Naive CD4-Cre A20$^{fl/fl}$ mice were analyzed for the spontaneous development of inflammation and autoimmune disorders. In the thymus, we observed no defect in T cell development. T lymphocytes developed normally and were released into the periphery.

In CD4-Cre A20$^{fl/fl}$ mice we observed a mild leukocyte infiltration and inflammation in spleen, liver (data not shown) and lymph nodes similar to symptoms of Sézary syndrome. In addition, serum cytokines were slightly increased, confirming a mild inflammation in CD4-Cre A20$^{fl/fl}$ mice. However, ALT levels in serum, an indicator of liver damage, were not significantly increased, indicating that the integrity of the liver was not disturbed. No aggravation of organ inflammation and skin lesions were observed in aged mice.

A similar mild inflammatory condition was observed by Giordano et al. (2014), upon A20 deletion in mature T cells. Thereby we conclude that A20 in T cells does not induce severe autoimmunity. An increase of T$_{regs}$ in CD4-Cre A20$^{fl/fl}$ mice (data not shown), which play an important role in regulating immunological self-tolerance might explain the lack of severe autoimmunity.

Consistent with previous reports on the role of A20 in other cell types, *in vitro* TCR stimulation of A20-deficient T cells induced increased NF-κB- and MAPK-activation.

Activation of these signaling pathways led to increased activation, proliferation and cytokine production in CD8$^+$ T cells. Similar results were observed by Giordano et al. (2014), indicating that A20 regulates TCR signaling. Preliminary evidence suggests that A20 negatively regulates NF-κB signaling by catalyzing the cleavage of K63-polyubiquitin chains from MALT1 in Jurkat cells, a human T cell line (Düwel et al., 2009). However, it has been shown that the TCR signaling of Jurkat T cells is altered compared to other human T cell lines (Bartelt et al., 2009). Therefore, it remains to be investigated, if the mechanism of NF-κB regulation in murine T cells is similar to the immortalized acute T cell leukemia-derived cell line.

Since enhanced activation of NF-κB in A20-deficient T cells resulted in increased T cell activation, we hypothesized, that CD4-Cre A20$^{fl/fl}$ mice mount a stronger T cell response leading to faster clearance of pathogens upon infection. To test this hypothesis, we infected CD4-Cre A20$^{fl/fl}$ mice and A20$^{fl/fl}$ control mice with *L. monocytogenes*, which induces a strong CD8$^+$ T cell response.

4.2 A20 regulates magnitude of T cell responses to infection with *L. monocytogenes*

The control of intracellular infections requires a strong protective CD8$^+$ T cell response which is typically classified into three phases: i) the expansion phase, which is initiated upon antigen encounter, leading to the final elimination of the pathogen, ii) the contraction phase, when the majority of pathogen-specific T cells undergo cell death, leaving behind a small pool of memory T cells, which then in the last phase, iii) the memory phase, rapidly expands upon a reinfection. In this study we intensively investigated the role of A20 during these phases of the T cell response.

After the first antigen encounter in peripheral lymphoid organs, T cells are activated, undergo clonal expansion and relocate to the site of infection, where they produce effector molecules for the activation and recruitment of more leukocytes (e.g. IFN-γ and TNF) and the killing of infected cells (granzyme B and perforin). These characteristics are essential for the effective elimination of the pathogen. NF-κB initiates these processes, as the upregulation of NF-κB induces activation, proliferation and cytokine production of immune cells. We observed that A20, a suppressor of NF-κB activation is upregulated upon TCR stimulation and, thus, seems to be important in impeding T cell responses.

A20 is extensively studied in the context of autoimmune diseases, however, less is known about the function of A20 during infection. Maelfait et al. (2012) reported that myeloid

cell-specific deletion of A20 in mice protected against Influenza A virus infection. Increased NF-κB activation induced enhanced cytokine and chemokine production, which in turn recruited more macrophages and neutrophils to the site of infection, leading to reduced viral load and body weight loss.

We focused on determining the outcome of bacterial infection in mice lacking A20 in T cells. During acute primary infection with the intracellular bacterium *L. monocytogenes*, pathogen-specific CD8$^+$ T cell response was augmented in CD4-Cre A20$^{fl/fl}$ mice, characterized by an increased expansion as well as IFN-γ- and granzyme B production, resulting in improved pathogen control. IFN-γ and granzyme B are regulated by NF-κB (Huang et al., 2006; Sica et al., 1997), thus, the increased pathogen-specific CD8$^+$ T cell response might be very well explained by the upregulation of NF-κB in the absence of A20. However, after pathogen clearance, we detected a rapid reduction of *L. monocytogenes*-specific CD8$^+$ T cells in CD4-Cre A20$^{fl/fl}$ mice with a decrease in IFN-γ and granzyme B production, indicating a loss of function. When we rechallenged these mice, we observed a phenotype contrary to the primary infection. A20-deficient CD8$^+$ T cells failed to expand and produced less effector molecules compared to A20-sufficient CD8$^+$ T cells.

Upon T cell activation, the co-inhibitory receptor PD-1 is shortly upregulated and after the clearance of infection, PD-1 expression subsides, as we observed in A20$^{fl/fl}$ control mice. However, in CD4-Cre A20$^{fl/fl}$ mice, even after clearance of a bacterial infection, pathogen-specific CD8$^+$ T cells expressed high levels of PD-1. The expression of PD-1 is associated with increased T cell activation and correlates with dysfunction and exhaustion during chronic viral infection (Keir et al., 2008). T cell exhaustion is induced upon persistent NF-κB activation. In T cells, PD-1 activation inhibits TCR signaling through dephosphorylation of PI3K and ZAP-70, and thereby, impeding T cell activation (Chemnitz et al., 2004; Sheppard et al., 2004). In the absence of A20, a strong and prolonged activation was observed in T cells which might induce PD-1 expression. The defective granzyme B and IFN-γ production as well as the failure in re-expansion might be explained by the overexpression of PD-1 on pathogen-specific CD8$^+$ T cells in CD4-Cre A20$^{fl/fl}$ mice. Noteworthy, Utzschneider et al. recently reported a new subset of memory CD8$^+$ T cells that express PD-1 but had sustained T$_{CM}$ function in a chronic viral infection model (Utzschneider et al., 2016). However, the role of PD-1 on memory T cells remains unclear. Further studies are necessary, to identify the function of PD-1 in our acute infection model, and to determine if A20 can directly regulate PD-1 expression, e.g. by interaction with Blimp-1 (B lymphocyte induced maturation protein 1), which can repress PD-1.

In the course of T cell exhaustion, a stepwise loss of function is ultimately leading to death of the exhausted cell through the upregulation of pro-apoptotic factors and non-

responsiveness to IL-7 and IL-15, the major cytokines regulating T cell homeostasis (Yi et al., 2010). Since the memory response was defective, we further aimed to understand if memory T cell conversion was impaired in A20-deficient CD8$^+$ T cells. We performed a detailed analysis of the fate of *L. monocytogenes*-specific CD8$^+$ T cells and we observed, that A20-deficient pathogen-specific CD8$^+$ T cells rapidly undergo cell death, while survival of A20-sufficient cells was improved. Therefore, we investigated whether A20 regulates memory T cell conversion.

The important factors for the cell-fate decision have not been completely identified. Expression of IL-7Rα (CD127) has been defined as a marker for long-living memory precursor cells. IL-7Rα^{high} cells are more likely to survive beyond the contraction phase, while IL-7Rα^{low} terminally differentiated effector cells, are prone to cell death (Kaech et al., 2003). In addition, KLRG-1 was used as a marker for terminally differentiated effector cells, and in combination with CD127, a detailed kinetic of SLEC and MPEC cells was performed to determine a possible role of A20 in memory T cell formation.

At the peak of infection, equal relative numbers were observed in both groups. However, while at day 21 p.i. the MPEC phenotype was dominant among A20-sufficient *L. monocytogenes*-specific CD8$^+$ T cells, in CD4-Cre A20$^{fl/fl}$ mice the pathogen-specific pool of CD8$^+$ T cells consisted of almost equal relative numbers of MPEC and SLEC. Absolute numbers of SLEC reduced in both groups, but slightly more in CD4-Cre A20$^{fl/fl}$ mice. The pathogen-specific MPEC population in A20$^{fl/fl}$ mice remained stable over time, which is consistent with current research, proposing that the fate of SLEC and MPEC is predefined. The loss of SLEC is not due to a transition into MPEC, but moreover due to their sensitivity to cell death induction, while MPECs seem to be resistant to cell death (Joshi et al., 2007). In CD4-Cre A20$^{fl/fl}$ mice, however, MPECs reduced significantly over time, explaining the major differences in the relative numbers as well.

The maintenance of MPECs is crucial for T$_{mem}$ generation, as they further transform into T$_{CM}$ and T$_{EM}$, which mount an immediate immunity to recurrent infections (Huster et al., 2004). While relative numbers of T$_{CM}$ were increased within the *L. monocytogenes*-specific CD8$^+$ T cell compartment of CD4-Cre A20$^{fl/fl}$ mice, absolute numbers of all subsets remained significantly reduced compared to control mice. Upon reinfection, absolute numbers of T$_{eff}$, T$_{CM}$ and T$_{EM}$ cells increased rapidly in A20$^{fl/fl}$ mice but only slightly increased in CD4-Cre A20$^{fl/fl}$ mice. These data indicate a major defect in the memory CD8$^+$ T cell compartment of CD4-Cre A20$^{fl/fl}$ mice. T$_{CM}$ harbor only reduced effector function, nevertheless, this does not account for the drastically impaired T$_{mem}$ response. Several other aspects could contribute to this phenotype. Currently, we can not rule out that A20 might directly regulate MPEC conversion to become T$_{CM}$, and that absence of A20 directly

inhibits T$_{mem}$ response, however, several more intrinsic and extrinsic factors regulate T$_{mem}$ formation, maintenance and function.

Not only the type but also the duration of an infection determines the longevity of CD8$^+$ T cells. It has been shown that reducing the duration of infection with antibiotic treatment, decreases secondary responses (Wirth et al., 2011).

Furthermore, it has been shown that PD-1 shapes memory T cell responses by impeding the accumulation of T$_{EM}$ (Charlton et al., 2013). In addition, blockage of PD-1 can rescue insufficient memory CD8$^+$ T cell responses (Fuse et al., 2009). Further studies are necessary to determine, if increased PD-1 expression in CD4-Cre A20$^{fl/fl}$ mice leads to the shift from T$_{EM}$ to T$_{CM}$ in the pathogen-specific CD8$^+$ T cell compartment and if PD-1 blockage could reverse the defective CD8$^+$ T$_{mem}$ response.

Previous reports suggest a significant impact of CD4$^+$ T helper cells for the generation of a robust CD8$^+$ T$_{mem}$ response upon *L. monocytogenes* infection (Shedlock and Shen, 2003; Sun and Bevan, 2003). In addition, the cytokine milieu contributes in shaping T$_{mem}$ formation. Especially signals from IL-2 and IL-12 support the differentiation into T$_{mem}$. Interestingly, only CD8$^+$ T cells receiving IL-2 signals during primary infection were able to mount a robust secondary response (Bachmann et al., 2007; Williams et al., 2006). When we analyzed the cytokine production of CD4$^+$ T cell in CD4-Cre A20$^{fl/fl}$ mice during primary and secondary response, we observed no differences to the A20$^{fl/fl}$ control group and, therefore, could rule out that defective CD4$^+$ T helper cells are the cause for the impaired T$_{mem}$ response in CD4-Cre A20$^{fl/fl}$ mice.

The signal strength the T cell receives from antigen, co-stimulatory molecules and cytokines contribute to the formation and maintenance of memory T cells (Daniels and Teixeiro, 2015). A gradient model was proposed, where a strong signal induces T$_{eff}$ formation but finally leads to cell death, but intermediate and low signal strength promote T$_{EM}$ and T$_{CM}$ generation, respectively (Kaech and Cui, 2012).

Interestingly, TRAF6 can regulate T$_{mem}$ formation, by modulating fatty acid metabolism (Pearce et al., 2009). It has been shown that A20 deubiquitinates TRAF6 in different human cell types, thereby inhibiting NF-κB signaling (Boone et al., 2004; Garg et al., 2013; Kelly et al., 2013). Further studies are necessary, to determine if A20 is involved in TRAF6-mediated T$_{mem}$ generation in murine T cells.

Furthermore, a tight regulation of NF-κB plays a fundamental role in the generation and maintenance of memory CD8$^+$ T cells. Mice expressing a dominant-negative form of IκBα, and thereby have reduced NF-κB activation, develop less memory-like CD8$^+$ T cells (Hettmann et al., 2003). Similarly, patients with autosomal-dominant anhidrotic ectodermal dysplasia with immunodeficiency (AD-EDA-ID), harboring a polymorphism in

the IκBα-encoding gene, which enhances the inhibitory function of IκBα, fail to develop memory T cells (Courtois et al., 2003). On the other hand, persistent NF-κB activation resulted in increased cell death of pathogen-specific CD8+ T cells, as demonstrated by Krishna et al. by generating mice with constitutive IKKβ activation (Krishna et al., 2012). In our model, we observed a similar loss of pathogen-specific CD8+ T cells, however, only after the peak of infection, leading to an improved primary response. A tight regulation of NF-κB activation is detrimental for the development and maintenance of T_{mem}.

The type, severity and duration of an infection can influence the T cell response. Further investigations are necessary to determine the T cell-specific role of A20 in other infection models. *L. monocytogenes* is a strong mediator of CD8+ T cell responses, which could explain that we did not observe an effect of A20 on the CD4+ T cell compartment. In infections, however, the role of A20 in CD4+ T cells is still not determined, thus, a CD4+ T cell- mediated infection model such as leishmaniasis could help to address this in more detail. In the model of EAE, a CD4+ T cell-driven autoimmune disease, it has recently been shown that A20-deficient CD4+ T cells undergo necroptosis and, thus, develop less severe EAE (Onizawa et al., 2015).

Hyperinflammatory conditions such as the model of allergic asthma, induced by hyperactive T_h2 cells could be further investigated. In these models, A20 might be a potential therapeutic target to reduce symptoms of inflammation. Additionally, chronic infections like toxoplasmosis or lymphocytic choriomeningitis virus might be of interest to further address the possibility of exhaustion in A20-deficient T cells.

To summarize, A20-deficient CD8+ T cells show no typical features of memory T cells; i) they have a low proliferative capacity compared to A20-sufficient memory CD8+ T cells, ii) effector functions can not be rapidly reactivated and iii) A20-deficient CD8+ T cells fail to survive long-term. In the current study we extensively focused on the role of A20 in all three phases of CD8+ T cell responses: expansion, contraction and memory phase. In addition to the defective memory response of CD8+ T cells, we continued to study the role of A20 in the contraction phase, as this also contributes to the impaired recall-response by reduced survival of MPECs.

4.3 A20 regulates CD8+ T cell contraction phase

Activation of NF-κB is required for an efficient primary CD8+ T cell response as well as for the development of memory T cells (Gerondakis and Siebenlist, 2010; Hettmann et al., 2003; Zehn et al., 2012). However, excessive or prolonged activation of the NF-κB signaling

pathway can induce autoimmune reactions or programmed cell death (Chandok and Farber, 2004).

During the contraction phase, the majority of pathogen-specific T cells undergo cell death, an important feature of the immune system to prevent the accumulation of remaining pathogen-specific cells. Few cells survive and form a heterogeneous pool of memory T cells. Initially, AICD, an extrinsic CD95-dependent process, has been identified as a mediator of T cell contraction (Alderson et al., 1995; Brunner et al., 1995; Dhein et al., 1995; Russell et al., 1993). However, studies involving LCMV infection reported a CD95-independent T cell contraction using CD95-deficient mice (Lohman et al., 1996; Zimmermann et al., 1996). Several independent studies published contradictory results using superantigen staphylococcal enteroxin B, where T cell contraction was reported either CD95-dependent (Bonfoco et al., 1998; Mogil et al., 1995; Renno et al., 1995) or -independent (Hildeman et al., 2002). Recent studies show an involvement of the intrinsic cell death pathway in the regulation of T cell contraction, mainly by the regulation of the Bcl-2 family members (Hildeman et al., 2002; Pellegrini et al., 2003; Wojciechowski et al., 2006). Intrinsic and extrinsic cell death pathways seem to counterregulate the T cell contraction phase (Bouillet and O'Reilly, 2009). Inhibition of both pathways leads to massive leukocyte accumulation in Bim (a pro-apoptotic member of the Bcl-2 family)- and CD95-double-deficient mice (Hughes et al., 2008; Hutcheson et al., 2008). In humans, the autoimmune lymphoproliferative syndrome (ALPS), leading to lymphadenopathy, splenomegaly and autoimmune disease, is caused by a mutation in CD95 (Martin et al., 1999; Müllauer et al., 2008), making clear that CD95 is an important regulator in the deletion of peripheral T cells. In *L. monocytogenes* infected mice, the contraction phase after bacterial clearance is mediated by CD95 (Fuse et al., 1997), indicating that different cell death mechanisms play a role, depending on the underlying infection.

Upon CD95 stimulation, apoptosis is initiated by the activation of terminal effector caspases including caspase-3 and -7. Under certain conditions, such as inhibition of caspase-8, CD95 stimulation can also initiate necroptosis, a RIPK3-dependent cell death (Silke et al., 2015). Quantification of apoptosis and necroptosis during the contraction phase of pathogen-specific CD8^{+} T cells *in vivo* is challenging and has not been reported so far, due to complications in differentiating apoptosis from necroptosis, as specific surface markers are not described so far. In the present study we used IFC which combines quantitative single cell microscopy with flow cytometry. This enabled us to quantify apoptotic and necroptotic *L. monocytogenes*-specific CD8^{+} T cells *ex vivo* based on morphological differences.

Morphologically, apoptotic cells are defined by phosphatidylserine exposure on the cell surface followed by membrane blebbing, chromatin condensation, a decrease in cell size and formation of apoptotic bodies (Henry et al., 2013). In contrast, necroptotic cells include rapid cytoplasmic and nuclear swelling as well as organelle breakdown, finally leading to the rupture of the plasma membrane (Pietkiewicz et al., 2015).

Independent of A20, necroptosis and apoptosis contributed to the contraction of *L. monocytogenes*-specific CD8^{+} T cells at day 7 and 11 p.i. However, in the absence of A20 both apoptosis and necroptosis were augmented (day 11 p.i.) and A20 preferentially suppressed necroptosis (day 7 and 11 p.i.). These data suggest that i) both necroptosis and apoptosis participate in the contraction phase and ii) A20 is a suppressor of necroptosis as well as apoptosis in CD8^{+} T cells. A previous study from Onizawa et al. (2015) described a protective role of A20 in CD4^{+} T cells against necroptosis. In sharp contrast to our results, apoptosis was completely abolished in A20-deficient CD4^{+} T cells. These conflicting results might be explained by intrinsic differences between CD4^{+} and CD8^{+} T cells as well as the choice of the disease model.

On a molecular level activation of effector caspase-3 is a hallmark for the induction of apoptosis, whereas necrosome formation is characterized by RIPK1/RIPK3 complex formation. Western blot analysis confirmed increased caspase-3 and -8 cleavage, but also RIPK1/RIPK3 complex formation in *in vitro* stimulated CD8^{+} T cells, confirming that both signaling pathways play a role in CD8^{+} T cells. However, cleavage of caspase-3 does not necessarily indicate its activity. Previous reports demonstrate that caspase-3 activity can be restrained by certain molecules such as cIAP2, XIAP or Bcl-XL (Clem et al., 1998; Kavanagh et al., 2014; Paulsen et al., 2008). Therefore, we measured caspase-3/7 activity *in vitro* and *ex vivo* with a DEVD-substrate-based assay. We first performed an *in vitro* kinetic, where we observed a correlation between proliferation and caspase-3/7 activity in A20-deficient CD8^{+} T cells resulting in increased cell death, while in A20-sufficient CD8^{+} T cells caspase-3/7 activity was only slightly elevated. Similar results were obtained from *ex vivo* staining of *L. monocytogenes*-specific CD8^{+} T cells. In conclusion, these data confirm that not only cleavage of effector caspase-3 is enhanced in A20-deficient CD8^{+} T cells, but also its activity, providing further evidence that A20 regulates apoptosis in CD8^{+} T cells. In addition, it has been shown that certain thresholds of effector caspase-3 and -7 activity can correlate with NF-κB and AKT activation, by cleaving Poly (ADP-ribose)-polymerase 1 and the RasGTPase activating protein (Hassa et al., 2001; Yang and Widmann, 2001). Furthermore, caspase-8 not only mediates cell death but, in addition, caspase-8 deficient T cells show defects in activation and proliferation (Kennedy et al., 1999; Salmena et al., 2003). It has been shown that caspase-8 is important for IKK-activation, and subsequently

NF-κB activation (Su et al., 2005). Thus, morphological analysis is an important tool to precisely determine cell death events on a single cell level. And indeed, IFC analysis after *in vitro* anti-CD3/CD28-stimulation revealed reduced survival and increased apoptosis and necroptosis of A20-deficient CD8^{+} T cells, confirming the role of A20 in the regulation of cell death.

Since it has been reported that the termination of the CD8^{+} T cells response after *L. monocytogenes* infection is mediated via CD95 signaling (Fuse et al., 1997), we determined CD95 expression *ex vivo*. A20-deficient *L. monocytogenes*-specific CD8^{+} T cells significantly upregulated the cell death receptor CD95, correlating with increased caspase-3/7 activity. Corresponding to our *ex vivo* findings, A20-deficient CD8^{+} T cells strongly upregulated CD95 expression upon TCR stimulation *in vitro,* indicating that upregulation of CD95 could be initiated upon NF-κB activation. Blocking of NF-κB activation *in vitro* using an IKK-inhibitor, resulted in downregulation of CD95 in A20-sufficient and -deficient CD8^{+} T cells. Furthermore, the difference between both groups was completely abolished, providing a strong evidence that A20, by inhibiting NF-κB activation, indirectly suppresses CD95 expression. In addition, A20 could also be directly involved in the death receptor pathways. RIPK1, a known target of A20, is a key regulator in both, CD95- and TNF-R signaling pathways (Festjens et al., 2007; Ma and Malynn, 2012). Further studies could provide insight into the regulation of death receptor pathways by A20 in T cells.

CD95 expression does not only induce cell death but the threshold of CD95 signaling determines whether cell death or T cell activation is induced (Paulsen and Janssen, 2011). CD95L stimulation resulted in increased caspase-dependent apoptosis of A20-deficient CD8^{+} T cells *in vitro*. However, we can not rule out that CD95 signaling may initially also contribute to the augmented activation of A20-deficient CD8^{+} T cells.

The regulation of expansion versus AICD of pathogen-specific T cells is necessary to regain immune homeostasis after bacterial clearance. AICD-experiments showed an increased activity of caspase-3/7 in A20-deficient CD8^{+} T cells, which is induced by interaction of CD95 with CD95L after repeated stimulation of cells (Krueger et al., 2003).

CD95 expression was increased not only on *in vitro* stimulated CD8^{+} T cells but also *in vivo* on pathogen-specific CD8^{+} T cells. It has been shown, that CD95 is upregulated upon NF-κB activation (Chan et al., 1999), thus, we hypothesized that NF-κB activation is restricted by A20 and thereby reduces apoptosis by limiting CD95 expression. To support this, we used an IKK-inhibitor, which impedes IκB degradation and translocation of NF-κB to the nucleus, thus, preventing NF-κB-mediated gene expression. The IKK-inhibitor abolished the difference in CD95 expression between both A20-sufficient

and -deficient CD8^{+} T cells, confirming an indirect effect of A20 on the regulation of CD95 expression.

Dudani et al. reported that CD95/CD95L did not influence the expansion or contraction of pathogen-specific CD8^{+} T cells, but is important for memory CD8^{+} T cell response (Dudani et al., 2008). To prove the involvement of CD95 during the contraction phase in our model, mice with A20- and CD95 double-deficient T cells should be generated. At present, we can not assume that only CD95 regulates T cell contraction, but also other factors might play a role, such as TNF-R signaling, the intrinsic cell death pathway or cytokine signaling. Previous reports could show an involvement of the TNF/TNF-R complex as well as CD40L, another member of the TNF-R family, in regulating the contraction phase and memory T cell formation (Borrow et al., 1996; Suresh et al., 2005; Whitmire and Ahmed, 2000; Zhou et al., 2002). Moreover, *in vitro* stimulation of CD8^{+} T cells with TNF induced cleavage of caspase-8 and caspase-3 in both groups, but A20-deficient CD8^{+} T cells exhibited increased sensitivity towards TNF stimulation. However, *in vitro* experiments can not fully reflect the complex inflammatory environment *in vivo*, thus, indicating that death of A20-deficient pathogen-specific CD8^{+} T cells is mediated by several mechanism, including TNF and CD95.

Taken together, our study uncovers that A20 restricts expansion of pathogen-specific CD8^{+} T cell during primary response, regulates the contraction phase and is important for memory T cell formation, survival and re-expansion.

In conclusion, A20 has a essential function in the regulation of pathogen-specific CD8^{+} T cells, which cannot be compensated by other DUBs. This places A20 in an important position, indicating that therapeutic manipulation of A20 may be an attractive strategy to either augment or suppress CD8^{+} T cell responses in human diseases.

4.4 Conclusions

The present study uncovers the opposing role of A20 for the CD8$^+$ T cell response *in vivo*. In primary listeriosis, A20 restricts CD8$^+$ T cell expansion resulting in an improved pathogen control. However, A20 positively regulated memory CD8$^+$ T cell formation and survival, resulting in an improved pathogen control upon secondary infection.

In addition, we used for the very first time IFC to determine the type of pathogen-specific CD8$^+$ T cell death and demonstrated that both, apoptosis and necroptosis contribute to the contraction of pathogen-specific CD8$^+$ T cells in primary infection. Furthermore, we could show that A20 inhibits both pathways in CD8$^+$ T cells.

Not only the reduced number of pathogen-specific CD8$^+$ T cells, but also a defective expansion and impaired production of effector molecules lead to increased bacterial burden in reinfected CD4-Cre A20$^{fl/fl}$ mice, indicating that A20 promotes re-expansion and function of memory CD8$^+$ T cells.
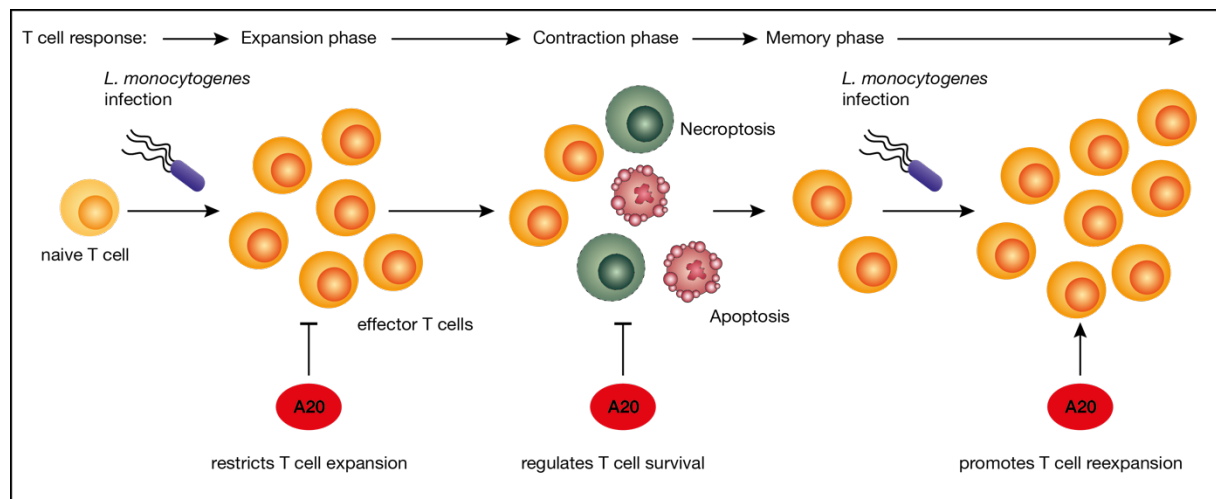
Figure 29: Graphical summary of this study.
Upon systemic *L. monocytogenes* infection, CD4-Cre A20$^{fl/fl}$ mice had reduced bacterial loads at the peak of infection and were able to clear the pathogen faster. During the contraction phase, however, increased cell death of A20-deficient pathogen-specific CD8$^+$ T cells occurred, resulting in an impaired memory T cell response after reinfection.

Understanding the maintenance and regulation of immunological memory is important for improving vaccination strategies and immunotherapies. Identification of molecules and pathways, regulating T cell responses can be used in a therapeutic manner to help in designing new vaccines to boost T cell immunity and treat autoimmune disorders.

The present study complements our knowledge of how the immune system is regulated by deubiquitinating enzymes and demonstrates their important role in immune regulation and provides the basis to further explore the therapeutic potential of A20-modulating drugs.

REFERENCE LIST

Adhikari, A., Chen, Z.J., 2009. Previews Diversity of Polyubiquitin Chains. *Dev. Cell* 16, 485–486.

Alderson, M.R., Tough, T.W., Davis-Smith, T., Braddy, S., Falk, B., Schooley, K.A., Goodwin, R.G., Smith, C.A., Ramsdell, F., Lynch, D.H., 1995. Fas Ligand Mediates Activation-induced Cell Death in Human T Lymphocytes. *J. Exp. Med.* 181, 71–77.

Arvelo, M.B., Cooper, J.T., Longo, C., Daniel, S., Grey, S.T., Mahiou, J., Czismadia, E., Abu-Jawdeh, G., Ferran, C., 2002. A20 protects mice from D-galactosamine/lipopolysaccharide acute toxic lethal hepatitis. *Hepatology* 35, 535–543.

Bachmann, M.F., Wolint, P., Walton, S., Schwarz, K., Oxenius, A., 2007. Differential role of IL-2R signaling for CD8+ T cell responses in acute and chronic viral infections. *Eur. J. Immunol.* 37, 1502–1512.

Barmada, M.M., Brant, S.R., Nicolae, D.L., Achkar, J., Duerr, R.H., 2004. A Genome Scan in 260 Inflammatory Bowel Disease-Affected Relative Pairs. *Inflamm Bowel Dis* 10, 15–22.

Bartelt, R.R., Cruz-Orcutt, N., Collins, M., Houtman, J.C.D., 2009. Comparison of T cell receptor-induced proximal signaling and downstream functions in immortalized and primary T cells. *PLoS One* 4.

Bedoya, S.K., Lam, B., Lau, K., Larkin, J., Bedoya, S.K., Lam, B., Lau, K., Larkin, J., 2013. Th17 Cells in Immunity and Autoimmunity. *Clin. Dev. Immunol.* 2013, 1–16.

Berzins, S.P., Smyth, M.J., Baxter, A.G., 2011. Presumed guilty: natural killer T cell defects and human disease. *Nat. Rev. Immunol.* 11, 131–42.

Bhoj, V.G., Chen, Z.J., 2009. Ubiquitylation in innate and adaptive immunity. *Nat. Rev. Insight* 458.

Blake, S.J.P., Ching, A.L.H., Kenna, T.J., Galea, R., Large, J., Yagita, H., Steptoe, R.J., 2015. Blockade of PD-1/PD-L1 promotes adoptive T-Cell immunotherapy in a tolerogenic environment. *PLoS One* 10, 1–21.

Blanco, P., Pitard, V., Viallard, J.F., Taupin, J.L., Pellegrin, J.L., Moreau, J.F., 2005. Increase in activated CD8+ T lymphocytes expressing perforin and granzyme B correlates with disease activity in patients with systemic lupus erythematosus. *Arthritis Rheum.* 52, 201–211.

Bonfoco, E., Stuart, P.M., Brunner, T., Lin, T., Griffith, T.S., Gao, Y., Nakajima, H., Henkart, P.A., Ferguson, T.A., Green, D.R., 1998. Inducible Nonlymphoid Expression of Fas Ligand Is Responsible for Superantigen-Induced Peripheral Deletion of T Cells. *Immunity* 9, 711–720.

Boone, D.L., Turer, E.E., Lee, E.G., Ahmad, R.C., Wheeler, M.T., Tsui, C., Hurley, P., Chien, M., Chai, S., Hitotsumatsu, O., McNally, E., Pickart, C., Ma, A., 2004. The ubiquitin-modifying enzyme A20 is required for termination of Toll-like receptor responses. *Nat. Immunol.* 5, 1052–1060.

Borrow, P., Tishon, A., Lee, S., Xu, J., Grewal, I.S., Oldstone, M.B.A., Flaveur, R.A., 1996. CD40L-deficient Mice Show Deficits in Antiviral Immunity and Have an Impaired Memory CD8+ CTL Response. *J.Exp.Med* 183, 2129–2142.

Bouillet, P., O'Reilly, L. a, 2009. CD95, BIM and T cell homeostasis. *Nat. Rev. Immunol.* 9, 514–519.

Braun, F.C.M., Grabarczyk, P., Möbs, M., Braun, F.K., Eberle, J., Beyer, M., Sterry, W., Busse, F., Schröder, J., Delin, M., Przybylski, G.K., Schmidt, C. a, 2011. Tumor suppressor TNFAIP3 (A20) is frequently deleted in Sézary syndrome. *Leukemia* 25, 1494–501.

Brunner, T., Mogil, R.J., Drake, L., Jin Yoo, N., Mahboubi, A., Echeverri, F., Martin, S.J., Force, W.R., Lynch, D.H., Ware, C.F., Green, D.R., 1995. T Cell-autonomous Fas/FasL interaction mediates activation-induced apoptosis. *Nature* 373, 441–444.

Chackerian, A., Alt, J., Perera, V., Samuel, M., Behar, S.M., 2002. Activation of NKT Cells Protects Mice from Tuberculosis Activation of NKT Cells Protects Mice from Tuberculosis. *Infect. Immun.* 70, 6302–6309.

Chan, H., Bartos, D.P., Owen-Schaub, L.B., 1999. Activation-dependent transcriptional regulation of the human Fas promoter requires NF-κB p50-p65 recruitment. *Mol Cell Biol* 19, 2098–2108.

Chandok, M.R., Farber, D.L., 2004. Signaling control of memory T cell generation and function. *Semin. Immunol.* 16, 285–293.

Charlton, J.J., Chatzidakis, I., Tsoukatou, D., Boumpas, D.T., Garinis, G. a, Mamalaki, C., 2013. Programmed death-1 shapes memory phenotype CD8 T cell subsets in a cell-intrinsic manner. *J. Immunol.* 190, 6104–14.

Chemnitz, J.M., Parry, R. V., Nichols, K.E., June, C.H., Riley, J.L., 2004. SHP-1 and SHP-2 Associate with Immunoreceptor Tyrosine-Based Switch Motif of Programmed Death 1 upon Primary Human T Cell Stimulation, but Only Receptor Ligation Prevents T Cell Activation. *J. Immunol.* 173, 945–954.

Choudhuri, K., van der Merwe, P.A., 2007. Molecular mechanisms involved in T cell receptor triggering. *Semin. Immunol.* 19, 255–261.

Chu, Y., Vahl, J.C., Kumar, D., Heger, K., Bertossi, A., Wójtowicz, E., Soberon, V., Schenten, D., Mack, B., Reutelshöfer, M., Beyaert, R., Loo, G. Van, Schmidt-supprian, M., Dc, W., Wo, E., Reutelsho, M., Amann, K., 2011. B cells lacking the tumor suppressorTNFAIP3/A20 display impaired differentiation and hyperactivation and cause inflammation and autoimmunity in aged mice. *Blood* 117, 2227–2236.

Clem, R.J., Cheng, E.H., Karp, C.L., Kirsch, D.G., Ueno, K., Takahashi, a, Kastan, M.B., Griffin, D.E., Earnshaw, W.C., Veliuona, M. a, Hardwick, J.M., 1998. Modulation of cell death by Bcl-XL through caspase interaction. *Proc. Natl. Acad. Sci. U. S. A.* 95, 554–559.

Conrad, M., Angeli, J.P.F., Vandenabeele, P., Stockwell, B.R., 2016. Regulated necrosis: disease relevance and therapeutic opportunities. *Nat. Rev. Drug Discov.*

Courtois, G., Smahi, A., Reichenbach, J., Döffinger, R., Cancrini, C., Bonnet, M., Puel, A., Chable-bessia, C., Yamaoka, S., Feinberg, J., Dupuis-girod, S., Bodemer, C., Livadiotti, S., Novelli, F., Rossi, P., Fischer, A., Israël, A., Munnich, A., Deist, F. Le, Casanova, J., 2003. A hypermorphic IκBα mutation is associated with autosomal dominant anhidrotic ectodermal dysplasia and T cell immunodeficiency. *J. Clin. Invest.* 112, 1108–15.

Daniel, S., Arvelo, M.B., Patel, V.I., Longo, C.R., Shrikhande, G., Shukri, T., Mahiou, J., Sun, D.W., Mottley, C., Grey, S.T., Ferran, C., 2004. A20 protects endothelial cells from TNF-, Fas-, and NK-mediated cell death by inhibiting caspase 8 activation. *Blood* 104, 2376–2384.

Daniels, M.A., Teixeiro, E., 2015. TCR Signaling in T Cell Memory 6, 1–10.

Dhein, J., Walczak, H., Bäumler, C., Debatin, K.M., Krammer, P.H., 1995. Autocrine T-cell suicide mediated by APO-1/(Fas/CD95). *Nature*.

Donnell, M.A.O., Legarda-addison, D., Skountzos, P., Yeh, W.C., Ting, A.T., 2007. Report Ubiquitination of RIP1 Regulates an NF-κB-Independent Cell-Death Switch in TNF Signaling. *Curr. Biol.* 17, 418–424.

Dudani, R., Russell, M., van Faassen, H., Krishnan, L., Sad, S., 2008. Mutation in the Fas pathway impairs CD8+ T cell memory. *J. Immunol.* 180, 2933–41.

Düwel, M., Welteke, V., Oeckinghaus, A., Baens, M., Kloo, B., Ferch, U., Darnay, B.G., Ruland, J., Marynen, P., Krappmann, D., 2009. A20 Negatively Regulates T Cell Receptor Signaling to NF-κB by Cleaving Malt1 Ubiquitin Chains. *J. Immunol.* 182, 7718–7728.

Festjens, N., Vanden Berghe, T., Cornelis, S., Vandenabeele, P., 2007. RIP1, a kinase on the crossroads of a cell's decision to live or die. *Cell Death Differ.* 14, 400–410.

Fung, E., Smyth, D.J., Howson, J.M.M., Cooper, J.D., Walker, N.M., Stevens, H., Wicker, L.S., Todd, J.A., 2009. Analysis of 17 autoimmune disease-associated variants in type 1 diabetes identifies 6q23 / TNFAIP3 as a susceptibility locus. *Genes Immun.* 4, 188–191.

Fuse, S., Tsai, C.-Y., Molloy, M.J., Allie, S.R., Zhang, W., Yagita, H., Usherwood, E.J., 2009. Recall responses by helpless memory CD8+ T cells are restricted by the up-regulation of PD-1. *J. Immunol.* 182, 4244–54.

Fuse, Y., Nishimura, H., Maeda, K., Yoshikai, Y., 1997. CD95 (Fas) may control the expansion of activated T cells after elimination of bacteria in murine listeriosis. *Infect. Immun.* 65, 1883–1891.

Garg, A. V, Ahmed, M., Vallejo, A.N., Ma, A., Gaffen, S.L., 2013. The deubiquitinase A20 mediates feedback inhibition of interleukin-17 receptor signaling. *Sci. Signal.* 6, ra44.

Germain, R.N., 2002. T-cell development and the CD4-CD8 lineage decision. *Nat. Rev. Immunol.* 2, 309–322.

Gerondakis, S., Siebenlist, U., 2010. Roles of the NF-κB pathway in lymphocyte development and function. *Cold Spring Harb. Perspect. Biol.* 2, 1–29.

Ghosh, S., Hayden, M.S., 2008. New regulators of NF-κB in inflammation. *Nat. Rev. Immunol.* 8, 837–848.

Ghosh, S., May, M.J., Kopp, E.B., 1998. NF-κB AND REL PROTEINS : Evolutionarily Conserved Mediators of Immune Responses. *Annu. Rev. Immunol.* 16, 225–260.

Graham, K.L., Krishnamurthy, B., Fynch, S., Mollah, Z.U., Slattery, R., Santamaria, P., Kay, T.W., Thomas, H.E., 2011. Autoreactive cytotoxic T lymphocytes acquire higher expression of cytotoxic effector markers in the islets of NOD mice after priming in pancreatic lymph nodes. *Am. J. Pathol.* 178, 2716–2725.

Graham, R.R., Cotsapas, C., Davies, L., Hackett, R., Lessard, C.J., Leon, J.M., Burtt, N.P., Guiducci, C., Parkin, M., Gates, C., Plenge, R.M., Behrens, T.W., Wither, J.E., Rioux, J.D., Fortin, P.R., Cunninghame, D., Wong, A.K., Vyse, T.J., Daly, M.J., Altshuler, D., Moser, K.L., Gaffney, P.M., 2008. Genetic variants near TNFAIP3 on 6q23 are associated with systemic lupus erythematosus. *Nat. Genet.* 40, 1059–1061.

Hammer, G.E., Turer, E.E., Taylor, K.E., Fang, C.J., Advincula, R., Oshima, S., Barrera, J., Huang, E.J., Hou, B., Malynn, B.A., Reizis, B., DeFranco, A., Criswell, L.A., Nakamura, M.C., Ma, A., 2011. Expression of A20 by dendritic cells preserves

immune homeostasis and prevents colitis and spondyloarthritis. *Nat. Immunol.* 12, 1184–1193.

Hamon, M., Bierne, H., Cossart, P., 2006. Listeria monocytogenes: a multifaceted model. *Nat. Rev. Microbiol.* 4, 423–434.

Harhaj, E.W., Dixit, V.M., 2010. Deubiquitinases in the regulation of NF-κB signaling. *Cell Res.* 21, 22–39.

Hassa, P.O., Covic, M., Hasan, S., Imhof, R., Hottiger, M.O., 2001. The Enzymatic and DNA Binding Activity of PARP-1 Are Not Required for NF-??B Coactivator Function. *J. Biol. Chem.* 276, 45588–45597.

Heger, K., Fierens, K., Vahl, J.C., Aszodi, A., Peschke, K., Schenten, D., Hammad, H., Beyaert, R., Saur, D., Loo, G. Van, Roers, A., Lambrecht, B.N., Kool, M., Schmidt-supprian, M., 2014. A20-Deficient Mast Cells Exacerbate Inflammatory Responses In Vivo. *Plos Biol.* 12.

Henry, C.M., Hollville, E., Martin, S.J., 2013. Measuring apoptosis by microscopy and flow cytometry. *Methods* 61, 90–7.

Hershko, A., Ciechanover, A., Varshavsky, A., 1998. The ubiquitin system. *Annu. Rev. Biochem.* 67, 425–479.

Hettmann, T., Opferman, J.T., Leiden, J.M., Ashton-Rickardt, P.G., 2003. A critical role for NF-κB transcription factors in the development of CD8+ memory-phenotype T cells. *Immunol. Lett.* 85, 297–300.

Hildeman, D.A., Zhu, Y., Mitchell, T.C., Bouillet, P., Strasser, A., Kappler, J., Marrack, P., 2002. Activated T cell death in vivo mediated by proapoptotic Bcl-2 family member Bim. *Immunity* 16, 759–767.

Hochstrasser, M., Amerik, A.Y., 2004. Mechanism and function of deubiquitinating enzymes. *Biochim. Biophys. Acta - Mol. Cell Res.* 1695, 189–207.

Honma, K., Tsuzuki, S., Nakagawa, M., Tagawa, H., Nakamura, S., Morishima, Y., 2009. TNFAIP3 / A20 functions as a novel tumor suppressor gene in several subtypes of non-Hodgkin lymphomas. *Blood* 114, 2467–2475.

Hövelmeyer, N., Reissig, S., Xuan, N.T., Adams-Quack, P., Lukas, D., Nikolaev, A., Schlüter, D., Waisman, A., 2011. A20 deficiency in B cells enhances B-cell proliferation and results in the development of autoantibodies. *Eur. J. Immunol.* 41, 595–601.

Huang, C., Bi, E., Hu, Y., Deng, W., Tian, Z., Dong, C., Sun, B., 2006. A Novel NF- B Binding Site Controls Human Granzyme B Gene Transcription. *J. Immunol.* 176, 4173–4181.

Hughes, P.D., Belz, G.T., Fortner, K.A., Budd, R.C., Strasser, A., Bouillet, P., 2008. Apoptosis Regulators Fas and Bim Cooperate in Shutdown of Chronic Immune Responses and??Prevention of Autoimmunity. *Immunity* 28, 197–205.

Husnjak, K., Dikic, I., 2012. Ubiquitin-Binding Proteins : Decoders of Ubiquitin- Mediated Cellular Functions. *Annu. Rev. Biochem.* 81, 291–322.

Huster, K.M., Busch, V., Schiemann, M., Linkemann, K., Kerksiek, K.M., Wagner, H., Busch, D.H., 2004. Selective expression of IL-7 receptor on memory T cells identifies early CD40L-dependent generation of distinct CD8+ memory T cell subsets. *Proc. Natl. Acad. Sci. U. S. A.* 101, 5610–5615.

Hutcheson, J., Scatizzi, J.C., Siddiqui, A.M., Haines, G.K., Wu, T., Li, Q.Z., Davis, L.S., Mohan, C., Perlman, H., 2008. Combined Deficiency of Proapoptotic Regulators Bim

and Fas Results in the Early Onset of Systemic Autoimmunity. *Immunity* 28, 206–217.

Ichiki, Y., Aoki, C.A., Bowlus, C.L., Shimoda, S., Ishibashi, H., Gershwin, M.E., 2005. T cell immunity in autoimmune hepatitis. *Autoimmun. Rev.* 4, 315–321.

Jameson, S.C., 2002. Maintaining the norm: T-cell homeostasis. *Nat. Rev. Immunol.* 2, 547–556.

Joshi, N.S., Cui, W., Chandele, A., Lee, H.K., Urso, D.R., Hagman, J., Gapin, L., Kaech, S.M., 2007. Inflammation Directs Memory Precursor and Short-Lived Effector CD8 + T Cell Fates via the Graded Expression of T-bet Transcription Factor. *Immunity* 27, 281–295.

Kaech, S.M., Cui, W., 2012. Transcriptional control of effector and memory CD8+ T cell differentiation. *Nat. Rev. Immunol.* 12, 749–761.

Kaech, S.M., Hemby, S., Kersh, E., Ahmed, R., 2002. Molecular and functional profiling of memory CD8 T cell differentiation. *Cell* 111, 837–851.

Kaech, S.M., Tan, J.T., Wherry, E.J., Konieczny, B.T., Surh, C.D., Ahmed, R., 2003. Selective expression of the interleukin 7 receptor identifies effector CD8 T cells that give rise to long-lived memory cells. *Nat. Immunol.* 4, 1191–8.

Kato, M., Sanada, M., Kato, I., Sato, Y., Takita, J., Takeuchi, K., Niwa, A., Chen, Y., Nakazaki, K., Nomoto, J., Asakura, Y., Muto, S., Tamura, A., Chiba, S., Mori, S., Ishikawa, Y., Okamoto, K., Tobinai, K., Nakagama, H., 2009. Frequent inactivation of A20 in B-cell lymphomas. *Nature* 459, 712–716.

Kavanagh, E., Rodhe, J., Burguillos, M.A., Venero, J.L., Joseph, B., 2014. Regulation of caspase-3 processing by cIAP2 controls the switch between pro-inflammatory activation and cell death in microglia. *Cell Death Dis.* 5, e1565.

Keir, M.E., Butte, M.J., Freeman, G.J., Sharpe, A.H., 2008. PD-1 and its ligands in tolerance and immunity. *Annu Rev Immunol* 26, 677–704.

Kelly, C., Williams, M.T., Mitchell, K., Elborn, J.S., Ennis, M., Schock, B.C., 2013. Expression of the nuclear factor-kB inhibitor A20 is altered in the cystic fibrosis epithelium. *Eur. Respir. J.* 41, 1315–1323.

Kennedy, N.J., Kataoka, T., Tschopp, J., Budd, R.C., 1999. Caspase activation is required for T cell proliferation. *J. Exp. Med.* 190, 1891–1896.

Kerscher, O., Felberbaum, R., Hochstrasser, M., 2006. Modification of Proteins by Ubiquitin and Ubiquitin-Like Proteins. *Annu. Rev. Cell Dev. Biol.* 22, 159–80.

Klein, L., Kyewski, B., Allen, P.M., Hogquist, K.A., 2016. Positive and negative selection of the T cell repertoire: what thymocytes see and don't see. *Nat. Rev. Immunol.* 14, 377–391.

Kool, M., van Loo, G., Waelput, W., De Prijck, S., Muskens, F., Sze, M., van Praet, J., Branco-Madeira, F., Janssens, S., Reizis, B., Elewaut, D., Beyaert, R., Hammad, H., Lambrecht, B.N., 2011. The ubiquitin-editing protein A20 prevents dendritic cell activation, recognition of apoptotic cells, and systemic autoimmunity. *Immunity* 35, 82–96.

Krammer, P.H., Arnold, R., Lavrik, I.N., 2007. Life and death in peripheral T cells. *Nat. Rev. Immunol.* 7, 532–542.

Kreuz, S., Siegmund, D., Rumpf, J.J., Samel, D., Leverkus, M., Janssen, O., H??cker, G., Dittrich-Breiholz, O., Kracht, M., Scheurich, P., Wajant, H., 2004. NF-κB activation by Fas is mediated through FADD, caspase-8, and RIP and is inhibited by FLIP. *J.*

Cell Biol. 166, 369–380.

Krishna, S., Xie, D., Gorentla, B., Shin, J., Gao, J., Zhong, X.-P., 2012. Chronic activation of the kinase IKKß impairs T cell function and survival. *J. Immunol.* 189, 1209–1219.

Krueger, A., Fas, S.C., Baumann, S., Krammer, P.H., 2003. The role of CD95 in the regulation of peripheral T-cell apoptosis. *Immunol. Rev.* 193, 58–69.

Lamothe, B., Besse, A., Campos, A.D., Webster, W.K., Wu, H., Darnay, B.G., 2007. Site-specific Lys-63-linked Tumor Necrosis Factor Is a Critical Determinant of IκB Kinase Activation *. *J. Biol. Chem.* 282, 4102–4112.

Lee, E.G., Boone, D.L., Chai, S., Libby, S.L., Chien, M., Lodolce, J.P., Ma, a, 2000. Failure to regulate TNF-induced NF-kappaB and cell death responses in A20-deficient mice. *Science* 289, 2350–2354.

Li, Q., Verma, I.M., Pines, N.T., 2002. NF-κB Regulation in the Immune System. *Nat. Rev. Immunol.* 2, 725–734.

Li, X., Jiang, S., Tapping, R.I., 2010. Toll-like receptor signaling in cell proliferation and survival. *Cytokine* 49, 1–9.

Lippens, S., Lefebvre, S., Gilbert, B., Sze, M., Devos, M., Verhelst, K., Vereecke, L., Guire, C.M., Guérin, C., Vandenabeele, P., Pasparakis, M., Mikkola, M.L., Beyaert, R., Declercq, W., van Loo, G., 2011. Keratinocyte-specific ablation of the NF-κB regulatory protein A20 (TNFAIP3) reveals a role in the control of epidermal homeostasis. *Cell Death Differ.* 18, 1845–1853.

Livak, K.J., Schmittgen, T.D., 2001. Analysis of relative gene expression data using real-time quantitative PCR and the 2^(-ΔΔCT) method. *Methods* 25, 402–408.

Lohman, B.L., Razvi, E.S., Welsh, R.M., 1996. T-lymphocyte downregulation after acute viral infection is not dependent on CD95 (Fas) receptor-ligand interactions. *J Virol* 70, 8199–8203.

Longo, C.R., Arvelo, M.B., Patel, V.I., Daniel, S., Mahiou, J., Grey, S.T., Ferran, C., 2003. A20 protects from CD40-CD40 ligand-mediated endothelial cell activation and apoptosis. *Circulation* 108, 1113–1118.

Ma, A., Malynn, B.A., 2012. A20: linking a complex regulator of ubiquitylation to immunity and human disease. *Nat. Rev. Immunol.* 12, 774–785.

Maelfait, J., Roose, K., Bogaert, P., Sze, M., Saelens, X., Pasparakis, M., Carpentier, I., van Loo, G., Beyaert, R., 2012. A20 (Tnfaip3) deficiency in myeloid cells protects against influenza A virus infection. *PLoS Pathog* 8, e1002570.

Malynn, B.A., Ma, A., 2010. Ubiquitin Makes Its Mark on Immune Regulation. *Immunity* 33, 843–852.

Martin, D.A., Zheng, L., Siegel, R.M., Huang, B., Fisher, G.H., Wang, J., Jackson, C.E., Puck, J.M., Dale, J., Straus, S.E., Peter, M.E., Krammer, P.H., Fesik, S., Lenardo, M.J., 1999. Defective CD95/APO-1/Fas signal complex formation in the human autoimmune lymphoproliferative syndrome, type Ia. *Proc. Natl. Acad. Sci. U. S. A.* 96, 4552–4557.

Matmati, M., Jacques, P., Maelfait, J., Verheugen, E., Kool, M., Sze, M., Geboes, L., Louagie, E., Mc Guire, C., Vereecke, L., Chu, Y., Boon, L., Staelens, S., Matthys, P., Lambrecht, B.N., Schmidt-Supprian, M., Pasparakis, M., Elewaut, D., Beyaert, R., van Loo, G., 2011. A20 (TNFAIP3) deficiency in myeloid cells triggers erosive polyarthritis resembling rheumatoid arthritis. *Nat. Genet.* 43, 908–12.

Mauro, C., Pacifico, F., Lavorgna, A., Mellone, S., Iannetti, A., Acquaviva, R., Formisano,

S., Vito, P., Leonardi, A., 2006. ABIN-1 binds to NEMO/IKKgamma and co-operates with A20 in inhibiting NF-κB. *J. Biol. Chem.* 281, 18482–18488.

Mogil, R.J., Radvanyi, L., Gonzalez-Quintial, R., Miller, R., Mills, G., Theofilopoulos, a N., Green, D.R., 1995. Fas (CD95) participates in peripheral T cell deletion and associated apoptosis in vivo. *Int. Immunol.* 7, 1451–8.

Müllauer, L., Emhofer, J., Wohlfart, S., Pichlhöfer, B., Stary, S., Ebetsberger, G., Mannhalter, C., Chott, A., 2008. Autoimmune lymphoproliferative syndrome (ALPS) caused by Fas (CD95) mutation mimicking sarcoidosis. *Am. J. Surg. Pathol.* 32, 329–334.

Nair, R.P., Duffin, K.C., Helms, C., Ding, J., Stuart, P.E., Goldgar, D., Gudjonsson, J.E., Li, Y., Tejasvi, T., Feng, B., Ruether, A., Schreiber, S., Weichenthal, M., Gladman, D., Rahman, P., Schrodi, S.J., Prahalad, S., Guthery, S.L., Fischer, J., Liao, W., Kwok, P., Menter, A., Lathrop, G.M., Wise, C.A., Begovich, A.B., Voorhees, J.J., Elder, J.T., Krueger, G.G., Bowcock, A.M., 2009. Genome-wide scan reveals association of psoriasis with IL-23 and NF-κB pathways. *Nat. Genet.* 41, 199–204.

Nijman, S.M.B., Luna-vargas, M.P.A., Velds, A., Brummelkamp, T.R., Dirac, A.M.G., Sixma, T.K., Bernards, R., 2005. Review A Genomic and Functional Inventory of Deubiquitinating Enzymes. *Cell* 123, 773–786.

Oeckinghaus, A., Ghosh, S., 2009. The NF-κB Family of Transcription Factors and. *Cold Spring Harb. Perspect. Biol.* 1–15.

Oeckinghaus, A., Wegener, E., Welteke, V., Ferch, U., Seda, C., Scheidereit, C., Krappmann, D., 2007. Malt1 ubiquitination triggers NF-κB signaling upon T-cell activation. *EMBO J.* 26, 4634–4645.

Onizawa, M., Oshima, S., Schulze-Topphoff, U., Oses-Prieto, J.A., Lu, T., Tavares, R., Prodhomme, T., Duong, B., Whang, M.I., Advincula, R., Agelidis, A., Barrera, J., Wu, H., Burlingame, A., Malynn, B.A., Zamvil, S.S., Ma, A., 2015. The ubiquitin-modifying enzyme A20 restricts ubiquitination of the kinase RIPK3 and protects cells from necroptosis. *Nat. Immunol.* 16, 618–627.

Opipari, a W., Boguski, M.S., Dixit, V.M., 1990. The A20 cDNA induced by tumor necrosis factor alpha encodes a novel type of zinc finger protein. *J. Biol. Chem.* 265, 14705–14708.

Opipari, a W., Hu, H.M., Yabkowitz, R., Dixit, V.M., 1992. The A20 zinc finger protein protects cells from tumor necrosis factor cytotoxicity. *J. Biol. Chem.* 267, 12424–7.

Pamer, E.G., 2004. Immune responses to Listeria monocytogenes. *Nat. Rev. Immunol.* 4, 812–823.

Pasparakis, M., Vandenabeele, P., 2015. Necroptosis and its role in inflammation. *Nature* 517, 311–320.

Patel, V.I., Daniel, S., Longo, C.R., Shrikhande, G. V, Scali, S.T., Czismadia, E., Groft, C.M., Shukri, T., Motley-Dore, C., Ramsey, H.E., Fisher, M.D., Grey, S.T., Arvelo, M.B., Ferran, C., 2006. A20, a modulator of smooth muscle cell proliferation and apoptosis, prevents and induces regression of neointimal hyperplasia. *FASEB J.* 20, 1418–1430.

Paulsen, M., Janssen, O., 2011. Pro- and anti-apoptotic CD95 signaling in T cells. *Cell Commun. Signal.* 9, 7.

Paulsen, M., Ussat, S., Jakob, M., Scherer, G., Lepenies, I., Sch??tze, S., Kabelitz, D., Adam-Klages, S., 2008. Interaction with XIAP prevents full caspase-3/-7 activation in proliferating human T lymphocytes. *Eur. J. Immunol.* 38, 1979–1987.

Pearce, E.L., Walsh, M.C., Cejas, P.J., Harms, G.M., Shen, H., Wang, L.-S., Jones, R.G., Choi, Y., 2009. Enhancing CD8 T-cell memory by modulating fatty acid metabolism. *Nature* 460, 103–107.

Pellegrini, M., Belz, G., Bouillet, P., Strasser, A., 2003. Shutdown of an acute T cell immune response to viral infection is mediated by the proapoptotic Bcl-2 homology 3-only protein Bim. *Proc. Natl. Acad. Sci. U. S. A.* 100, 14175–80.

Pickart, C.M., Eddins, M.J., 2004. Ubiquitin : structures , functions , mechanisms. *Biochim. Biophys. Acta - Mol. Cell Res.* 1695, 55–72.

Pietkiewicz, S., Schmidt, J.H., Lavrik, I.N., 2015. Quantification of apoptosis and necroptosis at the single cell level by a combination of Imaging Flow Cytometry with classical Annexin V/ propidium iodide staining. *J. Immunol. Methods* 423, 99–103.

Renno, T., Hahne, M., MacDonald, H.R., 1995. Proliferation is a prerequisite for bacterial superantigen- induced T cell apoptosis in vivo Proliferation is a prerequisite for bacterial superantigen- induced T cell apoptosis in vivo. *J. Exp. Med.* 181, 2283–2287.

Russell, J.H., Rush, B., Weaver, C., Wang, R., 1993. Mature T cells of autoimmune lpr/lpr mice have a defect in antigen-stimulated suicide. *Proc. Natl. Acad. Sci. U. S. A.* 90, 4409–13.

Sallusto, F., Geginat, J., Lanzavecchia, A., 2004. Central Memory and Effector Memory T cell subsets : Function, Generation, and Maintenance. *Annu. Rev. Immunol.* 22, 745–763.

Salmena, L., Lemmers, B., Hakem, A., Matysiak-Zablocki, E., Murakami, K., Billie Au, P.Y., Berry, D.M., Tamblyn, L., Shehabeldin, A., Migon, E., Wakeham, A., Bouchard, D., Yeh, W.C., McGlade, J.C., Ohashi, P.S., Hakem, R., 2003. Essential role for caspase 8 in T-cell homeostasis and T-cell-mediated immunity. *Genes Dev.* 17, 883–895.

Schmitz, R., Hansmann, M.-L., Bohle, V., Martin-Subero, J.I., Hartmann, S., Mechtersheimer, G., Klapper, W., Vater, I., Giefing, M., Gesk, S., Stanelle, J., Siebert, R., Küppers, R., 2009. TNFAIP3 (A20) is a tumor suppressor gene in Hodgkin lymphoma and primary mediastinal B cell lymphoma. *J. Exp. Med.* 206, 981–989.

Schuppler, M., Loessner, M.J., 2010. The Opportunistic Pathogen Listeria monocytogenes : Pathogenicity and Interaction with the Mucosal Immune System. *Int. J. Inflamm.* 2010, 1–12.

Seder, R.A., Ahmed, R., 2003. Similarities and differences in {CD}4+ and {CD}8+ effector and memory {T} cell generation. *Nat Immunol* 4, 835–842.

Shedlock, D.J., Shen, H., 2003. Requirement for CD4 T Cell Help in Generating Functional CD8 T Cell Memory. *Science (80-.).* 300, 337–339.

Shen, H., Tato, C.M., Fan, X., 1998. Listeria monocytogenes as a probe to study cell-mediated immunity. *Curr. Opin. Immunol.* 10, 450–458.

Sheppard, K.A., Fitz, L.J., Lee, J.M., Benander, C., George, J.A., Wooters, J., Qiu, Y., Jussif, J.M., Carter, L.L., Wood, C.R., Chaudhary, D., 2004. PD-1 inhibits T-cell receptor induced phosphorylation of the ZAP70/CD3?? signalosome and downstream signaling to PKC?? *FEBS Lett.* 574, 37–41.

Sica, A., Dorman, L., Viggiano, V., Cippitelli, M., Ghosh, P., Rice, N., Young, H. a, 1997. Interaction of NF-kappaB and NFAT with the interferon-gamma promoter. *J. Biol. Chem.* 272, 30412–30420.

Silke, J., Rickard, J.A., Gerlic, M., 2015. The diverse role of RIP kinases in necroptosis and

inflammation. *Nat. Immunol.* 16, 689–697.

Sprent, J., Tough, D.F., 2001. T Cell Death and Memory. *Science (80-.).* 293, 245–248.

Stavru, F., Archambaud, C., Cossart, P., 2011. Cell biology and immunology of Listeria monocytogenes infections: Novel insights. *Immunol. Rev.* 240, 160–184.

Storz, P., Döppler, H., Ferran, C., Grey, S.T., Toker, A., 2005. Functional dichotomy of A20 in apoptotic and necrotic cell death. *Biochem. J.* 387, 47–55.

Su, H., Nicholas, B., Lixin, Z., Cubre, A., Sakai, K., Dale, J., Salmena, L., Hakem, R., Straus, S., Lenardo, M., 2005. Requirement for Caspase-8 in NF- κB Activation by Antigen Receptor. *Science (80-.).* 307, 1465–1468.

Sun, J.C., Bevan, M.J., 2003. Defective CD8 T Cell Memory Following Acute Infection Without CD4 T Cell Help. *Science (80-.).* 300, 339–343.

Sun, S.-C., 2011. Non-canonical NF-κB signaling pathway. *Cell Res.* 21, 71–85.

Suresh, M., Singh, A., Fischer, C., 2005. Role of Tumor Necrosis Factor Receptors in Regulating CD8 T-Cell Responses during Acute Lymphocytic Choriomeningitis Virus Infection Role of Tumor Necrosis Factor Receptors in Regulating CD8 T-Cell Responses during Acute Lymphocytic Choriomeningitis Virus 79, 202–213.

Tavares, R.M., Turer, E.E., Liu, C.L., Advincula, R., Scapini, P., Rhee, L., Barrera, J., Lowell, C. a., Utz, P.J., Malynn, B. a., Ma, A., 2010. The Ubiquitin Modifying Enzyme A20 Restricts B Cell Survival and Prevents Autoimmunity. *Immunity* 33, 181–191.

Thome, M., Charton, J.E., Pelzer, C., Hailfinger, S., 2010. Antigen receptor signaling to NF-κB via CARMA1, BCL10, and MALT1. *Cold Spring Harb. Perspect. Biol.* 2.

Thomson, W., Barton, A., Ke, X., Eyre, S., Hinks, A., Bowes, J., Donn, R., Symmons, D., Hider, S., Bruce, I.N., Trust, W., Control, C., Wilson, A.G., Marinou, I., Morgan, A., Emery, P., Consortium, Y., Carter, A., Steer, S., Hocking, L., Reid, D.M., Wordsworth, P., Harrison, P., Strachan, D., Worthington, J., 2007. Rheumatoid arthritis association at 6q23. *Nat. Genet.* 39, 1431–1433.

Trembleau, S., Penna, G., Gregori, S., Chapman, H.D., Serreze, D. V, Magram, J., Adorini, L., 1999. Pancreas-infiltrating Th1 cells and diabetes develop in IL-12-deficient nonobese diabetic mice. *J. Immunol.* 163, 2960–2968.

Trynka, G., Zhernakova, A., Romanos, J., Franke, L., Hunt, K.A., Turner, G., Bruinenberg, M., Heap, G.A., Platteel, M., Ryan, A.W., Kovel, C. De, Holmes, G.K.T., Howdle, P.D., Walters, J.R.F., Sanders, D.S., Mulder, C.J.J., Mearin, M.L., Verbeek, W.H.M., Trimble, V., Stevens, F.M., Kelleher, D., Barisani, D., Bardella, M.T., Mcmanus, R., Heel, D.A. Van, Wijmenga, C., 2009. Coeliac disease-associated risk variants in TNFAIP3 and REL implicate altered NF-κB signalling. *Gut* 58, 1078–1083.

Utzschneider, D.T., Charmoy, M., Chennupati, V., Pousse, L., Ferreira, D.P., Calderon-Copete, S., Danilo, M., Alfei, F., Hofmann, M., Wieland, D., Pradervand, S., Thimme, R., Zehn, D., Held, W., 2016. T Cell Factor 1-Expressing Memory-like CD8+ T Cells Sustain the Immune Response to Chronic Viral Infections. *Immunity* 45, 415–427.

Vallabhapurapu, S., Karin, M., 2009. Regulation and Function of NF-κB Transcription Factors in the Immune System. *Annu. Rev. Immunol.* 27, 693–733.

Vanden Berghe, T., Linkermann, A., Jouan-Lanhouet, S., Walczak, H., Vandenabeele, P., Berghe, T. Vanden, Linkermann, A., Jouan-Lanhouet, S., Walczak, H., Vandenabeele, P., 2014. Regulated necrosis: the expanding network of non-apoptotic cell death pathways. *Nat. Rev. Mol. Cell Biol.* 15, 135–47.

Vereecke, L., Sze, M., Mc Guire, C., Rogiers, B., Chu, Y., Schmidt-Supprian, M.,

Pasparakis, M., Beyaert, R., van Loo, G., 2010. Enterocyte-specific A20 deficiency sensitizes to tumor necrosis factor-induced toxicity and experimental colitis. *J. Exp. Med.* 207, 1513–1523.

Verstrepen, L., Bekaert, T., Chau, T.L., Tavernier, J., Chariot, A., Beyaert, R., 2008. TLR-4, IL-1R and TNF-R signaling to NF-κB: Variations on a common theme. *Cell. Mol. Life Sci.* 65, 2964–2978.

Vignali, D.A.A., Collison, L.W., Workman, C.J., 2008. How regulatory T cells work. *Nat. Rev. Immunol.* 8, 523–532.

Wajant, H., Pfizenmaier, K., Scheurich, P., 2003. Non-apoptotic Fas signaling. *Cytokine Growth Factor Rev.* 14, 53–66.

Wang, H., Kadlecek, T.A., Au-Yeung, B.B., Goodfellow, H.E.S., Hsu, L.Y., Freedman, T.S., Weiss, A., 2010. ZAP-70: an essential kinase in T-cell signaling. *Cold Spring Harb. Perspect. Biol.* 2.

Wang, X., Deckert, M., Xuan, N.T., Nishanth, G., Just, S., Waisman, A., Naumann, M., Schlüter, D., 2013. Astrocytic A20 ameliorates experimental autoimmune encephalomyelitis by inhibiting NF-κB- and STAT1-dependent chemokine production in astrocytes. *Acta Neuropathol.* 3, 711–724.

Wang, X., Xu, Y., Liang, L., Xu, Y., Wang, C., Wang, L., Chen, S., Yang, L., Wu, X., Li, B., Luo, G., Tan, H., Li, W., Li, Y., 2014. Abnormal expression of A20 and its regulated genes in peripheral blood from patients with lymphomas. *Cancer Cell Int.* 14, 36.

Whitmire, J.K., Ahmed, R., 2000. Costimulation in antiviral immunity: differential requirements for CD4(+) and CD8(+) T cell responses. *Curr Opin Immunol* 12, 448–455.

Williams, M. a, Tyznik, A.J., Bevan, M.J., 2006. Interleukin-2 signals during priming are required for secondary expansion of CD8+ memory T cells. *Nature* 441, 890–893.

Wirth, T.C., Martin, M.D., Starbeck-Miller, G., Harty, J.T., Badovinac, V.P., 2011. Secondary CD8+ T-cell responses are controlled by systemic inflammation. *Eur. J. Immunol.* 41, 1321–1333.

Wojciechowski, S., Jordan, M.B., Zhu, Y., White, J., Zajac, A.J., Hildeman, D.A., 2006. Bim mediates apoptosis of CD127lo effector T cells and limits T cell memory. *Eur. J. Immunol.* 36, 1694–1706.

Xuan, N.T., Wang, X., Nishanth, G., Waisman, A., Borucki, K., Isermann, B., Naumann, M., Deckert, M., Schlüter, D., 2014. A20 expression in dendritic cells protects mice from LPS-induced mortality. *Eur. J. Immunol.* 45, 818–828.

Yang, J.Y., Widmann, C., 2001. Antiapoptotic signaling generated by caspase-induced cleavage of RasGAP. *Mol. Cell. Biol.* 21, 5346–58.

Ye, Y., Rape, M., 2009. Building ubiquitin chains: E2 enzymes at work. *Nat. Rev. Mol. Cell Biol.* 10, 755–64.

Yi, J.S., Cox, M.A., Zajac, A.J., 2010. T-cell exhaustion: Characteristics, causes and conversion. *Immunology* 129, 474–481.

Zehn, D., King, C., Bevan, M.J., Palmer, E., 2012. TCR signaling requirements for activating T cells and for generating memory. *Cell. Mol. Life Sci.* 69, 1565–1575.

Zhang, N., Bevan, M.J., 2011. CD8(+) T cells: foot soldiers of the immune system. *Immunity* 35, 161–8.

Zhou, S., Ou, R., Huang, L., Moskophidis, D., 2002. Critical role for perforin-, Fas/FasL-, and TNFR1-mediated cytotoxic pathways in down-regulation of antigen-specific T

cells during persistent viral infection. *J. Virol.* 76, 829–840.

Zhu, J., Paul, W.E., 2009. CD4 T cells: fates, functions, and faults. *Immunobiology* 112, 1557–1569.

Zimmermann, C., Rawiel, M., Blaser, C., Kaufmann, M., Pircher, H., 1996. Homeostatic regulation of CD8+ T cells after antigen challenge in the absence of Fas (CD95). *Eur. J. Immunol.* 26, 2903–10.

CURRICULUM VITAE

Personal details

Name	Sissy Just
Date of birth	March 14th, 1987
Place of birth	Eilenburg, Germany
Address	Amsdorfstr. 3
	39112 Magdeburg
Phone	0049 (0) 1771875201
Email	sissy.just@web.de

Education

Since 2013	PhD, Faculty of Natural Sciences, Otto-von-Guericke University, Magdeburg, Germany
2008-2010	Master of Science in Microbiology, Faculty of Natural Sciences, Friedrich-Schiller-University, Jena, Germany
2005-2008	Bachelor of Science in Biology, Faculty of Natural Sciences, Justus-Liebig-University, Giessen, Germany

Scientific experience

Since 2011	PhD thesis, Department of Medical Microbiology and Hospital Hygiene, University Hospital Magdeburg
2011	Research assistant, Department of Immunology, Fraunhofer Institute, Leipzig
2010	Master thesis, Department of Virology and Antiviral Therapy, University Hospital Jena
2009-2010	Internship, Department of Virology and Antiviral Therapy, University Hospital Jena
2009	Academic assistant, Department of Phytopathology, University Jena
2008	Bachelor thesis, Department of Ecology, University Giessen

Sissy Just • Amsdorfstr.3 • 39112 Magdeburg

DECLARATION OF ORIGINALITY

Hiermit erkläre ich, dass ich die von mir eingereichte Dissertation zu dem Thema

T cell specific function of the deubiquitinating enzyme A20 in murine listeriosis

selbstständig verfasst, nicht bereits als Dissertation verwendet habe und die benutzten Hilfsmittel und Quellen vollständig angegeben wurden.

Weiterhin erkläre ich, dass ich weder diese noch eine andere Arbeit zur Erlangung des akademischen Grades *doctor rerum naturalium* (Dr. rer. nat.) an anderen Einrichtungen eingereicht habe.

Magdeburg, 24. Oktober 2016

Sissy Just